공학박사 학위논문

Study on heteroepitaxial growth of GaN using sapphire nano-membrane for micro-light-emitting diodes

마이크로 발광 다이오드를 위한 사파이어 나노 멤브레인 위 GaN 이종성장 연구

2021 년 2 월

서울대학교 대학원

재료공학부

이 승 민

Study on heteroepitaxial growth of GaN using sapphire nano-membrane for micro-light-emitting diodes

지도교수 장 호 원

이 논문을 공학박사 학위논문으로 제출함

2020 년 12 월

서울대학교 대학원

재료공학부

이 승 민

이승민의 공학박사 학위논문을 인준함

2021 년 1 월

위 원 장	주 영 창
부위원장	장 호 원
위 원	김 진 영
위 원	윤 의 준
위 원	박 용 조

Abstract

Study on heteroepitaxial growth of GaN using sapphire nano-membrane for micro-light-emitting diodes

Seungmin Lee

Department of Materials Science and Engineering

College of Engineering

Seoul National University

III-nitride based semiconductors have advantages such as high quality, high efficiency, and long lifespan, and thus have attracted considerable interest in optoelectronic device applications such as light-emitting diodes, lasers, and solar cells over the past decades. The GaN epitaxial layer is mainly grown on heterogeneous substrates such as Si, SiC, and sapphire because epitaxial growth using the GaN substrate is not possible for economic and technical reasons. Among them, the sapphire substrate is widely used due to its high quality, transparency, and high temperature stability, but many problems arise due to the difference in lattice constant from the epilayer and the difference in thermal expansion coefficient. Due to the difference in lattice constant, high density of threading dislocation that directly affect the efficiency of the optical device are generated in the epilayer, and due to the difference in thermal expansion coefficient, a large compressive stress on the GaN

thin film and wafer bow occurs during cooling at room temperature after the epilayer growth at high temperature. These problems hinder the realization of high-efficiency GaN-based optical devices.

Compared to existing display technologies such as liquid crystal displays or organic light emitting diodes, micro light-emitting diodes (micro-LEDs) are in the spotlight as a next-generation display technology because they have excellent characteristics such as high brightness, fast response speed, ultra-high resolution, and low power consumption. In particular, in fields such as virtual reality and augmented reality, which are expected to be highly demanded in the future, displays become closer to the human eye, and ultra-high-definition micro-displays are required. However, low external quantum efficiency (EQE), high level of leakage current, and immature micro-LED transfer technology are obstacles to commercialization. The fabrication of conventional micro-LED uses a plasma etching process to form individual micro-LEDs after growing a LED epilayer on a substrate. Non-radiative recombination is increased by exposure of the multi-quantum wells (MQWs) serving as an active layer, thereby causing high level of leakage current and low external quantum efficiency.

In this study, a substrate with sapphire nano-membrane structures was proposed to obtain a high quality GaN epitaxial layer and to solve the problems of micro-LEDs. The growth of GaN on the sapphire nano-membrane was studied using an metalorganic chemical vapor deposition.

The GaN epitaxial layer grows in various shapes depending on the growth orientation and growth conditions, and various growth facets appear. In order to grow the desired micro-GaN epilayer on the sapphire nanomembrane, the study on growth behavior of GaN was first conducted to understand the growth aspect of the GaN on

the sapphire nano-membrane. The fabrication of sapphire nano-membrane was carried out by photolithography, amorphous alumina deposition using atomic layer deposition (ALD), photoresist (PR) removal, and crystallization through a subsequent heat treatment process. The amorphous alumina layer is crystallized into a single crystal α-phase alumina (sapphire) through solid phase epitaxy in the heat treatment process. In order to understand the growth behavior according to the growth direction, the growth of GaN was observed by varying the angle of the stripe pattern. The fastest lateral growth rate was seen in the stripe-shaped sapphire nano-membrane along with the sapphire $[11\bar{2}0]$ direction, and it was confirmed that the lateral growth rate repeats the maximum and the minimum every 30º rotation. By measuring the growth rate of facets formed differently depending on the direction, it could be understood that the growth shape of GaN was different according to the orientation. In addition, GaN grown in the bottom region between the membrane patterns was also observed. The Ga diffusion to the bottom region was inhibited by the GaN layer grown laterally on the membrane, showing the possibility that the GaN layer could be removed from the substrate by breaking the sapphire nano-membrane.

Secondly, a discrete micro-sized GaN layers were grown by designing a pattern, based on an understanding of the growth behavior on the sapphire nano-membrane. Since the sapphire nano-membrane was a closed structure, ashing method using an oxygen plasma was proposed to remove the PR. By controlling the thickness and density of the membrane, the PR removal rate was observed, and as a result, sapphire nano-membrane of various sizes could be successfully manufactured using suitable conditions. The direction and size of the pattern were appropriately designed using the direction with the fastest and slowest lateral growth rates, and the GaN layers

were merged only in the desired area, so that the micro-GaN separated from each other was grown. The micro-GaN layer had a 40% decrease in threading dislocation density (TDD) and a 36.5% increase in photoluminescence (PL) intensity compared to GaN grown on a planar sapphire substrate.

Finally, a discrete core-shell-like micro-LED array was grown on the 100 nm-thick sapphire nano-membrane without a harmful plasma etching process. It was confirmed that the sidewalls of MQWs were protected by p-GaN, and self-passivation by p-GaN is expected to prevent the decrease in EQE caused by the plasma etching process. TDD in the micro-LED formed on sapphire nano-membrane was reduced by 59.6% due to the sapphire nano-membranes, which serve as compliant substrates, compared to GaN formed on a planar substrate. In addition, Enhancements in internal quantum efficiency by 44% and 3.3 times higher PL intensity were also observed from it. Cathodic emission of 435 nm was measured in the c-plane multi-quantum well, while negligible levels of emission were observed in the lateral semipolar plane. Cathodoluminescence emission at 435 nm was measured from c-plane multiple quantum wells (MQWs), whereas negligible emissions were detected from semi-polar sidewall facets. A core-shell-like MQWs were formed on all facets, hopefully lowering concentration of non-radiative surface recombination centers and reducing leakage current paths. This study provides an groundbreaking platform for micro-LEDs by using sapphire nano-membrane.

Contents

List of Tables

List of Figures

Chapter 1. Introduction

1.1 III-nitride semiconductors

1.1.1 General properties of III-nitride materials

III-nitride materials, including gallium nitride (GaN), indium nitride (InN), aluminium nitride (AlN) and their alloys such as InGaN and AlGaN, have received considerable attention for optoelectronic device applications such as light-emitting diodes (LEDs) and laser diodes (LDs).[1,2] The III-nitrides and their alloys, typically grown in the wurtzite structure, form a continuous and direct band-gap from 0.7 eV (InN) to 6.2 eV (AlN), with GaN having a band-gap of 3.4eV. These optical properties of III-nitride materials allow the fabrication of optoelectronic devices of which wavelength ranges from infrared (IR) to ultraviolet (UV) region as well as visible light region, as shown in Fig. 1.1.[3,4] In addition, III-nitride materials exhibits superior properties such as large thermal conductivity, good thermal stability at high temperature, good chemical stability, high electron velocity and good mechanical strength. General properties of III-nitrides are illustrated in Table 1.1.[5] Therefore, III-nitride materials with their promising properties can be widely used not only for LEDs, LDs, solar cell and photodetector, but also for electronic devices such as high electron mobility transistor (HEMT) and field effect transistor (FET).[6]

1.1.2 GaN based LEDs and micro-LEDs

The III-nitride based LEDs have been considered as promising substitutes for conventional incandescent light bulbs or fluorescent lamps due to their advantages such as high efficiency, non-toxicity, long life span, and low energy consumptions.[7,8] The main field of research for III-nitride based LEDs has been the development of GaN-based visible LEDs for solid-state lighting. GaN-based epitaxial layers are often grown on foreign substrates such as Si, SiC and Al_2O_3.[9] Among them, sapphire (Al_2O_3) substrates are extensively used due to their high quality, transparency, and high temperature stability.[10] Figure 1.2 shows the schematic diagram of the conventional lateral type GaN-based LED structure on a sapphire substrate.[11] The LED structure consists of a stack of GaN-based epitaxial layers including un-doped GaN, n-GaN, InGaN/GaN multi-quantum wells (MQWs), p-GaN. The n and p-type GaN layers are generally doped with Si and Mg, respectively. When a forward voltage is applied to LED, radiative recombination of free electrons and holes occurs, and photon is emitted from the nitride semiconductors accordingly.

Recently, micro-LED is attracting much attention for next-generation display technology since it has many advantages over liquid-crystal display (LCD) and organic light-emitting diode display (OLED), as summarized in Table 1.2.[12] Low energy consumption for mobile/portable devices, high pixel density, high brightness for outdoor, and rapid response time are key performance factors. Micro-LED can be utilized in various applications with wide pixel density ranges as shown in Fig. 1.3.[12] Low pixel per inch (PPI) (~20), medium PPI (~500), high PPI (> 1000) displays can be used for TV, smartphone, and virtual reality (VR) / augmented reality (AR) applications, respectively.
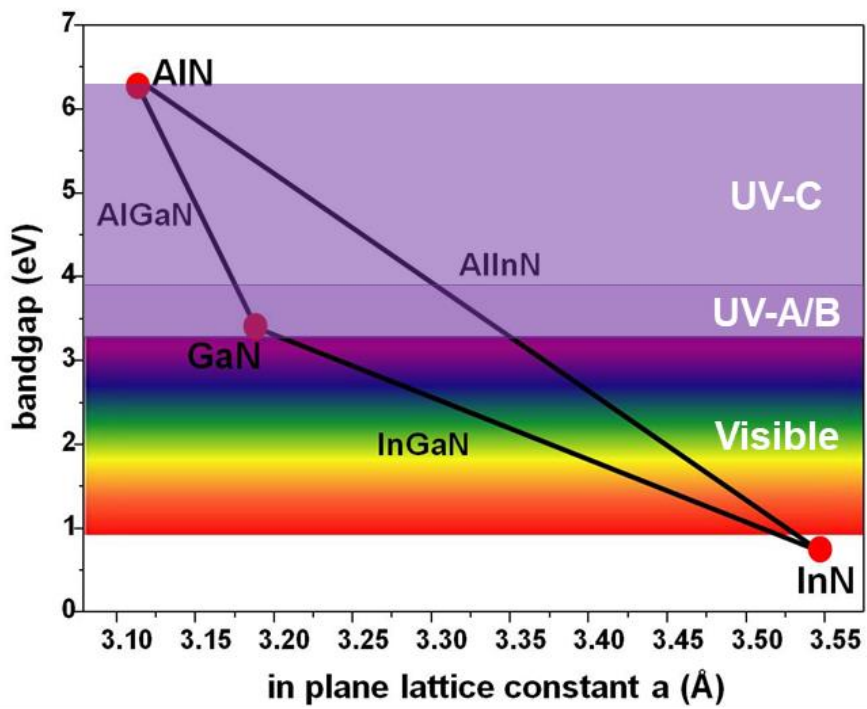
Figure 1.1. Bandgap of III-nitride versus lattice constant.

Table 1.1. General properties of III-nitrides.

Properties	GaN	AlN	InN
Bandgap energy (eV at RT)	3.39	6.2	0.7
Lattice constant (Å)	a=3.189 c=5.185	a=3.112 c=4.982	a=3.548 c=5.760
Thermal expansion coefficient (10^{-6}/K)	da/a=5.59 dc/c=3.17	da/a=5.27 dc/c=4.15	
Thermal conductivity (W/mK)	130	200	
Index of refraction	2.4	2.15	2.9
Dielectric constant (ε_0)	9.5	8.5	
Electron effective mass (m_0)	0.20		0.11
Melting point (^{o}C)	>2300	>2800	>1200
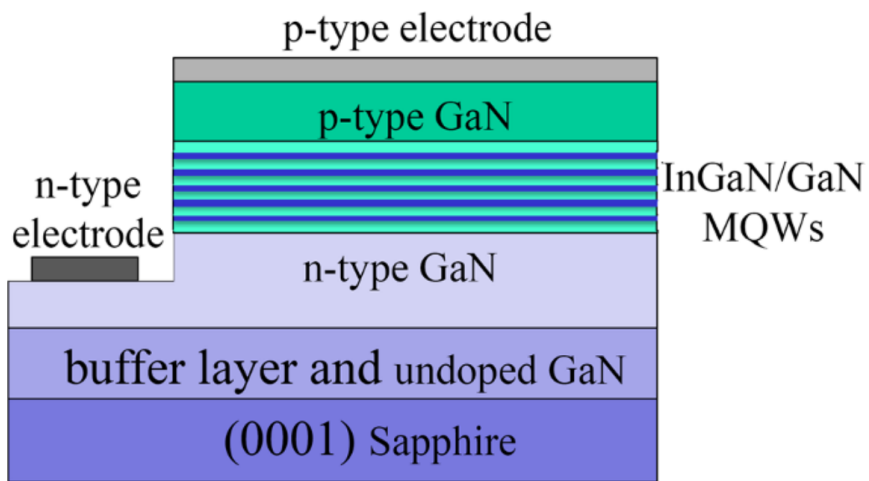
Figure 1.2. Schematic diagram of the typical lateral type GaN-based blue LED.[11]

Table 1.2. Comparisons with LCD and OLED.[12]

	LCD	OLED	Micro-LEDs
Energy consumption	Medium	Medium	Very low
Pixel density	Up to 1000 PPI	2500 PPI demonstrated	Up to 5000 PPI
Brightness	<2000 Cd/m^2	<1000 Cd/m^2	Up to 100000 Cd/m^2
Constrast	Low	High	High
Lifetime	Good	Medium	Best
Refresh rates	Low (ms)	High (µm)	Very high (ns)
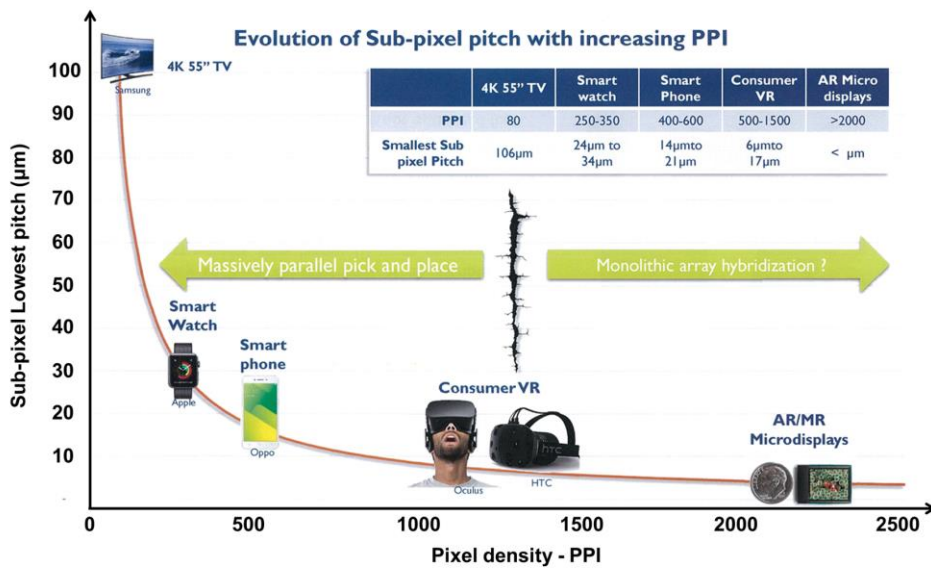
Figure 1.3. Various display applications with wide pixel density ranges.[12]

1.2 Technical issues with GaN based LEDs and micro-LEDs

1.2.1 Lattice mismatch and high dislocation density in GaN epilayers

The epitaxial growth means he growth of a single crystalline film on top of a crystalline substrate.[13] The substrate acts as a seed crystal and the crystal structure of the epitaxial film follows the crystal structure of the substrate. There are three types of epitaxy as follows: homoepitaxy; heteroepitaxy under fully strained state; and heteroepitaxy under strain relaxed state as shown in Fig. 1.4. Homoepitaxy refers to epitaxial film on a substrate with same material, whereas heteroepitaxy refers to epitaxial film on a substrate with different material. In the case of Homoepitaxy, the lattice constants of the substrate and thin film are the same, so high quality thin films of strain-free and dislocation-free are deposited. However, GaN thin film is typically deposited on other substrates, especially sapphire substrates, due to the size limitations and the high cost of GaN substrates. In heteroepitaxy of GaN on the sapphire substrate, the large lattice mismatch (~14%) between a sapphire substrate (d = 2.748 Å) and GaN film (d = 3.189 Å) accounts for evolution of misfit dislocations and high threading dislocation density in the GaN epitaxial film.[14] As the thickness of the deposited thin film becomes thicker, the strain caused by the lattice mismatch accumulates in the thin film, which eventually results in a strain-relaxed state as shown in Fig. 1.4(c), inducing the generation of misfit dislocations. The generated misfit dislocation, which occurs in the interface with the substrate, propagate to the top surface of the thin film and is called the treading dislocation. The threading dislocation are reported to be serve as undesirable non-radiative

recombination sites which results in the degradation of device performance.[15] A typical GaN epilayers has a high threading dislocation density (TDD) of $10^8 \sim 10^{10}$ cm^{-2}, so it is essential to lower the threading dislocation density to increase the internal quantum efficiency (IQE) of LEDs.

1.2.2 Film stress and wafer bow

The difference in coefficient of thermal expansion (CTE) between GaN and sapphire causes several severe problems in manufacturing high-efficiency optoelectronic devices.[16] The CTE of sapphire substrate is known as 7.50×10^{-6} K^{-1} while that of GaN is 5.59×10^{-6} K^{-1}, resulting in a 36% mismatch.[17] Because the CTE of sapphire is much larger than that of GaN, a severe wafer bow and a biaxial compressive stress in GaN occurs after cool-down to room temperature from the high growth temperature in metal-organic chemical vapor deposition (MOCVD).[18] Severe wafer bow impedes mass production of LEDs using large-area wafers and causes difficulties in subsequent device processing steps after the epitaxial growth of the LED structures.[19] Moreover, the large biaxial compressive stress causes charge separation in InGaN/GaN MQWs with a piezoelectric polarization field, leading to a reduction in the electron-hole wave function overlap and radiative recombination efficiency due to the quantum-confined Stark effect (QCSE).[20] To reduce the large stress in GaN, researchers have several approaches such as insertion of AlN/GaN superlattices[21], introduction of air voids in GaN film[22,23], control of the sapphire substrate's thickness[24,25], and deposition of low CTE material on the back side of the sapphire substrate[26]. Figure 1.5 shows the results of reducing the stress of GaN thin film by deposition of a SiO$_2$ layer with a low CTE on the back

side of the sapphire substrate.[26] The resulting reduction in compressive stress reduces the piezoelectric field in the LED structures, leading to an increase in IQE of LED devices.

1.2.3 Low light extraction efficiency

Light extraction efficiency (LEE) is defined as the number of photons extracted to free space per unit time to the number of photons emitted from active layer per unit time.[27] GaN film has a higher refractive index (n_{GaN} = 2.43), compared to that of air (n_{air} = 1) and sapphires ($n_{sapphire}$ = 1.7), leading to the low LEE.[28] Due to the difference in refractive index, the photon generated in the active layer is difficult to escape into the air and is reflected back inside , which is known as internal reflection. Based on Snell's law, when light passes through the interfaces of two different materials, the light is refracted and its velocity varies depending on the refractive index of the materials. Therefore, when light escapes from III-nitride semiconductors to air, the larger the refractive index of semiconductors, the smaller the critical angle, which is the angle at which the refraction angle becomes 90°. The critical angle of GaN/air is only 23.6°, calculated by using the refractive index of GaN and air. This calculation indicates that light generated in the LED structure can only escape into the air as much as the area of the escape cone determined by the critical angle as shown in Fig. 1.6.

1.2.4 Current issues with micro-LEDs

Micro-LEDs are defined as 1 ~ 100 μm-sized LEDs, and have recently been receiving a lot of attention and many studies have been reported. However, the conventional micro-LED has the following inherent drawbacks.

(1) Low micro-LED effieciency and etching loss in micro-LED chip singulation

The chip singulation of conventional micro-LEDs is done by plasma etching of the LED epitaxial film grown on the substrate. After chip singulation, the sidewalls of MQWs are exposed and heavily ion damaged during plasma etching and act as sites for non-radiative recombination, resulting in low external quantum efficiency (EQE) as shown in Fig. 1.7. The reported EQE of 10×10 μm^2 micro-LED is as low as 10%, compared to ~70% for large area LEDs.[29,30] Moreover, as LED chip size is reduced to obtain high PPI, a significant fraction of wafer is wasted. The chip singulation by plasma etching process ("kerf loss" ($\geq$ 2 μm)) would generate an unacceptable increase in cost.[12] For example, 40% of wafer is wasted for 1058 PPI displays as shown in Fig. 1.8.

(2) Difficulty in micro-LED transfer process

Application of micro-LED to displays requires an appropriate transfer process to move micro-LED chips to the target pixel. Millions of micro-LED transfer by traditional pick-and-place techniques would be impractical for manufacturing. Elastomeric stamp transfer, one of the typical pick-and-place techniques, is a low-yield and expensive lift-off process due to weak van der Waals force between chip

and stamp. Likewise, electrostatic transfer process may possibly induce damage to micro-LED due to charging/discharging phenomenon between chip and head. Additionally, in case of small micro-LEDs, conventional soldering process with small-pitch lateral contacts can cause short circuit problems due to the fine feature size pads and spacers in the backplane. Therefore, for micro-LEDs to be used as the next generation of display light sources, Many studies are needed for easy removal of micro-LEDs from the sapphire substrate and for process techniques that simply transfer large amounts of micro-LEDs to the target substrate.
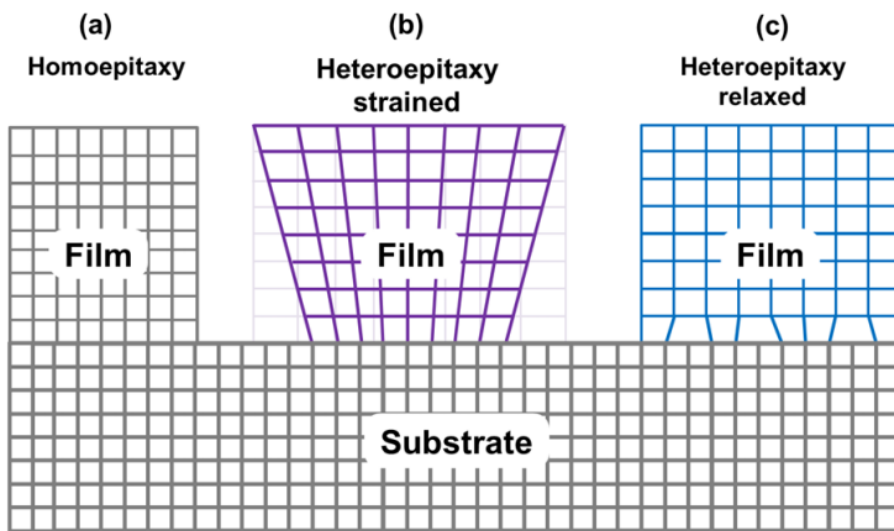
Figure 1.4. (a) Homoepitaxy, (b) heteroepitaxy of strained thin film, and (c) heteroepitaxy of strain-relaxed thin film.
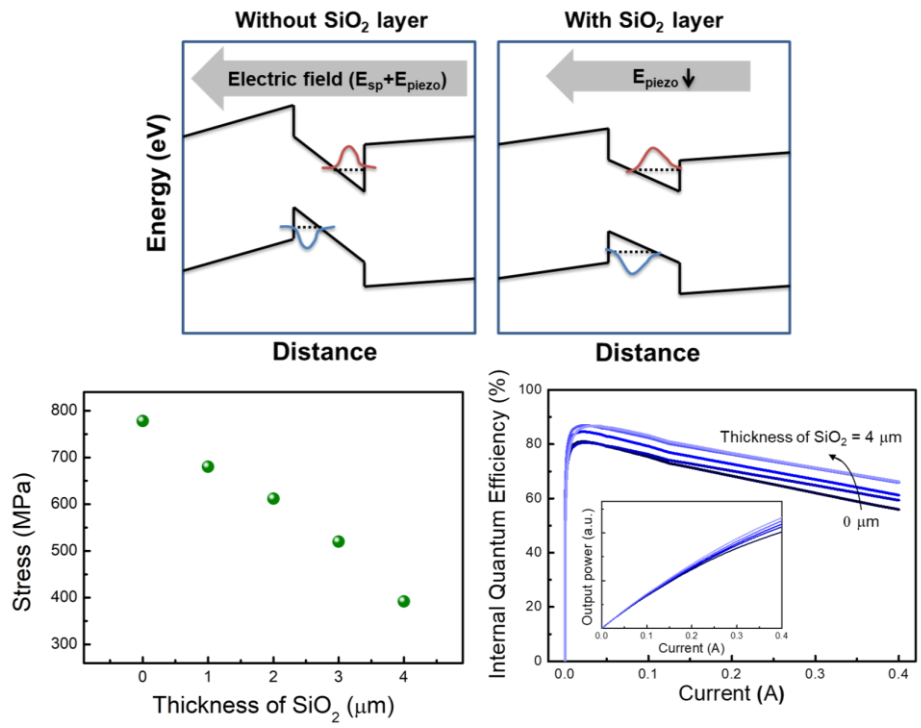
Figure 1.5. Schematic diagram of InGaN/GaN quantum well bandgap of sapphire substrate without SiO$_2$ layer and with SiO$_2$ layer. Calculated stress and IQE results of GaN thin film by deposition of a SiO$_2$ layer with a low CTE on the back side of the sapphire substrate.[26]

Air(n_{Air}: ~1)

Semiconductor
n_{GaN}: ~2.5

Light escape cone   GaN–air = 23.6°

$$\theta_c = \sin^{-1}\left(\frac{n_{out}}{n_{in}}\right)$$

θc

Extracted
(8.6%)

Quantum
Wells

Guided (68.4%)
in GaN

GaN

n=2.5

4 µm

Sapphire
Substrate

Guided in
Sapphire (23.3%)

n=1.7

130 µm
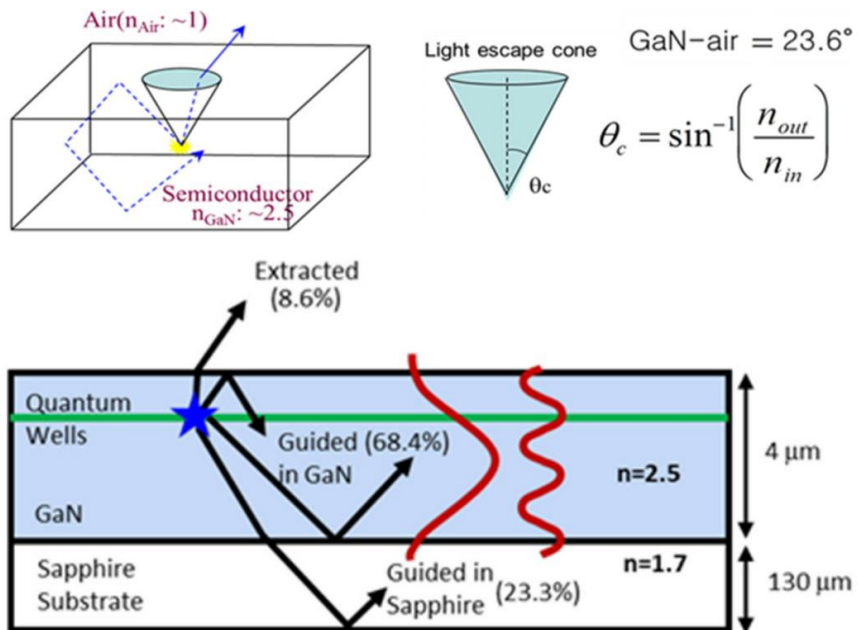
Figure 1.6. Critical angle of the total internal reflection and escape cone in GaN film.
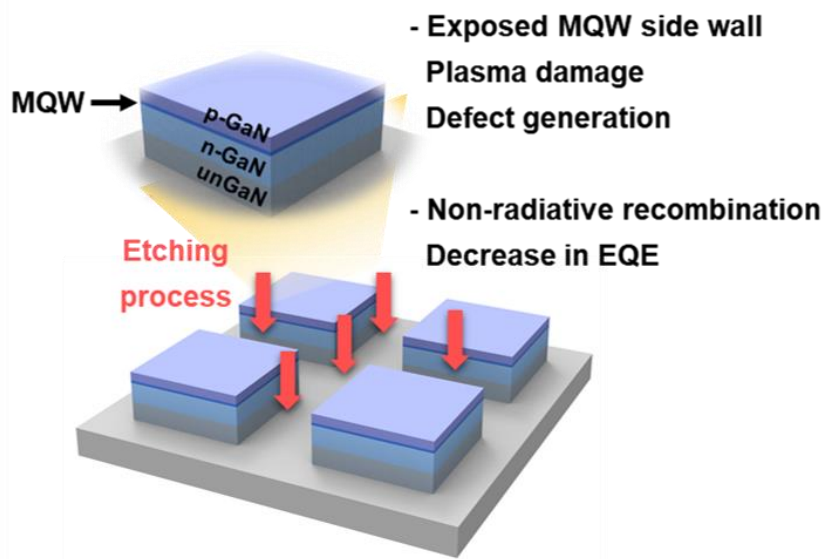
Figure 1.7. Schematic diagram of conventional micro-LED chip singulation by harmful plasma etching.

Die size: 100 μm
Sub-pixel pitch: 102 μm
(kerf loss: 2 μm)

Pixel-pitch

Kerf loss

Sub-pixel pitch

124 PPI
LED chip/substrate
area ratio: 83 %

Die size: 10 μm
Sub-pixel pitch: 12 μm
(kerf loss: 2 μm)

1058 PPI
LED chip/substrate
area ratio: 60 %
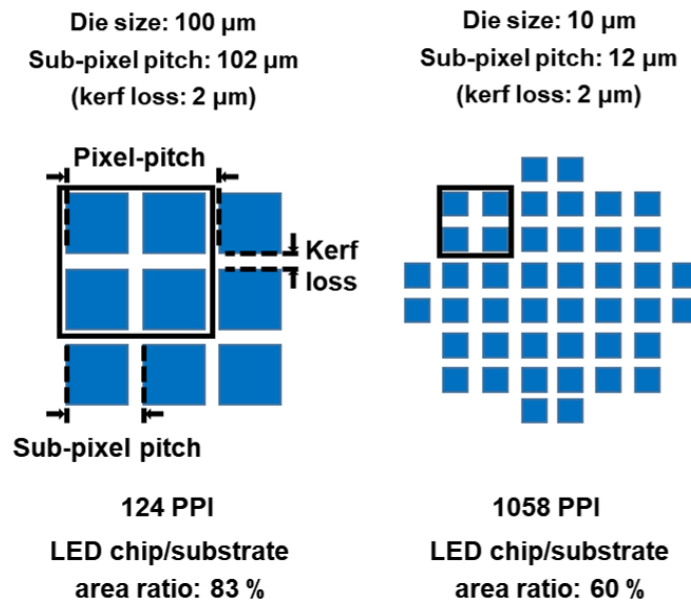
Figure 1.8. Decreased LED chip to substrate area ratio with increased PPI.

1.3 Compliant substrate and pendeo epitaxy

In heteroepitaxy on a thick substrate, There are many defects including misfit dislocation due to lattice mismatch. Compliant substrates represent one of the most promising defect engineering approaches in heteroepitaxial growth. By using a compliant substrate, the epilayer may be grown free from performance-degrading defects, and strain caused by lattice mismatch accumulates on the compliant substrate. Lo et al. first proposed the use of a compliant substrate to increase the critical thickness, which is the maximum thickness at which misfit dislocations do not occur.[31] As shown in Fig. 1.9, as the thickness of the substrate decreases, the critical thickness increases. D. Zubia and S. D. Hersee calculated the strain partitioning effect according to the thickness of the substrate and epilayer as shown in Fig. 1.10.[32] As the substrate becomes thinner than the epilayer, the substrate takes the strain caused by the lattice mismatch, and thus the misfit strain applied to the epilayer decreases, thereby suppressing the occurrence of dislocations. In order to suppress the occurrence of dislocations in heteroepitaxy as much as possible, many studies have been conducted on compliant substrates. Figure 1.11 shows the results of fabricating a membrane-type substrate to make a compliant substrate.[33,34]

Epitaxial lateral overgrowth (ELOG) and pendeo epitaxy (PE) are representative growth techniques to prevent the formation of dislocations, and many researchers have studied them. ELOG means regrowth through and over a masking layer previously deposited and patterned on a top a GaN seed layer, while PE means regrowth from previously etched or exposed sidewalls in a GaN seed layer.[35] Figure 1.12(a) and 1.12(b) shows pendeo-epitaxy of GaN on 6H-SiC(0001) and Si(111)

substrates, respectively. Since GaN regrows from the side of the GaN seed layer, the threading dislocation newly generated at the interface between the substrate and the epilayer decreases, and the threading dislocation is bent along with the lateral growth, so that a low TDD GaN thin film can be obtained. In this study, a sapphire nano-membrane that serves as a compliant substrate was used and GaN was grown with pendeo epitaxy on the membrane to maximize the reduction of dislocations.
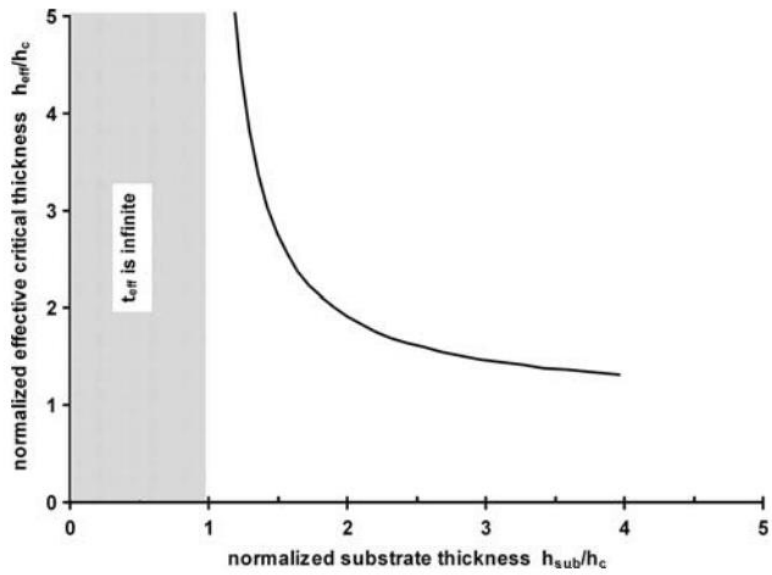
Figure 1.9. Normalized critical layer thickness versus the normalized substrate thickness for the growth of a mismatched heteroepitaxial layer on a compliant substrate.[31]
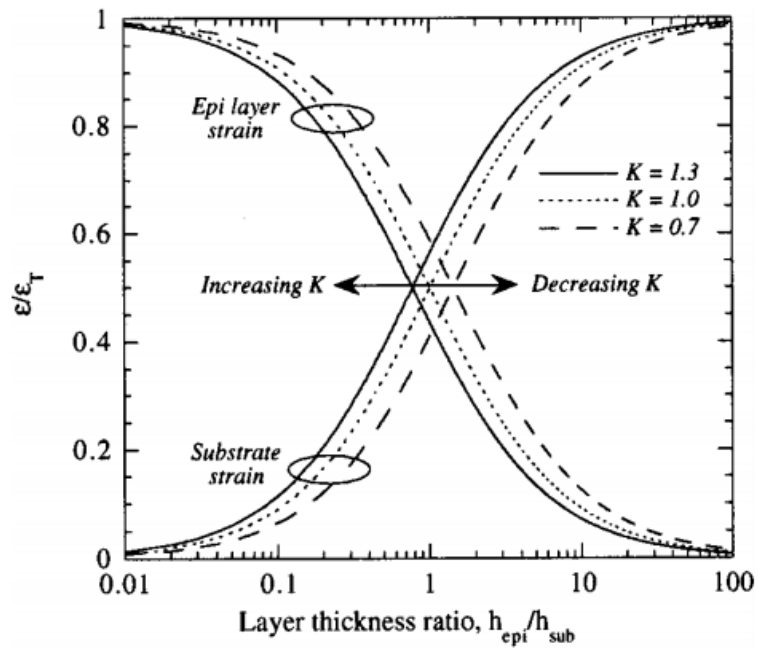
Figure 1.10. Strain partitioning for a planar substrate.[32]

(a) corner supported membrane

h_{sub}

(b)

5 µm

80 nm GaAs
100 nm AlGaAs

10µm
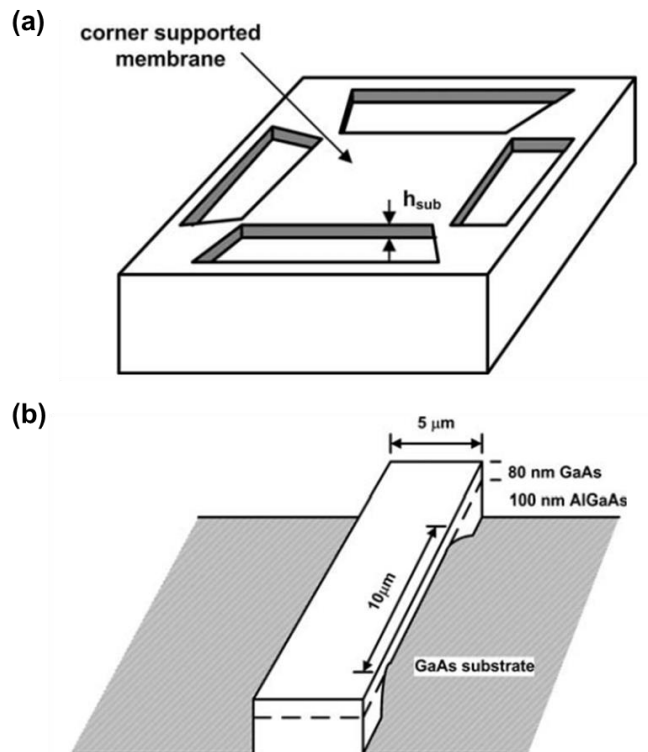
GaAs substrate

Figure 1.11. (a) Corner-supported cantilevered membrane and (b) cantilevered membrane with a bench structure.[33,34]
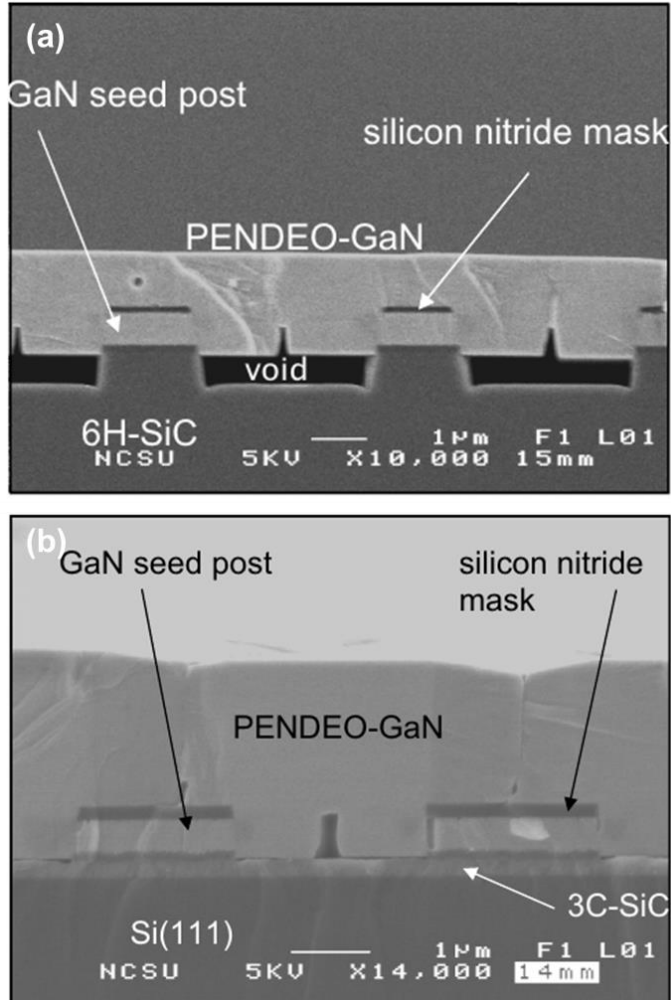
Figure 1.12. Cross-section SEM images of a pendeo-epitaxial grown GaN film on (a) 6H-SiC(0001) substrate and (b) Si(111) substrate.[35]

1.4 Epitaxial growth of GaN on sapphire nano-membrane

1.4.1 Solid-phase epitaxy in amorphous Al_2O_3 nano-membrane

For the fabrication of sapphire nano-membrane, amorphous Al_2O_3 is deposited on photoresist (PR) pattern by atomic layer deposition (ALD), and amorphous alumina must be crystallized into an alpha phase to make a template in which GaN can grow. There have been several investigations on the solid phase epitaxy (SPE) behavior of amorphous alumina layer formed by ion-implantation and e-beam evaporation.[37-39] While et al. reported that SPE of the amorphous Al_2O_3 layer occurs in two-step phase transformation from amorphous to metastable γ-phase and then subsequently to α-phase as shown in Fig. 1.13.[37] Due to difference in kinetics, a phase transformation to γ-phase occurs first, followed by a subsequent phase transformation into α-phase at the interface between the substrate and preceding γ-phase alumina. Figure 1.14 shows results of TEM investigation on an alumina membrane in which the SPE from a- to γ-phase and from γ- to α-phase are partially proceeded.[40] Since the activation energy of each phase transformation is different, all crystallization is performed in the γ-phase first, and crystallization proceeds to the alpha phase when the temperature is above a certain temperature.

1.4.2 The growth of GaN on ultra-thin sapphire nano-membrane

In order to solve the technical issues with GaN-based LEDs, recently, our group proposed ultra-thin sapphire membrane for the growth of high quality GaN.[41] The

sapphire membrane was fabricated by photolithography, deposition of Al_2O_3 by ALD, and crystallization by thermal treatment as shown in Fig. 1.15(a). Figure 1.15(b) and (c) shows plan-view and cross-section SEM images of GaN on the membrane after 40 min growth, respectively. The thicknesses of GaN layer grown on the top sapphire membrane and on the spacing regions were measured to be 1.4 μm and 0.6 μm, respectively. The GaN layers on the top sapphire membranes get closer to each other during lateral growth and limit the diffusion of reactants to the spacing regions. Since the sapphire membrane serving as a substrate is very thin, the strain generated by lattice mismatch in the GaN layer is greatly reduced based on the strain partitioning effect. As a result, as shown in Fig. 1.16, the average number of planes between misfit dislocations at the GaN/sapphire interface increased from 7.3 to 10.2. Figure 1.17(a) and 1.17(b) shows panchromatic cathodoluminescence (CL) images of GaN layers on the planar sapphire substrate, and on the ultra-thin sapphire membrane, respectively. The TDD obtained by counting the number of black spots decreased by 25% compared to the planar substrate. In addition, since the sapphire membrane can be easily modified in a desired shape by changing the pattern, it is expected that it can be easily applied to various fields.
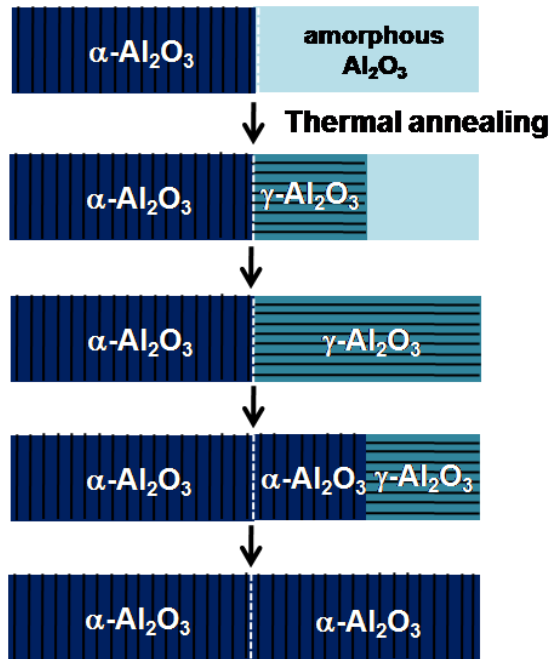
Figure 1.13. Phase transformation of amorphous-Al_2O_3 into alpha-Al_2O_3 by solid phase epitaxy.
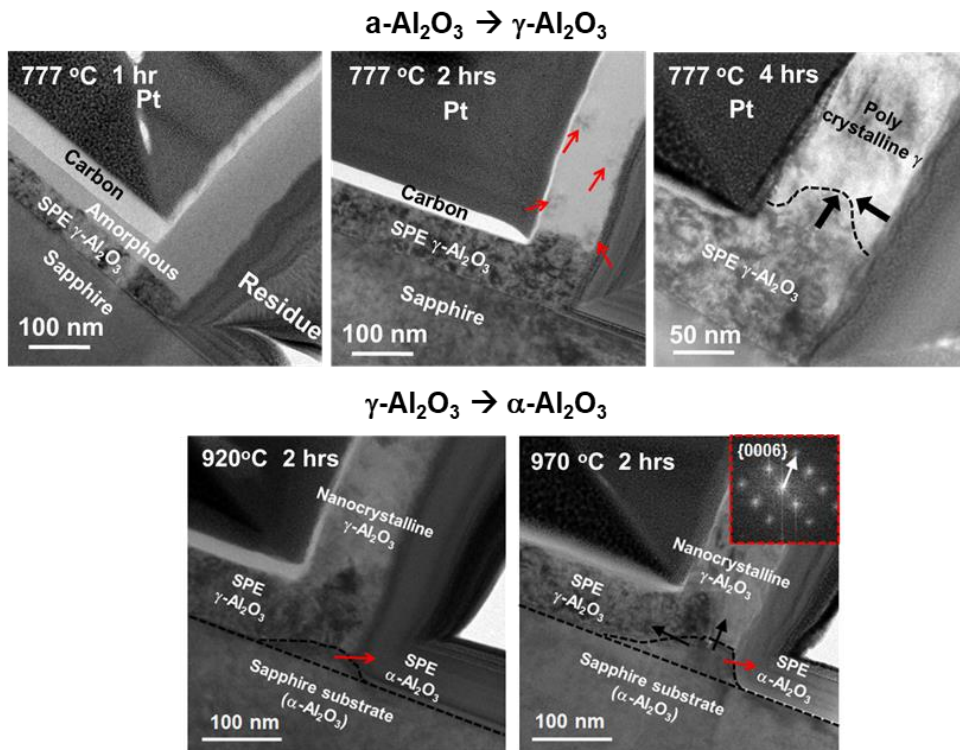
Figure 1.14. Cross-section TEM images of ALD alumina membrane phase transformation from a- to γ-phase and from γ- to α-phase Al_2O_3.

(a)

Alumina

PR   PR
Sapphire substrate

Atomic layer deposition of amorphous alumina

Removal of photoresist and crystallization of alumina

GaN growth by MOCVD

(b)

1 μm

(c)

(0001)

$\{11\bar{2}2\}$

GaN

1.4 μm

$\{11\bar{2}0\}$

Al_2O_3 membrane

0.6 μm

1 μm
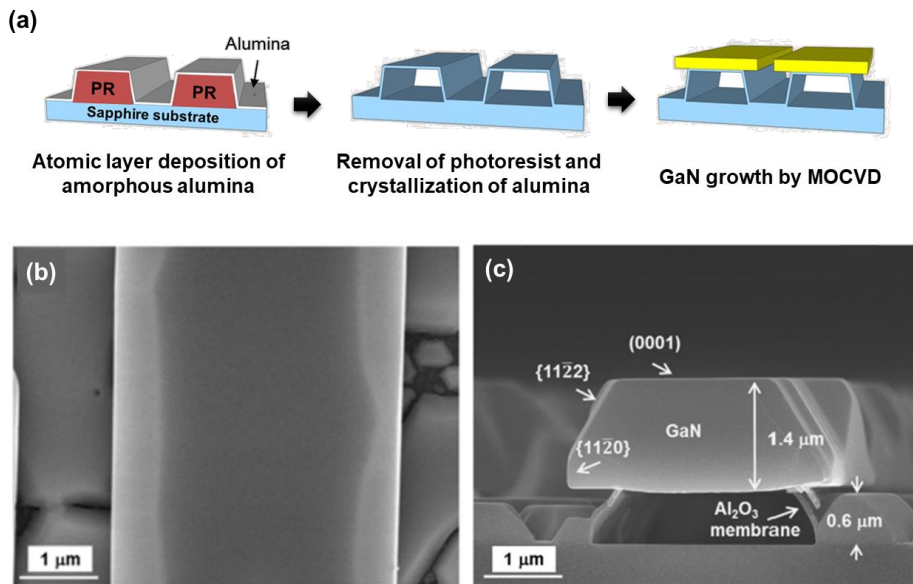
Figure 1.15. (a) Schematic diagrams for the fabrication of ultra-thin sapphire nano-membrane and the subsequent growth of a GaN. (b) Plan-view and (c) cross-section SEM images of GaN layer on a 26 nm thick sapphire membrane after 40 min growth.[41]
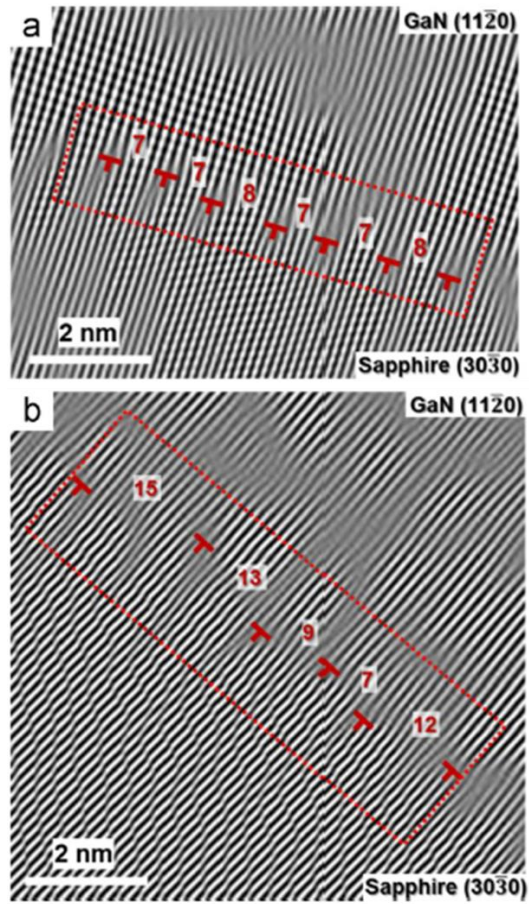
Figure 1.16. Reconstructed TEM images after Fourier filtering of (a) GaN on the conventional sapphire substrate and (b) GaN on the sapphire membrane.[41]
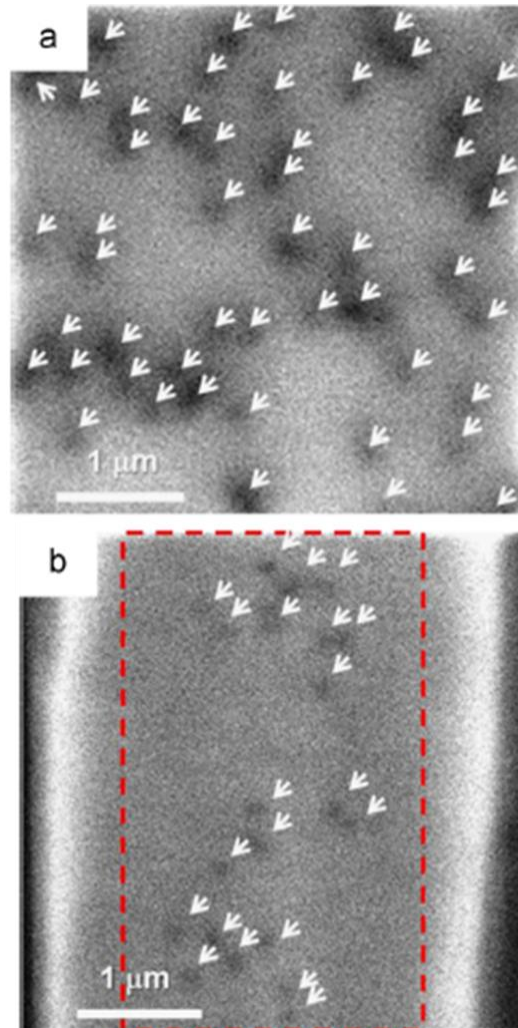
Figure 1.17. Panchromatic CL images of GaN layers (a) on the conventional sapphire substrate, and (b) on the sapphire membrane.[41]

1.5 Thesis contents and organization

In this thesis, the main goal is to realize high efficiency and dicing-free micro-LEDs using the sapphire nano-membrane. Since the sapphire nanomembrane structure serves as a compliant substrate, high-quality GaN having improved crystallinity can be grown. In addition, the shape and size of the membrane can be easily modified, making it a suitable technology for manufacturing micro-LEDs. Therefore, the sapphire nano-membrane was proposed as a new concept of micro-LEDs fabrication that can solve the technical problems of the conventional micro-LED. This thesis includes the study on the growth behavior of GaN on sapphire nano-membrane, the study on the growth of discrete micro-GaN layers with various sizes, the fabrication and characterization of highly efficient micro-LED arrays.

1. Although many studies on the growth aspects of epitaxial lateral overgrowth in GaN have been reported, there are few studies on the pendeo epitaxy of GaN, a epitaxy mode of growing GaN on the sapphire nano-membrane. In order to freely design the nano-membrane, observation of the growth of GaN is required. The growth behavior of GaN on the stripe-patterned sapphire nano-membrane with various orientations was observed in the chapter 3. The growth shape of GaN changed according to the direction of the sapphire nano-membrane, which was identified by analyzing the growth rate of the growth facets in GaN generated differently in each direction. In addition, by measuring the growth rate of GaN on the spacing region for each orientation, it has been demonstrated that the GaN

epilayer can be easily transferred by breaking the sapphire nano-membrane with mechanical force.

2. In a typical micro-LED, the active layer, MQWs, is exposed on the side of the LED chip by plasma etching for chip singulation. Since the exposed MQWs area, which increases as the size of the micro-LED decreases, induces non-radiative recombination, the external quantum efficiency decreases significantly as the chip size decreases. To prevent this problem, the sapphire nano-membrane was used to grow GaN layers separated from each other. A discrete micro-GaN array was grown on the sapphire nano-membrane structure by using the growth behavior of GaN previously studied. Pattern was designed by considering the lateral growth rate of growth facets and 14×14 and 50×50 μm^2 discrete micro-GaN arrays were grown by controlling the number and spacing of the membrane structure. The improved structural and optical properties of micro-sized GaN layers were analyzed due to the sapphire nanomembrane serving as a compliant substrate.

3. Micro-LEDs are attractive as light sources of next-generation displays, but their commercialization is limited due to problems such as low efficiency and difficulty in transferring, etc. The fabrication of micro-LED arrays using the sapphire nano-membrane has been proposed to overcome technical issues of micro-LEDs. A 4×16 μm^2 size micro-LED array was grown on a sapphire nano membrane array. The structural properties such as reduced film stress and threading dislocation density of GaN epilayers

were analyzed. The self-passivation of MQWs was also investigated and thereby improved optical properties were evaluated. In addition, the emission properties of multi-facets, which are advantageous for displays, and their causes were investigated. Finally, it was demonstrated that the micro-LED array could be easily transferred using mechanical lift-off, and vertical type micro-LED devices were fabricated and characterized.

1.6 Bibliography

[1] S. Nakamura, T. Mukai, and M. Senoh, "Candela-class high-brightness InGaN/AlGaN double-heterostructure blue-light-emitting diodes", *Appl. Phys. Lett.* **64**, 1687 (1994).

[2] S. Nakamura, M. Senoh, S. Nagahama, N. Iwasa, T. Yamada, T. Matsushita, H. Kiyoku, and Y. Sugimoto, "Laser diodes", *Jpn. J. Appl. Phys.* **35**, L74 (1996).

[3] J. W. Orton and C. T. Foxon, "Group III nitride semiconductors for short wavelength light-emitting diodes", *Rep. Prog. Phys.* **61**, 1 (1998).

[4] J. Wu, W. Walukiewicz, K. M. Yu, J. W. Ager III, E. E. Haller, H. Lu, W. J. Schaff, Y. Saito, and Y. Nanishi, "Unusual properties of the fundamental band gap of InN", *Appl. Phys. Lett.* **80**, 3967 (2002).

[5] S. C. Jain, M. Willander, J. Narayan and R. Van Overstraten, "III–nitrides: Growth, characterization, and properties", *J. Appl. Phys.* **87**, 965 (2000).

[6] M.-A. di Forte Poission, M. Magis, M. Tordjman, R. Aubry, N. Sarazin, M. Peschang, E. Morvan, S. L. Delage, J. di Persio, R. Quere, B. Grimbert, V. Hoel, E. Delos, D. Ducatteau, and C. Gaquiere, "LP-MOCVD growth of GaAlN/GaN heterostructures on silicon carbide: application to HEMT devices", *J. Cryst. Growth* **272**, 305 (2004).

[7] E. F. Schubert and J. K. Kim, "Solid-State Light Sources Getting Smart", *Science* **308**, 1274 (2005).

[8] S. Pimputkar, James S. Speck, Steven P. DenBaars and S. Nakamura, "Prospects for LED lighting", *Nature Photonics* **3**, 180 (2009).

[9] A. Kuramata, K. Horino, and K. Domen, "GaN-based blue laser diodes grown on SiC substrate as light source of high-density optical data storage", *FUSITSU Sci. Tech. J.* **34**, 191 (1998).

[10] L. Liu and J. H. Edgar, "Substrates for gallium nitride epitaxy", *Mater. Sci. Eng. R Rep.* **37**, 61 (2002).

[11] X. Sun, D. Li, H. Song, Y. Chen, H. Jiang, G. Miao, and Z. Li, "Short-wavelength light beam in situ monitoring growth of InGaN/GaN green LEDs by MOCVD", *Nanoscale Res. Lett.* **7**, 1 (2012).

[12] E. Virey, "MicroLED displays: hype and reality, hopes and challenges", *Yole Development*, (2017).

[13] M. Ohring, "Materials science of thin films: deposition and structure" 2nd edition (Academic Press, San Diego, 2002).

[14] D. Zhu, D. J. Wallis and C. J. Humphreys, "Prospects of III-nitride optoelectronics grown on Si", *Rep. Prog. Phys.* **76**, 106501 (2013).

[15] J. S. Speck and S. J. Rosner, "The role of threading dislocations in the physical properties of GaN and its alloys", *Physica B: Condensed Matter.* **24**, 273 (1999).

[16] L. Liu and J. H. Edgar, "Substrates for gallium nitride epitaxy", *Mater. Sci. Eng. R Rep.* **37**, 61 (2002).

[17] L. Zhang, J. Yu, X. Hao, Y. Wu, Y. Dai, Y. Shao, H. Zhang and Y. Tian, "Influence of stress in GaN crystals grown by HVPE on MOCVD-GaN/6H-SiC substrate", *Scientific Reports* **4**, 4179 (2014)

[18] T. Kozawa, T. Kachi, H. Kano, and H. Nagase, "Thermal stress in GaN epitaxial layers grown on sapphire substrates", *J. Appl. Phys.* **77**, 4389 (1995).

[19] A. Dadgar, F. Schulze, T. Zettler, K. Haberland, R. Clos, G. Straßburger, J. Bläsing, A. Diez, and A. Krosta, "In situ measurements of strains and stresses in GaN heteroepitaxy and its impact on growth temperature", *J. Cryst. Growth* **272**, 72 (2004).

[20] J. S. Speck, and S. F. Chichibu, "Nonpolar and semipolar group III nitride-based materials", *MRS Bull.* **34**, 304 (2009).

[21] E. Feltin, B. Beaumont, M. Laugt, P. Mierry, P. Vennegues, H. Lahreche, M. Leroux, and P. Gibart, "Stress control in GaN grown on silicon (111) by metalorganic vapor phase epitaxy", *Appl. Phys. Lett.* **79**, 3230 (2001).

[22] C-H. Chiu, C-C. Lin, H-V. Han, C-Y. Liu, Y-H. Chen, Y-P. Lan, P. Yu, H-C. Kuo, T-C. Lu, and S-C. Wang, "High efficiency GaN-based light-emitting diodes with embedded air voids/SiO_2 nanomasks", *Nanotechnology* **23**, 045303 (2012).

[23] J. Jang, D. Moon, H-J. Lee, D. Lee, D. Choi, D. Bae, H. Yuh, Y. Moon, Y. Park, and E. Yoon, "Incorporation of air-cavity into sapphire substrate and its effect on GaN growth and optical properties", *J. Cryst. Growth* **430**, 41 (2015).

[24] J-H. Lee, N. S. Kim, D. Y. Lee, and J-H. Lee, "Effect of residual stress and

sidewall emission of InGaN-based LED by varying sapphire substrate thickness",
IEEE Photon. Technol. Lett. **21**, 1151 (2009).

[25] W. Z. Tawfik, S. Bae, S. B. Yang, T. Jeong, and J. K. Lee, "Stress engineering
by controlling sapphire substrate thickness in 520 nm GaN-based light-emitting
diodes", *Appl. Phys. Express* **6**, 122103 (2013).

[26] S. Lee, J. Kim, C-H. Oh, J-I. Shim, Y. Park, and E. Yoon, "Fabrication of Less
Bowed Light-Emitting Diodes on Sapphire Substrates with a SiO_2 Thin Film on
Their Back Sides", *J. Korean Phys. Soc.* **75**, 480 (2019).

[27] E. F. Schubert, "Light-emitting diodes", 2nd edition (Cambridge University
Press, New York, 2006).

[28] E. Ejder, "Refractive index of GaN", *Phys. Status Solidi (a)* **6**, 445 (1971).

[29] F. Templier, "GaN-based emissive microdisplays: A very promising technology
for compact, ultra-high brightness display systems", *J. Soc. Inf. Display* **24**, 669
(2016).

[30] F. Olivier, S. Tirano, L. Dupré, B. Aventurier, C. Largeron, F. Templier,
"Influence of size-reduction on the performances of GaN-based micro-LEDs for
display application", *J. Lumin.* **191**, 112 (2017).

[31] Y. H. Lo, "New approach to grow pseudomorphic structures over the critical
thickness", *Appl. Phys. Lett.* **59**, 2311 (1991).

[32] D. Zubia and S. D. Hersee, "Nanoheteroepitaxy: The Application of
nanostructuring and substrate compliance to the heteroepitaxy of mismatched

semiconductor materials", *J. Appl. Phys.* **85**, 6492 (1999).

[33] D. Teng and Y.H. Lo, "Dynamic model for pseudomorphic structures grown on compliant substrates: An approach to extend the critical thickness", *Appl. Phys. Lett.* **62**, 43 (1993).

[34] C. L. Chua, W. Y. Hsu, C. H. Lin, G. Christensen, and Y. H. Lo, "Overcoming the pseudomorphic critical thickness limit using compliant substrates", *Appl. Phys. Lett.* **64**, 3640 (1994).

[35] T. Gehrke, "Review of structured thin films in wide bandgap semiconductors: pendeo-epitaxy of GaN and AlGaN", *J. Nanophotonics* **2**, 021990 (2008).

[37] C. W. White, L. A. Boatner, P. S. Sklad, C. J. McHargue, and M. J. Aziz, "Ion implantation of crystalline oxides and ceramics", *Nucl. Instrum. Methods Phys. Res. B* **32**, 11-22 (1988).

[38] J. C. McCallum, T.W. Simpson, and I.V. Mitchell, "Time resolved reflectivity measurements of the amorphous-to-gamma and gamma-to-alpha phase transitions in ion-implanted Al$_2$O$_3$, *Nucl. Instrum. Methods Phys. Res. B* **91**, 60-62 (1994).

[39]. D. R. Clarke, "Epitaxial phase transformations in aluminium oxide", *Phys. Stat. Sol. (a)* **166**, 183 (1998).

[40] J. Jang, D. Yang, D. Moon, D. Choi, H. J. Lim, S. Kang, D. Bae, H. N. Han, Y. Park, E. Yoon, "Solid-phase epitaxy of a cavity-shaped amorphous alumina nanomembrane structure on a sapphire substrate", *J. Cryst. Growth* **498**, 130 (2018).

[41] D. Moon, J. Jang, D. Choi, I. -S. Shin, D. Lee, D. Bae, Y. Park, and E. Yoon,

"An ultra-thin compliant sapphire membrane for the growth of less strained, less defective GaN", *J. Cryst. Growth* **441**, 52 (2016).

Chapter 2. Experiments and analysis

2.1 Growth equipment

2.1.1 Metalorganic chemical vapor deposition (MOCVD)

In this work, Thomas Swan 6 x 2" (incorporated 6 substrates of 2 inch size) close-coupled showerhead MOCVD system was used to grow III-nitride epitaxial layers. Trimethylgallium (TMGa, $(CH_3)_3Ga$) and trimethylindium (TMIn, $(CH_3)_3In$) was used as precursors for group III sources, and ammonia (NH_3) of 99.9999% purity was used for group V sources. Bis(cyclopentadienyl)magnesium (CP$_2$Mg, $(C_2H_5)_2Mg$) and 10 ppm diluted silane (SiH_4) was installed for p-type and n-type doping, respectively. Schematic of gas delivery system of MOCVD is in Fig. 2.1.

2.1.2 Atomic layer deposition (ALD)

ALD system (Lucida D100) was used for the deposition of an amorphous alumina (a-Al_2O_3) layer. Trimethylaluminum (TMA, $(CH_3)_3Al$) and deionized water (H_2O) were used as the precursors of Al and O, respectively. Nitrogen gas (N_2) with the purity of 99.9999% with the oxygen content less than 0.2 ppm was used as carrier gas and for the purge of non-reacted reactants and by-products. The gaseous sources are transported sequentially by separate pulses into heated reaction chamber. Subsequently, reactive chemical sources in vapor phase are used for the chemical reaction on the substrate surface. The surface termination is controlled to actively

react with the gaseous precursor before the other source is transported into the reaction chamber. A pulse of TMA source provides the aluminum source of the Al_2O_3 layer (1st pulse). The first chemically reacted precursor bonds to the surface and changes the dominant surface termination. After chemical adsorption when the entire surface is terminated with CH_3 of TMA precursor, nitrogen gas removes the non-reacted reactants and the gaseous by-products (1st purge). This step suppresses the reaction of each reactant in the chamber and allows the reactants to be sequentially deposited into the atomic layer. The same pulse and purge steps occur for H_2O, the second reactant, to provide the oxygen of Al_2O_3 (2nd pulse - 2nd purge). The film thickness can be easily controlled by adjusting the number of cycles in ALD system.

Figure 2.1. Thomas Swan 6 x 2'' MOCVD system.

2.2 Analysis tools

2.2.1 Field emission scanning electron microscopy (FE-SEM)

In each step of fabrication for sapphire nano-membrane and growth of III-nitrides by MOCVD, structural characteristics such as the dimensional properties and shapes were observed by FE-SEM (Hitachi S-4800). The growth morphology of GaN epitaxial layers were also measured by FE-SEM operated at 15 kV. Platinum was coated on the samples to avoid charging effects before measurements.

2.2.2 Transmission electron microscopy (TEM)

The TEM specimens were thinned to a thickness of ~100 nm by using focused ion beam (FIB, NOVA 600 Nanolab). Bright-field and high-resolution TEM images were obtained by JEOL JEM-2100F with the acceleration voltage of 200 kV. After the thermal annealing, the sapphire nano-membrane with embedded cavities was analayzed by selected area diffraction patterns. The thicknesses of InGaN/GaN quantum wells on various growth facets were measured by scanning TEM (STEM).

2.2.3 Micro-Raman spectroscopy

Micro-Raman measurements was carried out for micro-sized GaN layers to compare the amount of strain state. Raman spectra were taken using Horiba LabRAM HR Evolution with a 633 nm He-Ne laser. A hydride vapor phase epitaxy

(HVPE) GaN sample (stress-free bulk GaN) was used as a reference to calculate the film stress in micro-sized GaN by obtaining the Raman shift.

2.2.4 Micro-photoluminescence (Micro-PL)

The optical properties of the samples were analyzed by Micro-PL system (Dongwoo Optron micro-PL system). The PL measurement is a non-destructive method of examining the electronic structure of materials. When the laser is incident directly onto a sample, it is absorbed and transmits excess energy to the material in a process called "photo-excitation". The way to release this excess energy is through the emission of light called photoluminescence. The PL intensity and spectra is a direct measure of material properties such as bandgap energy, stress state and crystallinity. PL measurement was performed at room temperature using He-Cd laser 325 nm line. The PL signal was dispersed by a monochromator and detected by charge coupled device (CCD) detector. The laser spot size of micro-PL system used in this study was 3 μm.

2.2.5 Cathodoluminescence (CL)

Gatan Mono CL4 system was used to evaluate luminescence properties of III-nitride epilayers as well as to investigate the density of threading dislocations by measuring the dark spot density under panchromatic mode. Spatially-resolved CL and monochromatic CL measurements from each facet of micro-LEDs were carried out at room temperature with the acceleration voltage of 5 kV.

Chapter 3. The study on growth behavior of GaN on sapphire nano-membrane

3.1 Introduction

Light-emitting diodes (LEDs) use heterogeneous epitaxy to grow GaN on foreign substrates such as sapphire, SiC, and Si due to the high price of GaN substrates.[1-3] In these cases, a large number of threading dislocations are generated that lowers the efficiency of the LED due to lattice mismatch between GaN and the substrates.[4,5] Some researchers investigated a compliant substrate to obtain high quality epilayers of SiGe, GaN, and InGaAs as shown in Fig. 3.1.[6-9] Using a compliant substrate whose substrate thickness is smaller than the thickness of the epilayer, the strain resulting from the lattice mismatch is distributed to the epilayer and the substrate. This suppresses the generation of lattice mismatch dislocations of the epilayer, and thus a high crystalline epilayer can be obtained. Our group reported that the interval of lattice mismatch dislocations per unit length is reduced by 28% by growing GaN on an ultra-thin compliant sapphire membrane of 26 nm thickness.[10]

In order to grow a desired shape of GaN array for micro-LED application, it is necessary to deeper understanding of the growth behavior of GaN on the sapphire nano-membrane. The epitaxial lateral overgrowth (ELOG) of GaN on the sapphire substrate has been demonstrated to reduce the threading dislocation density (TDD) in GaN film.[11-13] The rates of lateral overgrowth and the equilibrium facets depend on both the crystallographic orientation and the parameters of growth such as

pressure, temperature and V/III ratio in Metalorganic chemical vapor deposition (MOCVD) system. K. Hiramatsu et al. investigated the morphology in ELOG of GaN observing from either $<11\bar{2}0>$ or $<1\bar{1}00>$ orientation as a function of a reactor pressure (P) or growth temperature (T) as shown in Fig. 3.2.[14] D. Kapolnek reported anisotropic epitaxial lateral growth in GaN using star shape as shown in Fig. 3.3.[15] Figure 3.4 illustrates the ideal structure of $\{11\bar{2}0\}$ and $\{11\bar{2}2\}$ facets, which consists of Ga and N dangling bonds.[16] Because the amount of dangling bond density varies depending on the growth facets, the growth rate varies depending on the facet of GaN. The growth of GaN on the sapphire nano-membrane is a pendeo epitaxy, which has not yet been studied for growth aspects such as ELOG. In this study, the observation of the growth of GaN was performed to analysis the growth behavior of GaN on the membrane with various orientations by using different growth rates of each growth facet in GaN,

13 μm diameter

300 nm $In_{0.15}Ga_{0.85}As$

300 nm $In_{0.15}Ga_{0.85}As$

10.5 nm $In_{0.4}Ga_{0.6}As$ quantum well

40 nm $In_{0.05}Ga_{0.95}As$ compliant film

5-μm-tall $Al_{0.6}Ga_{0.4}As$ pedestal

GaAs substrate

(a)

5 μm
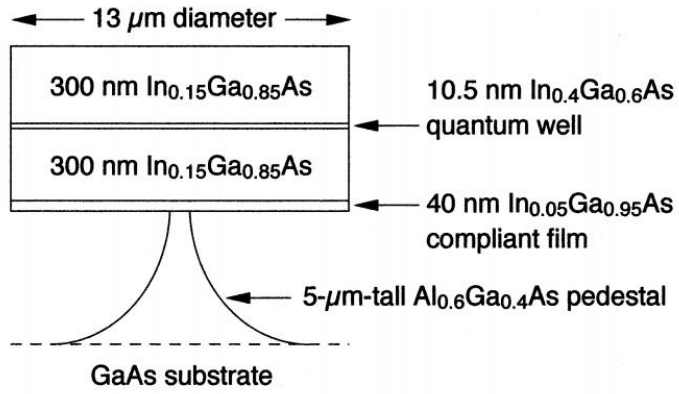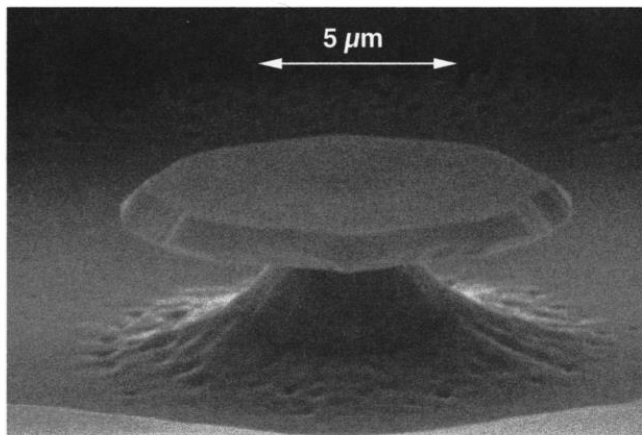
(b)

Figure 3.1. (a) Schematic diagram and (b) SEM image of InGaAs quantum well structure grown on a disk-shaped compliant membrane.[8]
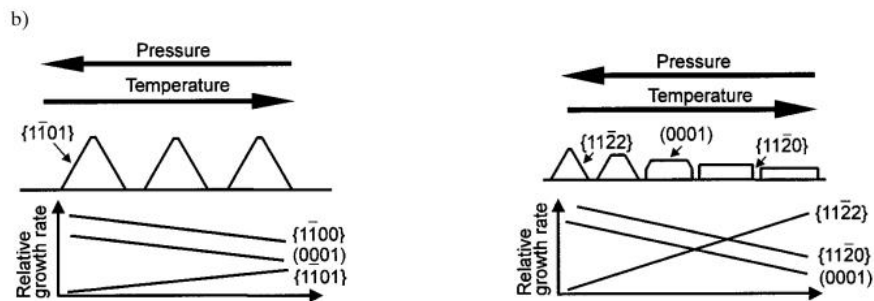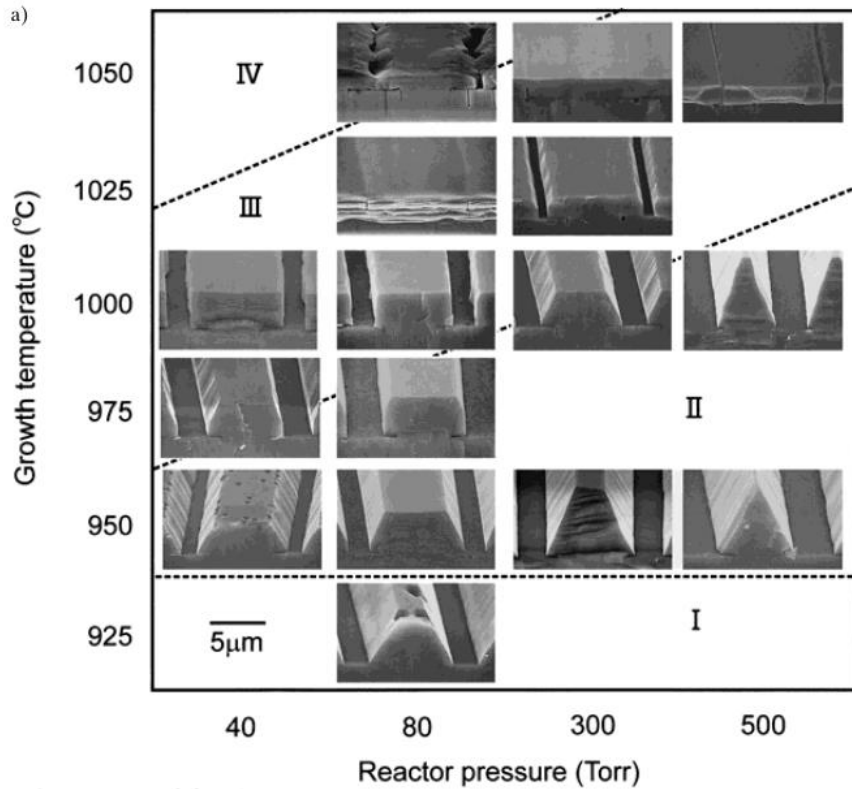
Figure 3.2. (a) SEM images of ELOG of GaN from $<1\bar{1}00>$ stripes at different pressure or temperature. (b) Schematic diagram of the morphology of ELOG GaN from $<11\bar{2}0>$ orientation (left) and $<1\bar{1}00>$ (right) orientation as a function of pressure and temperature.[14]
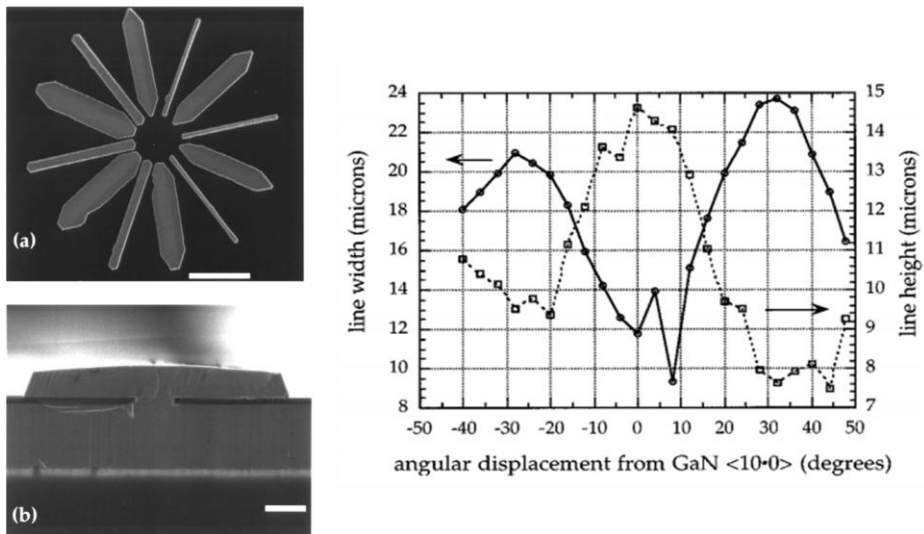
Figure 3.3. (a) Star feature illustrating in-plane anisotropic growth (bar = 50 μm). (b) Cross-sectional SEM image of a line oriented parallel to the GaN <1$\bar{1}$00> (bar = 1 μm). (c) Plot of GaN linewidth and height as a function of orientation.[15]
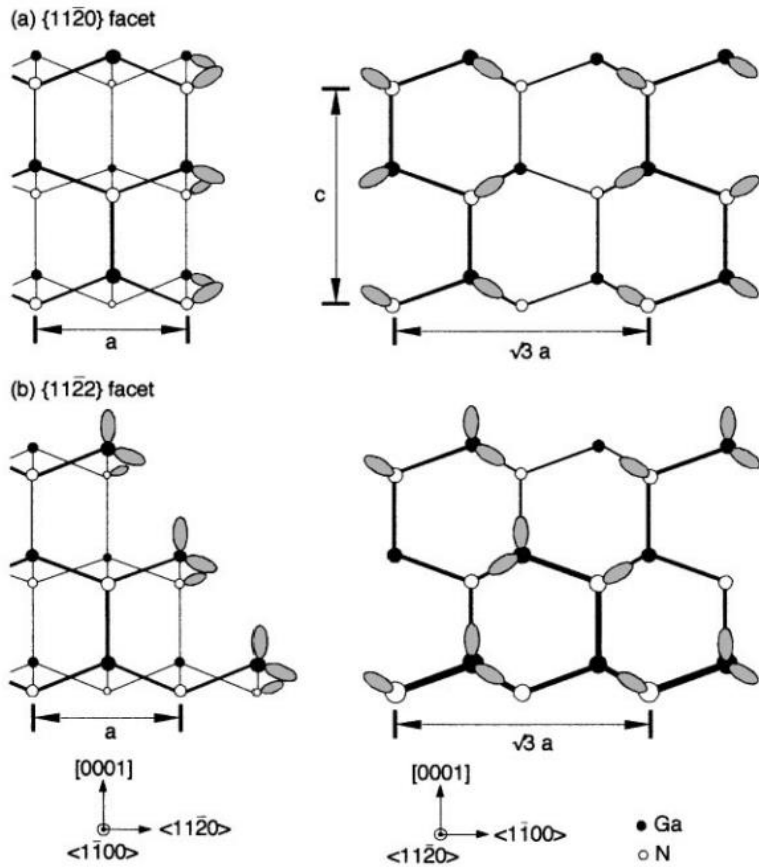
Figure 3.4. The ideal structure of $\{11\bar{2}0\}$ and $\{11\bar{2}2\}$ facets exposed during the lateral overgrowth of GaN.[16]

3.2 Experimental procedure

Figure 3.5 shows the schematics of experiments for growing GaN on thin sapphire nano-membrane. For the fabrication of thin sapphire nano-membrane, a photoresist (PR) pattern of a stripe with the width and the spacing of 2 μm was formed on a c-plane sapphire substrate. To observe the growth aspect of GaN on nano-membrane with various directions, the orientation of the stripe was changed from 0º to 60º in steps of 10º in consideration of the hexagonal symmetry of GaN. Direction of 0º means $[11\bar{2}0]_{sapphire}$, which is vertical to flat zone of substrate. Then, an amorphous alumina layer was deposited on the stripe-patterned sapphire substrate by atomic layer deposition (ALD). The ALD process was performed at 110 °C to maintain the pattern shape of the PR pattern, and 1500 cycles were performed to deposit an amorphous alumina with 120 nm thick. The substrate was dipped in acetone to removal PR after scratching the edge, leaving stripe cavities, and annealed at 1100 °C for 2 hours in air to crystallize the amorphous ALD alumina into single-crystalline α-phase (sapphire) for the GaN growth. Jang et al. reported that amorphous alumina membrane crystallizes in two steps through solid phase epitaxy (SPE).[17] As a first step, phase change occurs to gamma-phase alumina, which is a metastable phase at a relatively low temperature of about 800 °C. In the second phase, gamma-phase alumina is phase-changed into alpha-phase alumina at a sufficiently high temperature of about 1100 °C. The ALD alumna membrane is crystallized into the alpha phase alumina same with the sapphire substrate and becomes a place where GaN can grow. After crystallization, GaN layers were successfully grown on a sapphire nano-membrane structure by a Thomas Swan 3×2" MOCVD.

Trimethylgallium (TMGa) and NH_3 were used as precursors of Ga and N, and H_2 was used as a carrier gas. First, the low-temperature GaN buffer layer was grown at 560 °C and 100 Torr. An un-doped GaN layer was grown at a reactor temperature of 1040 °C and 300 Torr. To understand the growth behavior of GaN on the sapphire nano-membrane in each orientation, growth time was varied from 30 to 90 min with 30 min interval as shown in Fig. 3.6. The growth behaviors of GaN on the sapphire nano-membrane including the cavities were observed by field emission scanning electron microscope (FE-SEM) of Hitachi S-4800.
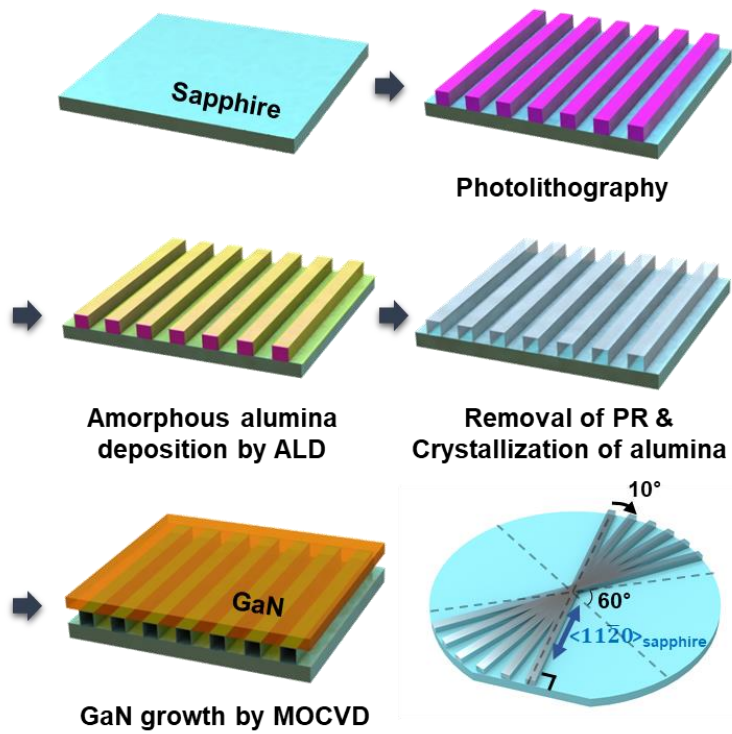
Figure 3.5. Schematic diagram of the growth of GaN on sapphire nano-membrane.
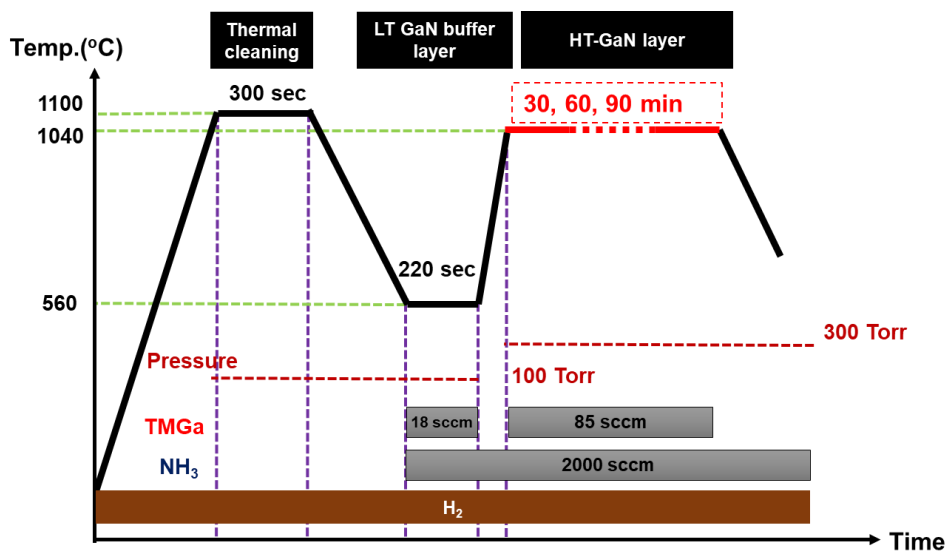
Figure 3.6. Schematic diagram of the growth procedure of un-doped GaN.

3.3 Results and discussion

3.3.1 Fabrication of sapphire nano-membrane

Figures 3.7(a) shows cross-section SEM image of stripe pattern with the width and the spacing of 2 μm using photolithography. As shown in the SEM image in Fig. 3.7(b), an amorphous Al_2O_3 layer with thickness of 120 nm was deposited on the stripe patterned PR by ALD. After dipping the samples in acetone, all PRs have been eliminated and cavity formed as shown in Fig. 3.7(c). Then the amorphous alumina membrane was crystallized into alpha-phase alumina through heat treatment. It is well known that typical alumina is crystallized in two stages through solid phase epitaxy (SPE).[18-20] In the first stage, the phase changes from a-phase alumina to semi-stable γ-phase alumina at a relatively low temperature of about 800 ℃, and in the second stage, the γ -phase alumina changes to α-phase alumina under a sufficiently high temperature of about 1100 ℃. The membrane structure is crystallized into an α-phase alumina, such as a sapphire substrate, and becomes a place for GaN to grow. The SEM image in Fig. 3.7(d) shows a sapphire membrane structure completely crystallized with α-phase alumina. The sapphire nano-membrane has the same phase with the sapphire substrate, so GaN can be deposited on the top of the membrane structure and between the stripe patterns. After the crystallization process, the cross-section of the sapphire nanomembrane shows that it has changed from a square to a trapezoidal shape. The shape change was caused by the increase in density when the amorphous alumina crystallized into α-phase alumina. The density of amorphous alumina is in the range from 2.5 to 3.0 g/cm^3

depending on the ALD process temperature and the density of α-phase alumina is 3.95 g/cm^3.[21] After the crystallization, the volume of the membrane is expected to decrease by 25 ~ 37% depending on the initial density of the amorphous alumina. So, the two lateral sides fixed to the sapphire substrate and the top of the square cavity are shrank, resulting in trapezoidal cavity. As a result of the measurement, the top part of the membrane contracted from 2 μm to 1.8 μm, and the thickness of the membrane contracted from 120 nm to 100 nm.
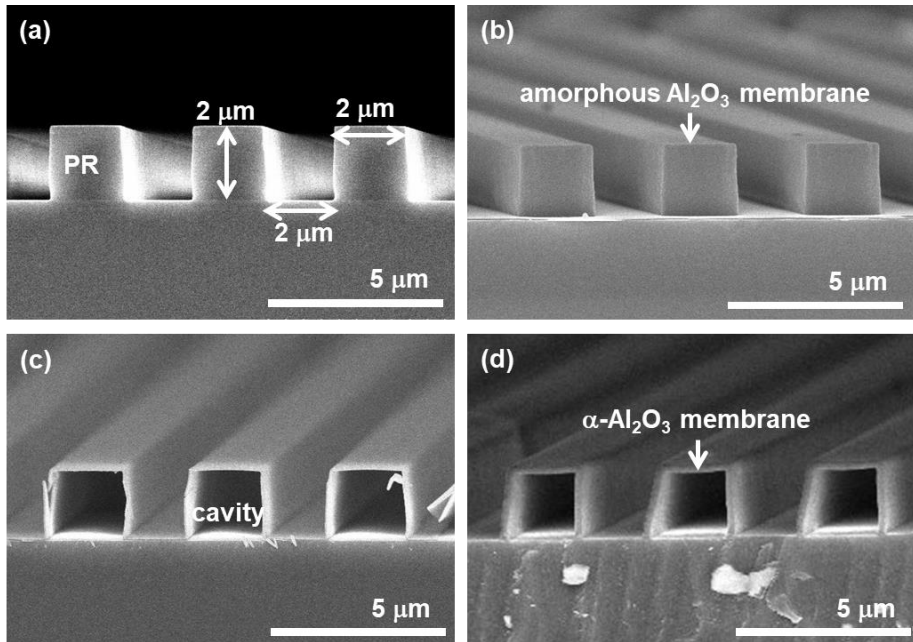
Figure 3.7. Cross-section SEM images of (a) stripe patterned photoresist (PR) (2 μm width and 2 μm spacing), (b) amorphous Al_2O_3 membrane deposited by ALD on stripe patterned PR, (c) amorphous Al_2O_3 membrane with cavity after PR removal by dipping in acetone, (d) crystallized sapphire (α-Al_2O_3) membrane after thermal treatment.

3.3.2 Growth behavior of GaN on sapphire nano-membrane with various orientations

Figure 3.8 and Fig. 3.9 show cross-section scanning electron microscopy (SEM) images of GaN growth on the sapphire nano-membrane. To confirm the growth behavior of GaN on the membrane, the crystal planes of GaN was observed with growth time and orientation. In the initial stage, GaN is deposited on top of the nano-membrane and also the bottom area between the patterns. The initial GaN grown on the membrane has (0001), $\{11\bar{2}0\}$, $\{11\bar{2}2\}$, and $\{1\bar{1}01\}$ growth facets along the direction.[22-24] As the growth progresses, the lateral to vertical growth rate ratio in each directions changes depending on the initial facet of GaN due to the difference in the surface energy of each facets. The ideal (0001), $\{11\bar{2}0\}$, and $\{11\bar{2}2\}$ facets have one, two, and three dangling bonds, respectively.[16] The growth rate of the facet having more dangling bonds is higher since the surface energy is higher. As the growth rate of $\{1\bar{1}01\}$ facet is slower than that of (0001) facet, the growth rate increases in the order of $\{1\bar{1}01\}$, (0001), $\{11\bar{2}0\}$, and $\{11\bar{2}2\}$ in this growth condition.[14] In the case of 0º, which is parallel to $[11\bar{2}0]_{sapphire}$, the $\{11\bar{2}2\}$ facet with the highest surface energy gradually disappears and the $\{11\bar{2}0\}$ facet remains. Similarly, the lateral growth is induced, because the surface energy of $\{11\bar{2}0\}$ facet is higher than that of the (0001) facet. This behavior is convex growth mode which means that slow-growing facets remain and ultimately define island shape while fast-growing facets disappear.[25] Also, as shown in SEM images of 30º case, which is parallel to $[1\bar{1}00]_{sapphire}$, $\{1\bar{1}01\}$ facet (lateral growth facet of GaN) with the lowest surface energy remains and (0001) facet grow to extinction as shown in Fig. 3.10(b). The measured growth rates of each facets in 0º and 30º directions are listed in Table

3.1. It can be seen that the facets with the slowest growth rate among the facets appearing at the same direction remain. Figure 3.10(a) shows the width and thickness of GaN on the sapphire nano-membrane. The lateral to vertical growth rate ratio decreases from 0º with 3.12 to 30º with 0.02, then increases again from 30º to 60º. Figure 3.11 shows plan-view SEM images of the GaN layer on the sapphire nano-membrane with each direction after 60 min growth. Green hexagon means a set of $\{11\bar{2}0\}$, and $\{11\bar{2}2\}$ facets, while blue hexagon means a set of $\{1\bar{1}01\}$ facet. It can be seen that the ratio of blue hexagon increases from 0º to 30º, and the rate of green hexagon increases again as it goes to 60º. In the direction of 10º, 20º, 40º, and 50º, the lateral growth facets with different growth rates are mixed. These behaviors exhibit hexagonal symmetry, with a 30º angular span between the lateral and vertical growth maxima and minima.
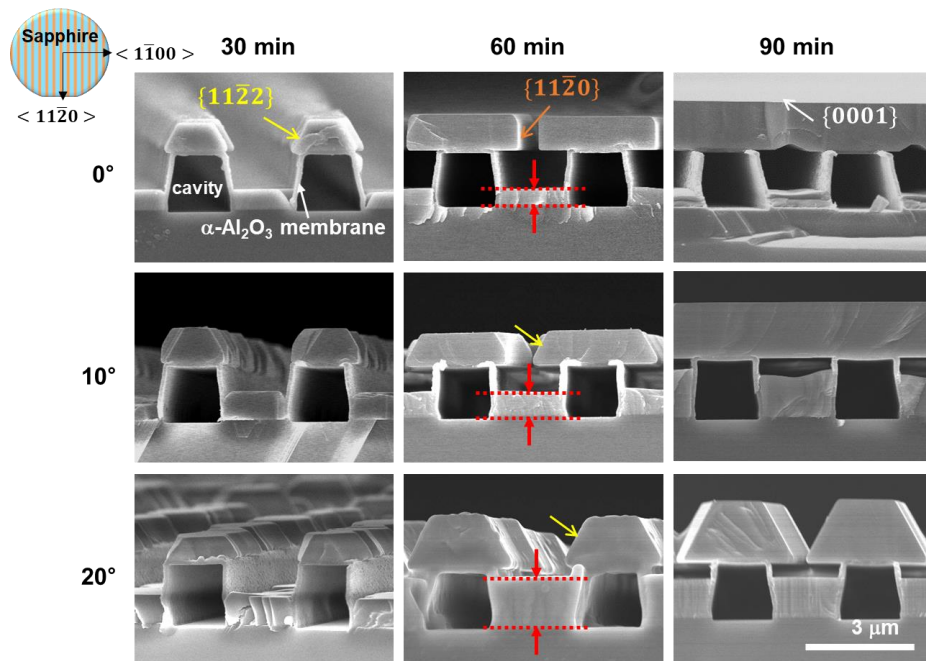
Figure 3.8. Cross-section SEM images of the growth of GaN layer on the sapphire nano-membrane with 0º, 10º, and 20º directions after 30, 60 and 90 min at 1040 °C and 300 Torr by MOCVD.
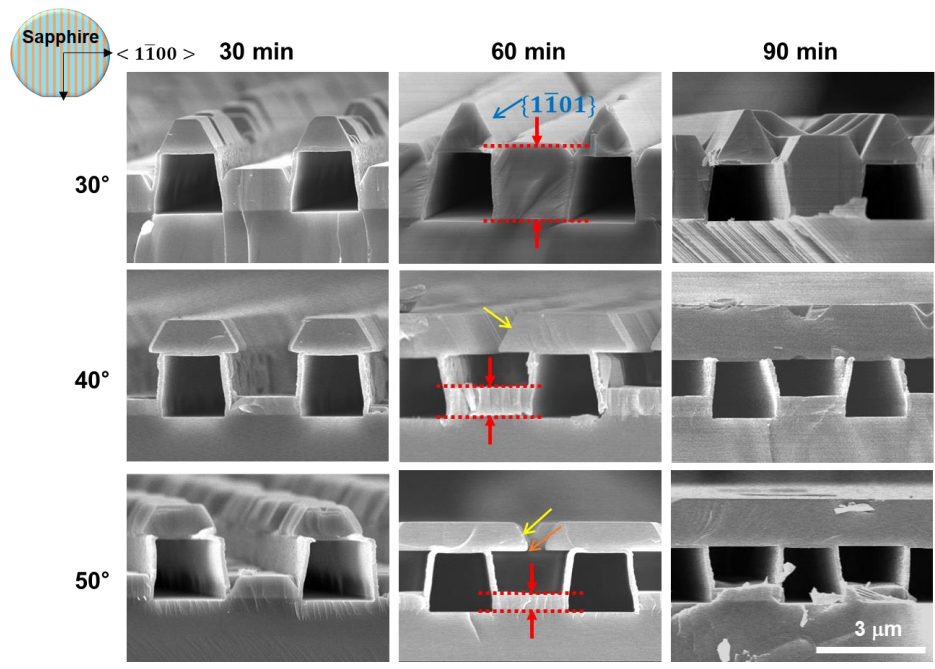
Figure 3.9. Cross-section SEM images of the growth of GaN layer on the sapphire nano-membrane with 30º, 40º, and 50º directions after 30, 60 and 90 min at 1040 ℃ and 300 Torr by MOCVD.

Table 3.1. The measured growth rates of each facets in 0° and 30° directions from 30 min growth to 60 min growth.

	Growth rate (µm/hr)			
	$\{0001\}$	$\{11\bar{2}0\}$	$\{11\bar{2}2\}$	$\{1\bar{1}01\}$
0°	0.26	0.81	1.18	-
30°	1.04	-	-	0.02
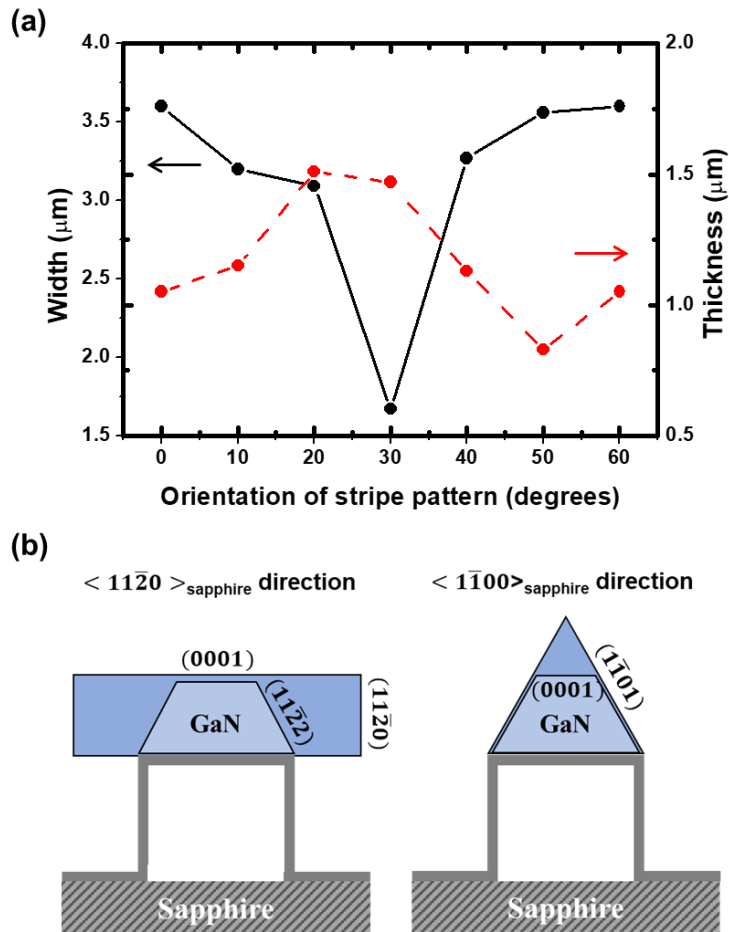
Figure 3.10. (a) Plot of with and thickness of GaN on the sapphire nano-membrane as a function of orientation. (b) Schematic diagram of the growth of GaN on the sapphire nano-membrane with $<11\bar{2}0>_{sapphire}$ and $<1\bar{1}00>_{sapphire}$ directions.
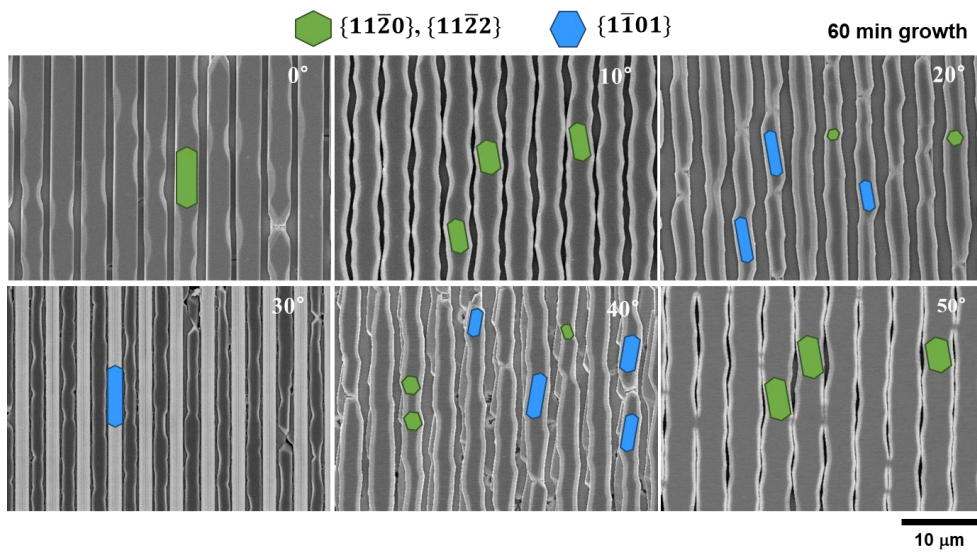
Figure 3.11. Plan-view SEM images of the GaN layer on the sapphire nano-membrane with various directions after 60 min growth.

3.3.3 Growth behavior of GaN on spacing region with various orientations

Except for the direction of 30º, GaN on the membrane grows laterally without contact with the bottom of the trench, namely, pendeo epitaxy (PE) (from the latin pendeo, meaning hanging on, suspended from).[26-29] Figure 3.12(b) shows the growth of GaN on spacing region which is between the membrane patterns as a function of orientation. As lateral growth of GaN on the top surface of membrane continues, the diffusion of Ga and N adatoms in the spacing region is disturbed by roof-shaped GaN layer. However, in 30º direction, since the lateral growth is slower than the vertical growth rate, Ga and N adatoms can be diffused to the bottom of spacing region without any interference. For this reason, GaN grows from the bottom like epitaxial lateral overgrowth (ELOG) instead of PE at 30º direction. In the case of the others, GaN growth in the spacing region becomes slower, resulting in coalescence of GaN on top surface of the membrane as shown in Fig. 3.12(c). This suggests that it is possible to apply an easy and damage-free mechanical lift-off (MLO) technique instead of laser lift-off, which can be costly and damaging in the sapphire substrate separation process. As shown in Fig. 3.13, the GaN stripes were successfully transferred to a Si substrate with Au/Ni as a bonding material. The side legs of the thin nano-membrane were easily broken by mechanical force, and the top of the sapphire nanomembrane was transmitted along with the GaN layer.
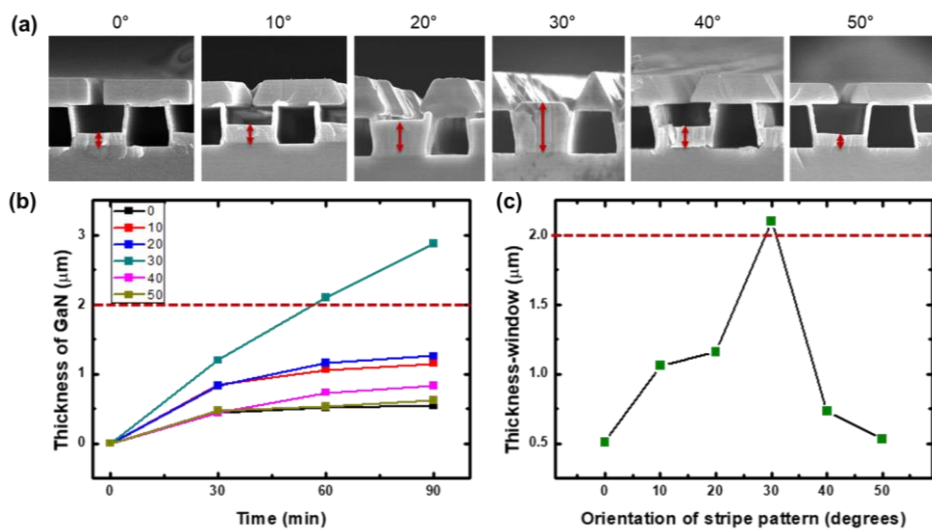
Figure 3.12. (a) Cross-section SEM images of the growth of GaN layer on the spacing region with various directions. Thickness of GaN on spacing region (between the membrane patterns) as a function of (b) time and (c) orientation. (red dot line: pattern height)
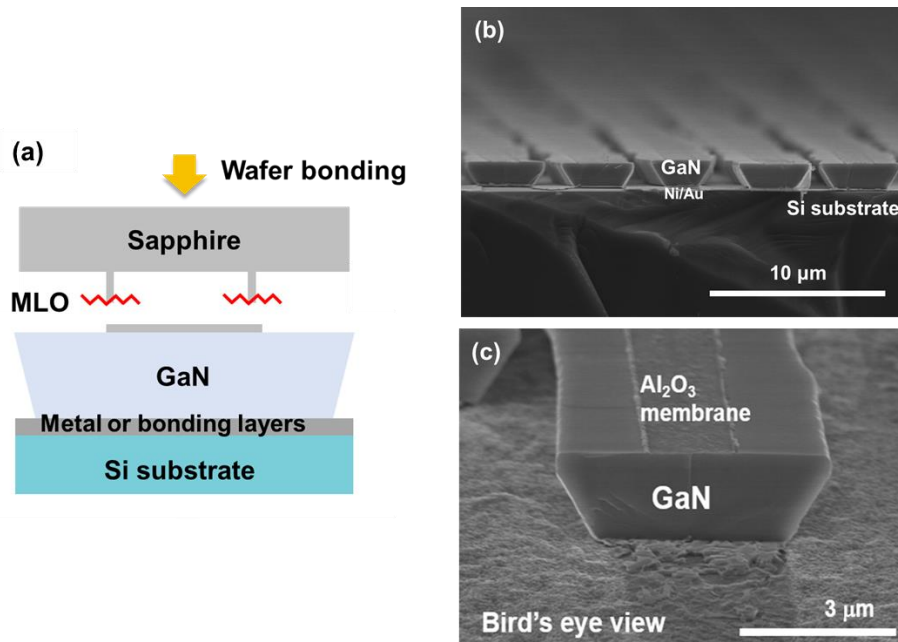
Figure 3.13. GaN layer transferred onto the Si substrate using mechanical lift-off (MLO), (a) Schematic of MLO process, (b) cross-section, and (c) bird's eye view SEM image. The top sapphire nano-membrane is visible on top of a GaN stripe.

3.4 Summary

In summary, the growth behavior of GaN on sapphire nano-membrane was investigated by varying the orientation of stripe pattern. The initial GaN grown on the membrane had (0001), $\{11\bar{2}0\}$, $\{11\bar{2}2\}$, and $\{1\bar{1}01\}$ growth facets along the orientation. Lateral to vertical growth rate ratio decreased gradually toward 30° pattern due to changing growth facets from $\{11\bar{2}0\}$ and $\{11\bar{2}2\}$ facets to $\{1\bar{1}01\}$ facet. These behaviors exhibit hexagonal symmetry, with a 30º angular span between the lateral and vertical growth maxima and minima. Especially, 0º orientation had linear GaN layer on pattern, whereas other orientations have nonlinear GaN layer, which means that it is advantages for LED configuration. GaN layer was deposited on spacing region without interruption at initial stage, but after lateral growth of GaN on pattern, growth of GaN on spacing region was interrupted by roof-shaped GaN. The result makes us expect to be able to grow discrete GaN arrays using the appropriate use of 0° with fast lateral growth rates and 30° with little progress in lateral growth.

3.5. Bibliography

[1] H. mano, N. Sawaki, I. Akasaki, and Y. Toyoda, "Metalorganic vapor phase epitaxial growth of a high quality GaN film using an AlN buffer layer", *Appl. Phys. Lett.* **48** 353 (1986).

[2] T.W. Weeks Jr., M. Bremser, K. Ailey, E. Carlson, W. Perry, E. Piner, M. El Masry, and R.F. Davis, "Undoped and doped GaN thin films deposited on high-temperature monocrystalline AlN buffer layers on vicinal and on-axis α(6H)-SiC(0001) substrates via organometallic vapor phase epitaxy", *J. Mater. Res.* **11**, 1011 (1996).

[3] A. Watanabe, T. Takeuch, K. Hirosawa, H. Amano, K. Hiramatsu, and I. Akasaki, "The growth of single crystalline GaN on a Si substrate using AlN as an intermediate layer", *J. Cryst. Growth* **128**, 391 (1993).

[4] T. Sugahara, H. Sato, M. Hao, Y. Naoi, S. Kurai, S. Tottori, K. Yamashita, K. Nishino, L. T. Romano, and S. Saki, Jpn. "Direct evidence that dislocations are non-radiative recombination centers in GaN", *J. Appl. Phys.* **37**, L398 (1998).

[5] S. Nakamura, M. Senoh, S. Nagahama, N. Isawa, T. Yamada, T. Matsushita, H. Kiyoku, Y. Sugimoto, T. Kozaki, H. Umemoto, M. Sano, and M. Chocho, "InGaN/GaN/AlGaN-based laser diodes with modulation-doped strained-layer superlattices grown on an epitaxially laterally overgrown GaN substrate", *Appl. Phys. Lett.* **72**, 211 (1998).

[6] Z. Yang, J. Alperin, W.I. Wang, T.S. Kuan, F. Semedy, and S.S. Iyer, "In situ relaxed $Si_{1-x}Ge_x$ epitaxial layers with low threading dislocation densities grown on

compliant Si-on-insulator substrates", *J. Vac. Sci. Technol. B* **16**, 1489 (1998).

[7] J. Cao, D. Pavlidis, Y. Park, J. Singh, A. Eisenbach, "Improved quality GaN by growth on compliant silicon-on-insulator substrates using metalorganic chemical vapor deposition", *J. Appl. Phys.* **83**, 3829 (1998).

[8] A.M. Jones, J.L. Jewell, J.C. Mabon, E.E. Reuter, S.G. Bishop, S.D. Roh, and J.J. Coleman, "Long-wavelength InGaAs quantum wells grown without strain-induced warping on InGaAs compliant membranes above a GaAs substrate", *Appl. Phys. Lett.* **74**, 1000 (1999).

[9] C.L. Chua, W.Y. Hsu, C.H. Lin, G. Chirstenson, and Y.H. Lo, "'Photopumped long wavelength vertical-cavity surface-emitting lasers using strain-compensated multiple quantum wells", *Appl. Phys. Lett.* **64**, 3395 (1994).

[10] D. Moon, J. Jang, D. Choi, I. S. Shin, D. Lee, D. Bae, Y. Park, and E. Yoon, "An ultra-thin compliant sapphire membrane for the growth of less strained, less defective GaN", *J. Cryst. Growth* **441**, 52 (2016).

[11] O. H. Nam, M. D. Bremser, T. S. Zheleva1 and R. F. Davis, "Lateral epitaxy of low defect density GaN layers via organometallic vapor phase epitaxy", *Appl. Phys. Lett.* **71**, 2638 (1997).

[12] Z. Yu, M.A.L. Johnson, J.D. Brown, N.A. El-Masry, J.W. Cook Jr, and J.F. Schetzina, "Study of the epitaxial–lateral-overgrowth (ELO) process for GaN on sapphire", *J. Cryst. Growth* **195**, 333 (1998).

[13] B. Beaumont, P. Vennegues and P. Gibart, "Epitaxial lateral overgrowth of GaN",

Phys. Status Solidi B **227**, 1 (2001).

[14] K. Hiramatsu, K. Nishiyama, A. Motogaito, H. Miyake, Y. Iyechika, and T. Maeda, "Recent progress in selective area growth and epitaxial lateral overgrowth of III-nitrides: effects of reactor pressure in MOVPE growth", *Phys. Stat. Sol. (a)* **176**, 535 (1999).

[15] D. Kapolnek, S. Keller, R. Vetury, R. D. Underwood, P. Kozodoy, S. P. Den Baars, and U. K. Mishra, "Anisotropic epitaxial lateral growth in GaN selective area epitaxy", *Appl. Phys. Lett.* **71**, 1204 (1997).

[16] H. Marchand, J.P. Ibbetson, P.T. Fini, S. Keller, S.P. DenBaars, J.S. Speck, and U.K. Mishra, "Mechanisms of lateral epitaxial overgrowth of gallium nitride by metalorganic chemical vapor deposition", *J. Crystal Growth*, **195**, 328, (1998)

[17] J. Jang, D. Yang, D. Moon, D. Choi, H. J. Lim, S. Kang, D. Bae, H. N. Han, Y. Park and E. Yoon, "Solid-phase epitaxy of a cavity-shaped amorphous alumina nanomembrane structure on a sapphire substrate", *J. Cryst. Growth* **498**, 130 (2018).

[18] C.W. White, L.A. Boatner, P.S. Sklad, C.J. McHargue, J. Rankin, G.C. Farlow and M.G. Aziz, "Ion implantation and annealing of crystalline oxides and ceramic materials", *Nucl. Instrum. Meth. B* **32**, 11 (1988).

[19] T.W. Simson, Q. Wen, N. Yu and D.R. Clarke, "Kinetics of the amorphous→γ →α transformations in aluminum oxide: effect of crystallographic orientation", *J. Am. Ceram. Soc.* **81**, 61 (1998).

[20] D. R. Clarke, "Epitaxial phase transformations in aluminum oxide", *Phys. Stat.*

Sol. (a) **166**, 183 (1998).

[21] M.D. Groner, F.H. Fabreguette, J.W. Elam and S.M. George, "Low-Temperature Al$_2$O$_3$ Atomic Layer Deposition", *Chem. Mater.* **16**, 639 (2004).

[22] H. Marchand, J. P. Ibbetson, P. T. Fini, S. Keller, S. P. DenBaars, J. S. Speck, and U. K. Mishra, "Mechanisms of lateral epitaxial overgrowth of gallium nitride by metalorganic chemical vapor deposition", *J. Cryst. Growth* **195**, 328 (1998).

[23] O. H. Nam, T. S. Zheleva, M. D. Bremser, and R. F. Davis, "Lateral epitaxial overgrowth of GaN films on SiO$_2$ areas via metalorganic vapor phase epitaxy", *J. Electron. Mater.* **27**, 233 (1998).

[24] J. Wang, R. S. Q. Fareed, M. Hao, S. Mahanty, S. Tottori, Y. Ishikawa, T. Sugahara, Y. Morishima, K. Nishino, M. Osinski, and S. Sakai, "Lateral overgrowth mechanisms and microstructural characteristics of bulk-like GaN layers grown by sublimation method", *J. Appl. Phys.* **85**, 1895 (1999).

[25] Q. Sun, C. D. Yerino, B. Leung, J. Han, and M. E. Coltrin, "Understanding and controlling heteroepitaxy with the kinetic Wulff plot: A case study with GaN", *J. Appl. Phys.* **110**, 053517 (2011).

[26] T. S. Zheleva, S. A. Smith, D. B. Thomson, K. J. Linthicum, P. Rajagopal, and R. F. Davis, "Pendeo-epitaxy: A new approach for lateral growth of gallium nitride films", *J. Electon. Mater.* **28**, L5 (1999).

[27] R. F. Davis, T. Gehrke, K. J. Linthicum, T. S. Zheleva, E. A. Preble, P. Rajagopal, C. A. Zorman, and M. Mehregany, "Pendeo-epitaxial growth of thin films of gallium

nitride and related materials and their characterization", *J. Cryst. Growth* **225**, 134 (2001).

[28] T. S. Zheleva, W. M. Ashmawi, and K. A. Jones, "Pendeo-Epitaxy versus Lateral Epitaxial Overgrowth of GaN: A Comparative Study via Finite Element Analysis", *Phys. Status Solidi (a)* **176**, 545 (1999).

[29] A. Strittmatter, S. Rodt, L. Reißmann, D. Bimberg, H. Schröder, E. Obermeier, T. Riemann, J. Christen, and A. Krost, "Maskless epitaxial lateral overgrowth of GaN layers on structured Si (111) substrates", *Appl. Phys. Lett.* **78**, 727 (2001).

Chapter 4. The growth of a discrete micro-GaN array with various sizes on sapphire nano-membrane

4.1 Introduction

4.1.1 Micro-LEDs as an emerging display technology and current issues

Micrometer-scale light emitting diodes (micro-LEDs) have attracted much attention due to potential applications to displays with high pixel density, high brightness, and low energy consumption.[1,2] However, there are still some issues for mass production of micro-LED displays such as low external quantum efficiency (EQE), leakage current, and costly and time-consuming transfer process onto a display backplane, etc.[3] Among them, it has been reported that the low EQEs and significant leakage current were attributed to plasma etching process, which was conventionally used for chip singulation.[4-9] During the plasma etching of an LED epitaxial structure, sidewalls of multiple quantum wells (MQWs) were inevitably exposed and damaged by plasma, resulting in generation of non-radiative surface recombination centers and leakage current paths. For the conventional LED chips with size over 1 mm x 1 mm, the non-radiative surface recombination and leakage current at low injection current level were not considered as severe problems. However, as the dimension of LEDs decreased, the surface to volume ratio increased, leading to the significant reduction in EQE and increases in leakage current. As shown in Table 4.1, typical micro-LEDs exhibited peak EQE under 10%.[8-16] As an effort to solve these problems, Tian et al. proposed thermal curing after the plasma

etching.[8] However, the thermally-cured micro-LEDs still showed EQE under 10%. Sidewall passivation methods for micro-LEDs using dielectric materials have been also reported.[6] There have even been attempts to change the etching method from inductively coupled plasma (ICP) to neutral beam etching (NBE), but as shown in Fig. 4.1, EQE was best at 3.4%.[15] Although improved optical or electrical characteristics were observed due to the sidewall passivation, plasma damages to the sidewalls of micro-LEDs still remains. It was reported that leakage current increased as dimension of micro-LEDs decreased, indicating incomplete suppression of sidewall damages. Therefore, if it is possible to fabricate a micro-LED array without harmful plasma etching process for chip singulation, the EQE and electrical properties would be greatly improved.

Table 4.1. External quantum efficiency of conventional micro-LED.

Year	Affiliation	Dimension (mm)	EQE$_{max}$ (%)
2012	Univ. of Strathclyde[8]	6 ~ 105 (diameter)	6 ~ 10
2014	Univ. of Strathclyde[10]	40 (diameter)	10
2016	LETI[11]	6.5 x 6.5	9.5
2017	LETI[9]	10 x 10	~5
2017	LETI[12]	5 x 5 ~ 100 x 100	6.5 ~ 13
2018	Tsinghua Univ.[13]	180 x 125	~12
2019	AIST (Japan) [14]	6, 10, 20, 40	0.7 ~ 3.4
2019	Univ. of California[15]	10 ~ 100 (KOH, ALD)	22 ~ 25
2020	Univ. of California[16]	1 ~ 30 (diameter)	2.5 ~ 7
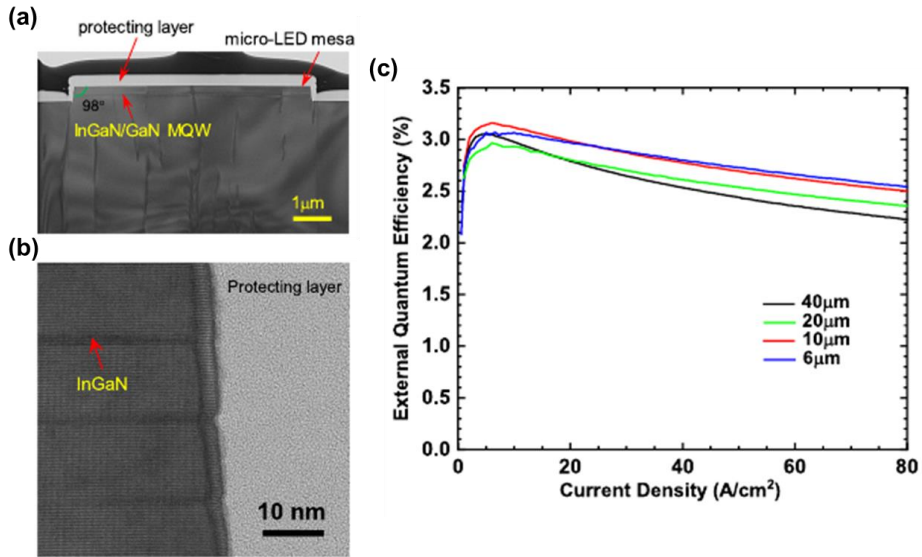
Figure 4.1. (a) Cross-sectional TEM image of a 6 μm micro-LED mesa fabricated by the NBE. (b) The high-resolution lattice image near the sidewall surface of the NBE sample. (c) EQE as a function of current density of micro-LEDs with different sizes fabricated by the NBE process.[15]

4.1.2 Sapphire nano-membrane for micro-LEDs

Due to the limited size and high cost of bulk GaN substrates, the commercial GaN-based LEDs are usually grown on c-plane sapphire substrates. However, the lattice mismatch and difference in thermal expansion coefficients between GaN and sapphire substrate induce high defect densities and high compressive stress in GaN layers, which causes deleterious effects on the LED performance.[17] Recently, our group demonstrated a 26 nm-thick ultra-thin sapphire nano-membrane structure, which served as a compliant substrate for the growth of less defective and less strained GaN.[18] The strain in GaN associated with the lattice mismatch between GaN and sapphire substrate could be shared with the ultra-thin sapphire nano-membrane. For the GaN grown on top surface of each membrane, the mean spacing between misfit dislocations was increased by 40% and the threading dislocation density (TDD) was reduced by 25%, compared to those of GaN grown on a conventional 430 μm-thick sapphire substrate. Significant reduction in piezoelectric electric field and resultant enhanced photoluminescence (PL) from InGaN/GaN MQWs grown on a 100 nm-thick sapphire nano-membrane were also observed.[19] It is expected that high-efficiency micro-LED chips can be obtained by growing high-quality GaN thin films with micro-size using sapphire nano membrane.

4.1.3 Pattern design for discrete GaN dies by using growth behaviors of GaN on sapphire nano-membrane

It is quite well known that facets of GaN show different growth rates under different growth condition such as temperature, pressure, and V/III ratio. Under

certain growth conditions, the growth rates of the growth facets vary depending on the orientation of growth, as shown in Fig. 4.2.[20] In chapter 3, through the study on growth behaviors of GaN on the sapphire nano-membrane, the growth rates were measured according to the growth facets, and the growth rates were increased in order of $\{1\bar{1}01\}$, (0001), $\{11\bar{2}0\}$, and $\{11\bar{2}2\}$. Moreover, the evolution of growth facets of GaN is determined by whether the facet is under convex or concave growth conditions. Under a convex growth condition, "slow growth facet" would remain. On the other hand, under a concave growth condition, "slow growth facet" would disappear, as illustrated in Fig. 4.3(a). When we use the test nano-membrane pattern in Fig. 4.3(b), the $\{1\bar{1}01\}$ and $\{11\bar{2}2\}$ facets would complete in both concave and convex conditions, the shape of GaN would change from left to right in Fig. 4.3(c) with growth time. The use of sapphire nano-membrane with the designed pattern, as shown in Fig. 4.4, would result in square-like micro-LED dies in various sizes.

In this chapter, Based on previous studies on the fabrication of a sapphire nano-membrane structure and the anisotropic growth characteristics of GaN, we designed the array of nano-membrane patterns with different lengths and spacings between a group of patterns. In the result, we demonstrated the growth of a discrete micro-GaN array on the sapphire nano-membrane without etching process, where the sidewalls of the active layer was not exposed. In addition, it was confirmed that a less defective GaN layer was obtained by growing GaN on the thin sapphire nano-membrane.
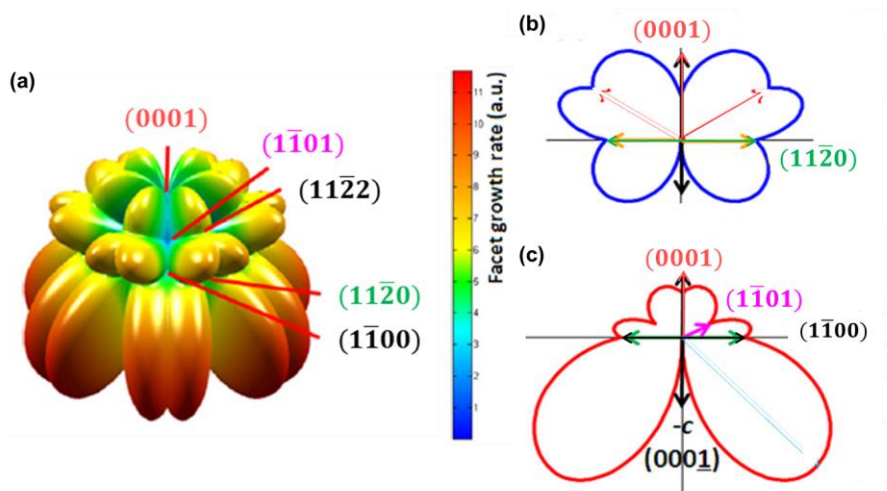
Figure 4.2. (a) Kinetic Wulff plots (vplots) for a low reactor pressure and low V/III ratio condition. 2D v-plots for the orientations within (b) the m-plane and (c) the a-plane.[20]
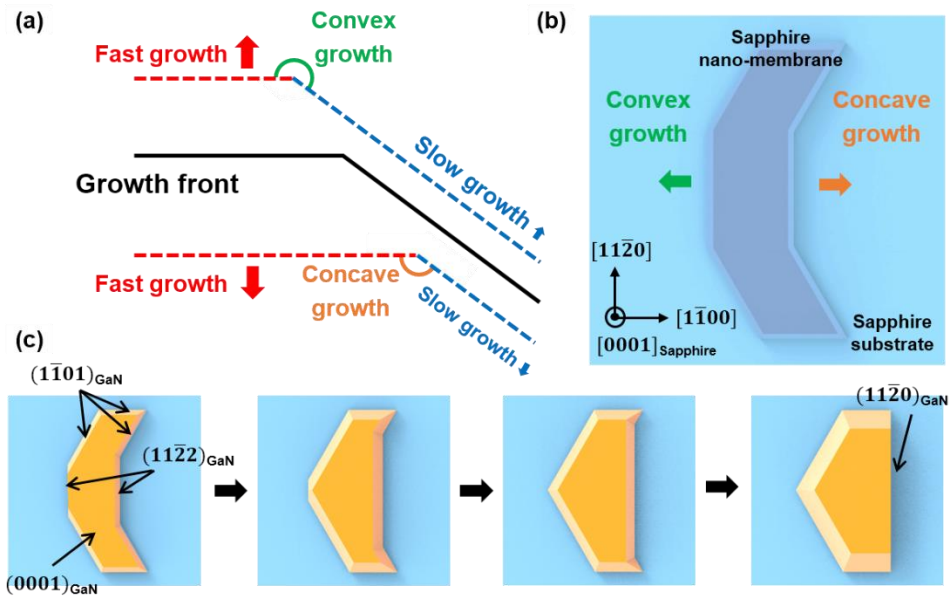
Figure 4.3. (a) Morphological evolution for convex and concave growth. (b) Pattern design of sapphire nano-membrane for the study on the growth behavior of GaN. (c) Expected morphology of GaN grown on the sapphire nano-membrane.
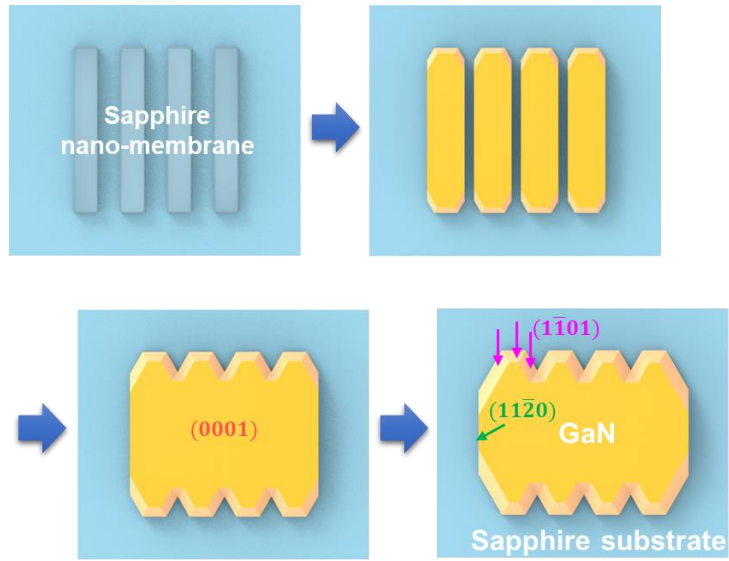
Figure 4.4. Schematics of the growth of GaN on a designed sapphire nano-membrane structure.

4.2 Experimental procedure

For the growth of a discrete micro-GaN array, the membrane pattern was designed using different growth rates for each growth facet of GaN. Figure 4.5 shows the schematics of experiments for growing a discrete GaN array on the sapphire nano-membrane. For the fabrication of sapphire nano-membrane structure, first, photoresist(PR) pattern of a stripe with the width and the spacing of 2 μm was formed on a sapphire substrate. The size of pattern groups is 6×6, 14×14, and 50×50 μm^2 and the stripe length and the number of stripe arrays determine the size of the discrete micro-GaN layers. Then, an amorphous Al_2O_3 layer with a thickness of 120 nm was deposited by atomic layer deposition(ALD) at 110 °C. After PR removal, the substrate was annealed at 1100 °C for 2 hours in air to crystallize the ALD alumina into α-phase for the GaN growth as described in our previous study.[21] Fabrication process of stripe patterned sapphire nano-membrane were described in chapter 3.2. However, in this case, it is impossible to remove PR by dipping in acetone because the edge cannot be opened. For PR removal, microwave asher of ULVAC Enviro II was used. Oxygen plasma was made with O_2 gas of 2500 sccm and N_2 gas of 250 sccm under a microwave power of 2000 W, a pressure of 1000 mTorr, and a temperature of 140 °C. Cooling was performed every 300 seconds for 60 seconds and ashing was carried out for 1 hour to remove PR. The ashing process was carried out by changing the thickness and density of the ALD alumina membrane to find conditions where PR is removed more easily. The remaining processes were the same with previous chapter and GaN was grown for 2 hours. Discrete GaN dies should be structurally and optically high quality to guarantee high EQE micro-LEDs. The

structural quality was assessed by field emission scanning electron microscopy (FE-SEM) and cathodoluminescence (CL) and the optical quality of GaN dies was observed by Photoluminescence (PL). The growth behaviors of GaN on the sapphire nano-membrane including the cavities were observed by FE-SEM of Hitachi S-4800. CL was measured with Gatan MonoCL4 at 5 kV, and PL was measured with a Dongwoo Optron micro-PL system using a 325 nm He-Cd laser.

Photolithography (Chip-sized pattern)

Amorphous alumina deposition by ALD

(110°C, 1500 cycles)

Removal of PR

(1040 °C, 300 torr)
GaN

(1100 °C, 2 hrs)

Discrete GaN array growth by MOCVD

Crystallization by thermal treatment
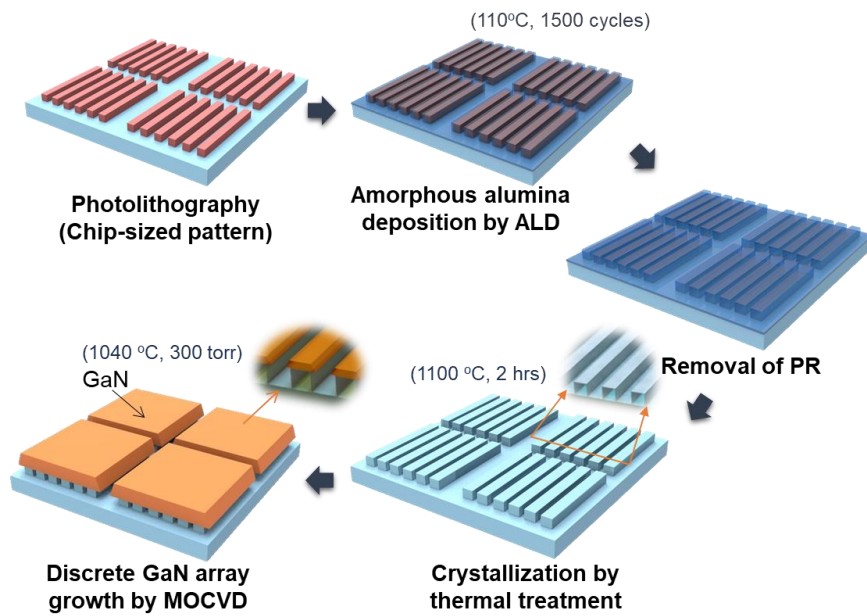
Figure 4.5. Schematic diagram of the growth of a disrete GaN array on sapphire nano-membrane array.

4.3 Results and discussion

4.3.1 PR removal by asher for fabrication of the sapphire nano-membrane array

Through the understanding of the GaN growth behavior on the membrane in chapter 3, a pattern design was performed to fabricate a discrete micro-GaN array, as shown in Fig. 4.6. The pattern was designed in a simple stripe pattern with a good lateral growth $[11\bar{2}0]_{sapphire}$ orientation and a poor lateral growth $[1\bar{1}00]_{sapphire}$ orientation. Since chip-sized patterns has been formed with all sides of membrane blocked, it is difficult to remove PR with acetone. Another PR removal method, heat treatment, causes the membrane to collapse because the PR quickly oxidizes and tries to escape the membrane. Therefore, as a way to solve this, we use an asher that is easy to control the rate of elimination of internal PR. PR can be removed by oxygen plasma generated from the microwave plasma asher as shown in Fig. 4.7. The oxygen radicals of the oxygen plasma react with the PR through the amorphous alumina membrane and the PR is removed by the oxidation reaction. Since the amorphous alumina membrane is porous, the reactants H_2O and CO_2 reacted inside the film are diffused and escaped to the outside of the film.

The thinner the thickness and the lower the density of amorphous alumina membrane, the easier the PR can escape. In order to find the optimum condition for removing PR, the amorphous alumina membrane thickness varied from 64.5 nm to 21.5 nm by changing the number of ALD cycles to 750, 500, and 250 cycles, and the density of membrane was changed by processing the deposition at temperature of 110 ℃ and 50 ℃. Since the deposition rate changes when the temperature is changed,

the process was performed at 675 cycles at 50 ℃ and 500 cycles at 110 ℃ to compare the same thickness. The membrane thickness and density according to each condition are shown in Table 4.2. Figure 4.8 shows SEM images after 15, 30, and 45 minutes of ashing on 50×50 μm^2 membranes with thicknesses of 21.5, 43, and 64.5 nm. The dark area of membrane is the area where the internal PR has been removed, and the bright area is where the PR remains inside. To make a quantitative comparison of PR removal rates, the removed PR to total PR ratio is given by

$$Ratio(\%) = \frac{Amount\ of\ Removed\ PR}{Amount\ of\ total\ PR} \times 100$$

$$= \frac{Length\ of\ removed\ PR}{Length\ of\ total\ PR} \times 100 \qquad [4-1]$$

with the fact that each stripe pattern has the same cross-sectional area. Figure 4.9 is a histogram graph measuring the length of the area where PR is removed from each pattern and Fig. 4.10 shows the plot of the removed PR to total PR ratio over time. Since PR was not uniformly removed in each stripe pattern, lengths of 260 lines were measured for each sample to obtain statistical values. In the case of 500 cycles and 750 cycles, histogram follows Gaussian distribution, but in case of 250 cycles, it is distributed very randomly. Ultra-thin alumina membrane is expected to cause cracks and holes in some areas because it cannot withstand the damage of the oxygen plasma and the rapid outflow of reactants. Therefore, an appropriate thickness of about 43 nm is needed to maintain the membrane shape.

Figure 4.11 shows SEM images after 15, 30, and 45 min ashing on 50×50 μm^2 membranes with deposition conditions of 675 cycles at 50 ℃ and 500 cycles at

110°C. The density of the membrane deposited at 50°C was 2.5 g/cm3, which is considerably lower than that at 110°C, and it can be seen that PR was quickly removed from the initial stage of ashing. The plot of the removed PR to total PR ratio over time was obtained in the same way as the previous calculation, and is shown in Fig. 4.12. As the density reduction increases the diffusion coefficient, the PR removal rate is faster for a sample with ALD at low temperature. In the sample with 50 °C ALD, however, the alumina membrane quickly collapsed and deformed. Furthermore, a thickness of about 100 nm is required to stably maintain the membrane while GaN is growing. Therefore, in order to prevent the deformation of the membrane and to easily remove the PR, ALD alumina was first deposited at 110 °C for 500 cycles, then the PR was removed, and 1000 cycles were additionally deposited before crystallization, as shown in Fig. 4.13(a). Figure 4.13(b) shows plan-view SEM images of each size membrane structure after PR removal and crystallization.

6 x 6 μm²

14 x 14 μm²

50 x 50 μm²
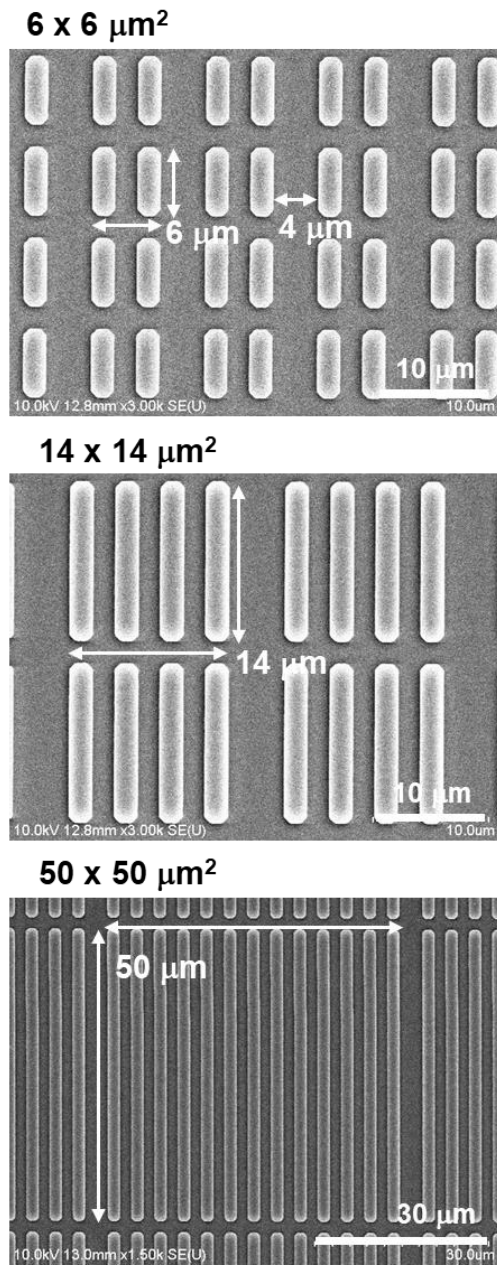
Figure 4.6. Plan-view SEM images 6 × 6, 14 × 14, and 50 × 50 μm² patterns after the deposition of .amorphous alumina membrane by ALD.

Figure 4.7. Schematics of PR ashing for the closed amorphous alumina membrane by oxygen plasma in microwave plasma asher.

Table 4.2. The thickness and density of ALD alumina membrane with various conditions.

Conditions	Thickness (nm)	Density (g/cm³)
750 cycles at 110 ℃	64.5	2.746
500 cycles at 110 ℃	43	2.746
250 cycles at 110 ℃	21.5	2.746
675 cycles at 50 ℃	43	2.500
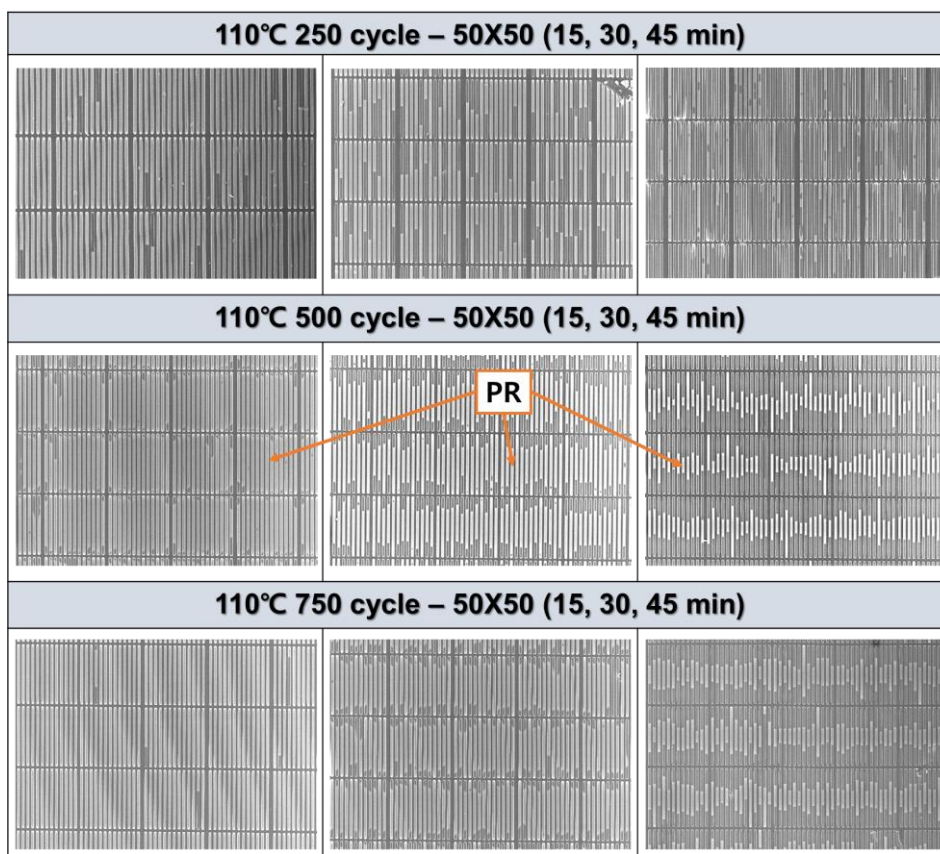
Figure 4.8. Plan-view SEM images of 50×50 μm^2 membranes after 15 min, 30 min, and 45 min of ashing on the membrane deposited in 250 cycles, 500 cycles, and 750 cycles ALD. (black bar = 50 μm)
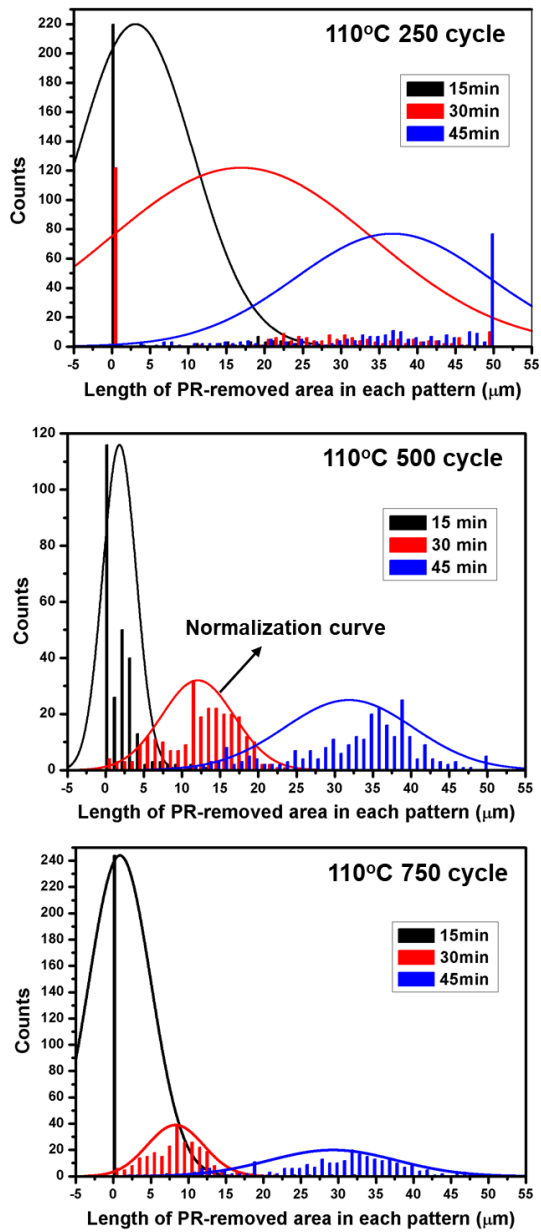
Figure 4.9. Histogram of PR-removed area in case of 250 cycles, 500 cycles, and 750 cycles.
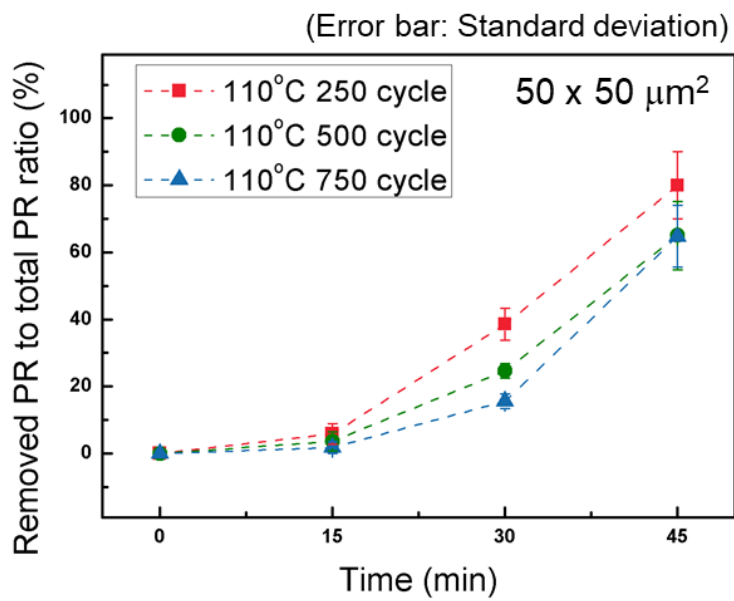
Figure 4.10. The plot of the removed PR to total PR ratio of the membranes with various thickness over time.
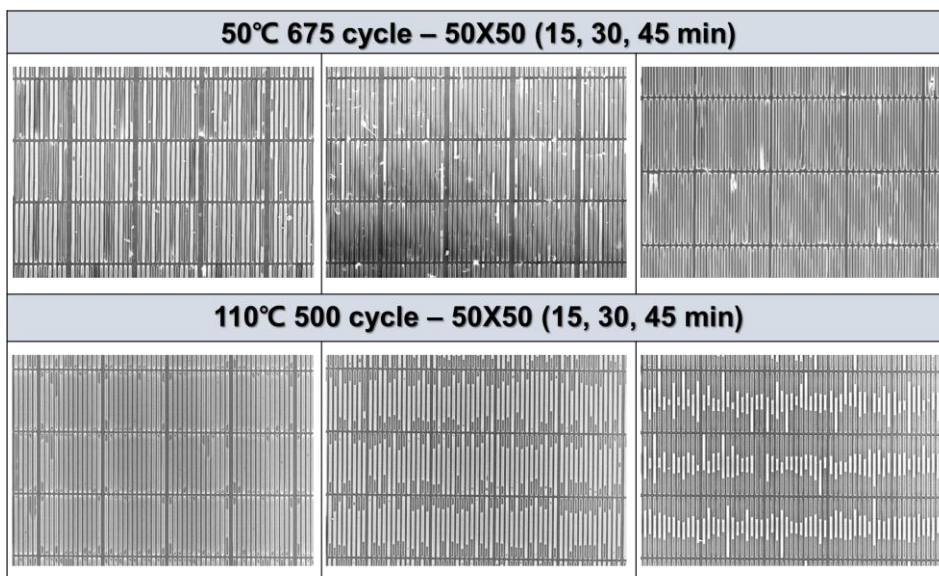
Figure 4.11. Plan-view SEM images of $50 \times 50\ \mu m^2$ membranes after 15 min, 30 min, and 45 min of ashing on the membrane with deposition conditions of 675 cycles at 50 °C and 500 cycles at 110 °C. (black bar = 50 μm)
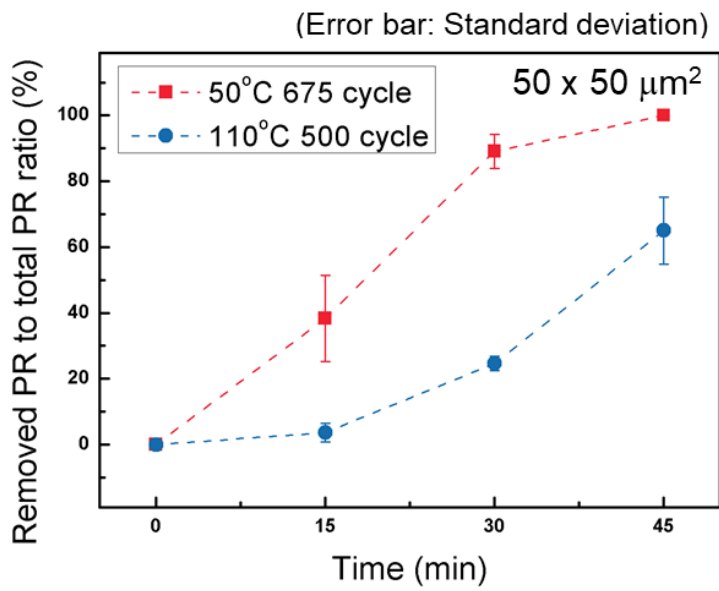
Figure 4.12. The plot of the removed PR to total PR ratio of the membranes with deposition temperature of 50 ℃ and 110 ℃ over time.

(a) ALD 110℃ 500 cycle + ashing   After SPE process

43 nm

ALD 110℃
1000 cycle

& Crystallization

~110 nm

2 μm   3 μm

(b)

20 μm   20 μm   30 μm
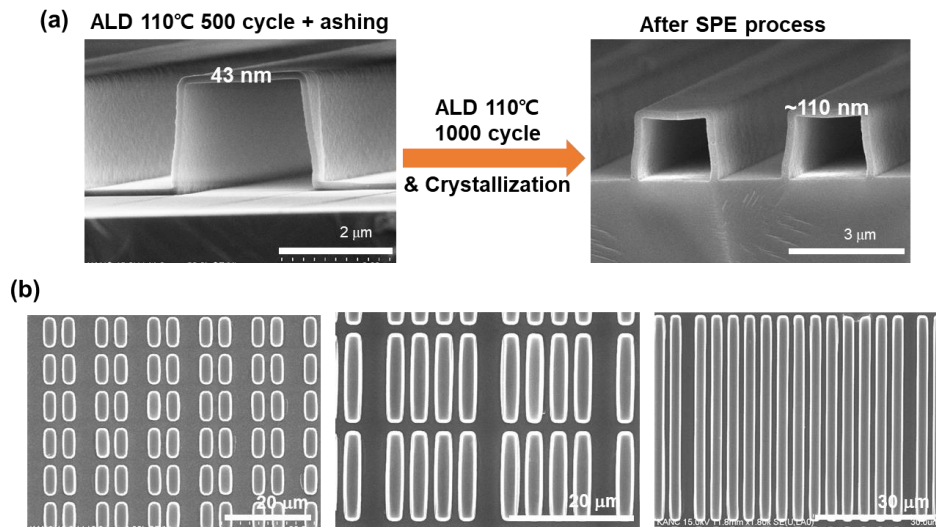
Figure 4.13. (a) Cross-section SEM images of PR removed membrane structure and crystallized membrane after additional deposition of ALD. (b) Plan-view SEM images 6 × 6, 14 × 14, and 50 × 50 μm² membrane structures after PR removal and crystallization.

4.3.2 Growth of a discrete micro-GaN array

Figure 4.14 shows the GaN layer on the sapphire nano-membrane with 6×6, 14×14, and 50×50 μm^2 sizes grown for 70 min after crystallization of amorphous alumina membrane. As previously anticipated, the GaN layer was grown in a convex growth mode consisting of $\{11\bar{2}0\}$ and $\{1\bar{1}01\}$ facets. Considering the lateral growth rate of GaN, the spacing between chip size pattern groups was adjusted to 4 μm for the horizontal direction and 2 μm for the vertical direction. GaN can be coalesced in the area of 2 μm spacing between the patterns, but, GaN cannot be coalesced in the area of 4 μm spacing in the horizontal direction. The $\{1\bar{1}01\}$ facet with hexagonal symmetry was observed at the top and bottom of the discrete GaN layers in bird's eye view SEM images, as shown in Fig. 4.15. The $\{1\bar{1}01\}$ facet of GaN in the vertical direction has the lowest growth rate, because it has lower surface energy than the $\{11\bar{2}0\}$ and (0001) facet of GaN. Therefore, lateral growth does not proceed in the vertical direction, and GaN is not coalesced. Figure 4.16 shows discrete micro-GaN arrays with 6×6, 14×14, and 50×50 μm^2 chip sizes grown for 2 hours. The 14×14 and 50×50 μm^2 sized GaN layers were grown not to merge with each other through proper lateral growth control, and also did not merge with the GaN grown in the spacing region as shown in Fig. 4.16(d) and 4.16(g). The 6×6 μm^2 sized GaN layers, however, has a relatively wide spacing region, so even if GaN is laterally grown, the diffusion of Ga to the bottom is not hindered. So, as shown in Fig. 4.16(a), GaN grown at the bottom of the substrate merged with GaN grown on the top of membrane.
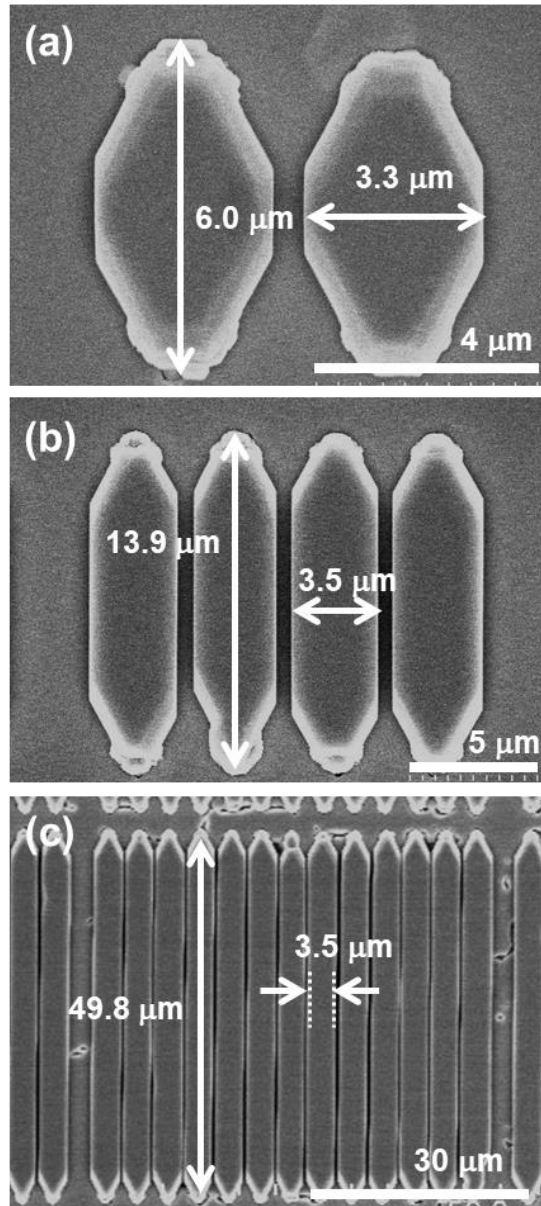
Figure 4.14. Plan-view SEM images of the GaN layer on the sapphire nano-membrane with (a) 6 × 6, (b) 14 × 14, and (c) 50 × 50 μm^2 sizes grown for 70 min.
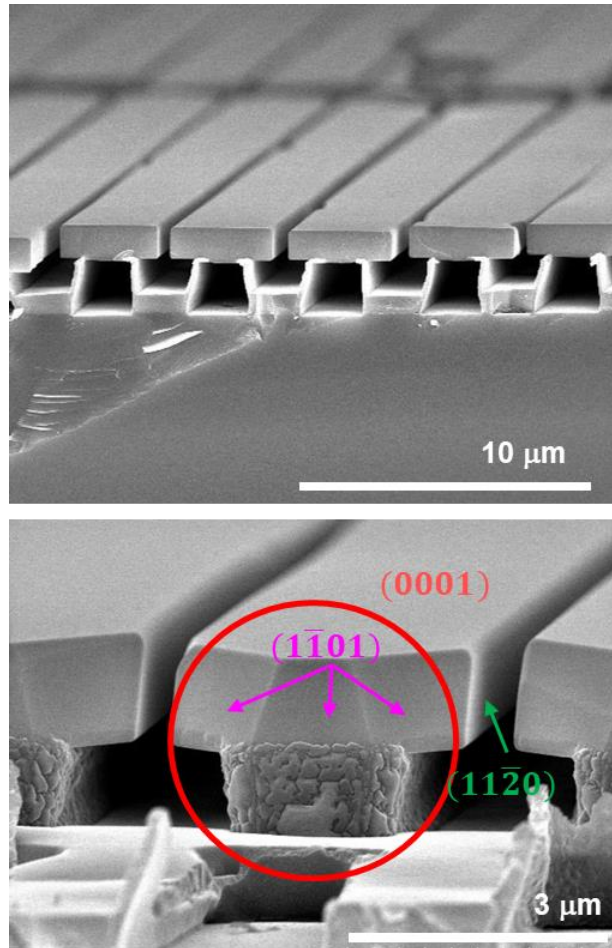
Figure 4.15. Bird's eye view SEM images of fast lateral growth in horizontal direction and slow lateral growth in vertical direction.
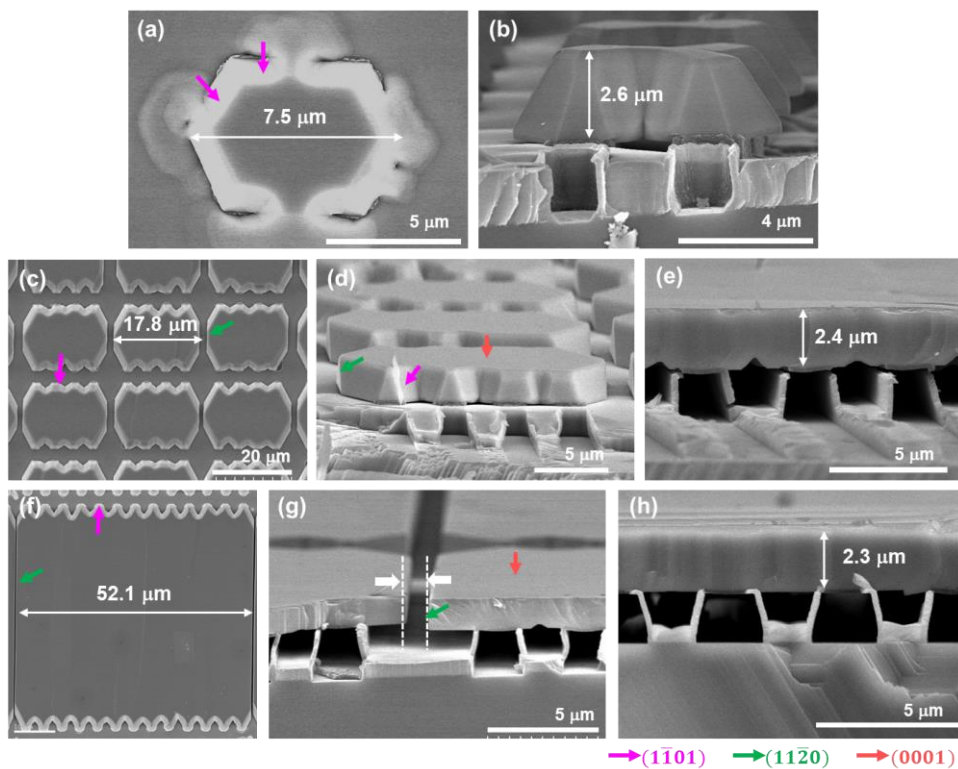
Figure 4.16. Plan-view, bird's eye view, and cross-section SEM images of the GaN layer on the sapphire nano-membrane with (a, b) 6×6 μm^2 size, (c, d, e) 14×14 μm^2 size, and (f, g, h) 50×50 μm^2 size grown for 120 min.

4.3.3 Threading dislocation density of micro-GaN layer

To measure the threading dislocation density (TDD) of micro-GaN layer, CL measurement was performed as shown in Fig. 4.17. TDD of the 14×14 and 50×50 μm^2 micro-GaN layers were measured to be 1.17×10^8 cm^{-2} and 1.31×10^8 cm^{-2}, respectively, which is 40% and 33% lower than that of GaN on the planar sapphire substrate (1.94×10^8 cm^{-2}). Moon et al. reported strain reduction of GaN layer on an ultra-thin sapphire membrane with a thickness of about 26 nm.[18] Stress occurs due to the lattice mismatch between sapphire and GaN. In the conventional case where GaN is grown on a sapphire substrate, GaN film takes this stress and a lattice mismatch dislocation is generated. However, when a very thin sapphire membrane acts as a substrate, strain caused by lattice mismatch is distributed to the sapphire membrane, i.e., strain partitioning.[22] As the thickness of the substrate becomes thinner, the strain applied to the epilayers becomes smaller due to strain partitioning. So, the misfit dislocation density is reduced, leading to a decrease in TDD. As a result, TDD decreased due to the reduction of the lattice mismatch dislocation and the lateral growth of GaN. In the merged area between yellow region in Fig. 4.18, however, threading dislocations are clustered in the form of lines. The yellow region is the stripe patterned membrane where GaN is grown and the region between them shows the area of GaN coalescence. As GaN grows laterally, the dislocations come up when the GaN layers merge with each other. Threading dislocations in which many are clustered can adversely affect the LED performance, so it is necessary to minimize the point of merging.
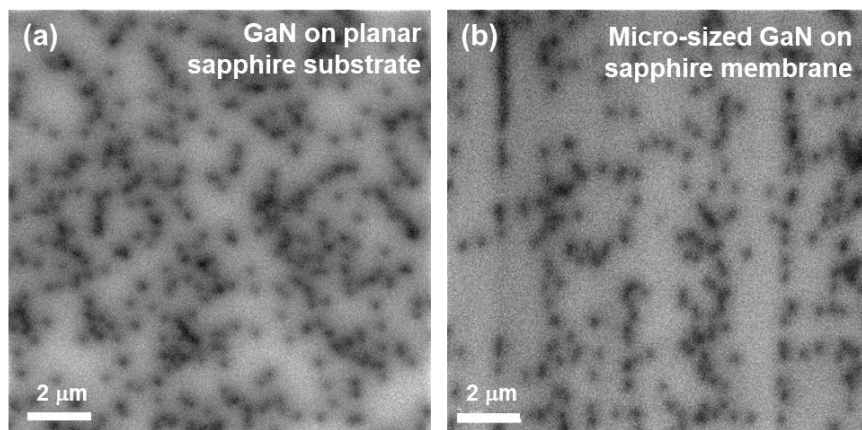
Figure 4.17. CL images of (a) GaN on planar sapphire substrate and (b) GaN layer
on the sapphire nano-membrane.
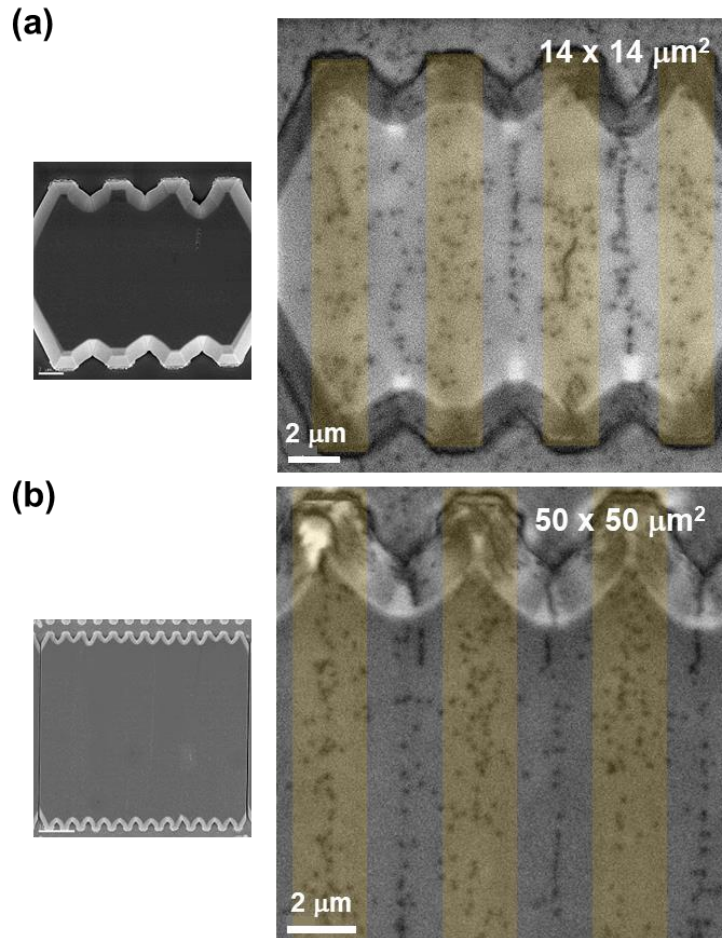
Figure 4.18. CL images of (a) 14 × 14 μm² and (b) 50 × 50 μm² size GaN layer on the sapphire nano-membrane. Yellow region is the stripe patterned membrane where GaN is grown on top of that.

4.3.4 Optical property of micro-GaN layer

Micro-PL measurement was performed to evaluate the optical properties of micro-sized GaN layers. Figure 4.19 shows near band edge (NBE) PL spectra at 10 K. The NBE emission peak intensity of GaN grown on the sapphire nano-membrane was found to be about 36.5% higher than that of GaN grown on the planar sapphire substrate. This is due to the low TDD of GaN on the sapphire membrane. The PL FWHM of GaN on the sapphire substrate and the sapphire membrane are 3.1 meV and 3.9 meV, respectively. Due to the density change ($2.1 \sim 3.5$ g/cm^3 $\rightarrow$ 3.99 g/cm^3)[21,23,24] resulting from the crystallization of the alumina membrane from the amorphous to the alpha phase, the membrane structure contracts and warps.[21] This results in a c-direction deformation at the top of the sapphire membrane, which is expected to affect the crystallinity of GaN. In addition, a red shift of the NBE emission peak from 355.16 nm to 356.71 nm was observed, indicating a reduction in the compressive stress of GaN on the sapphire membrane.
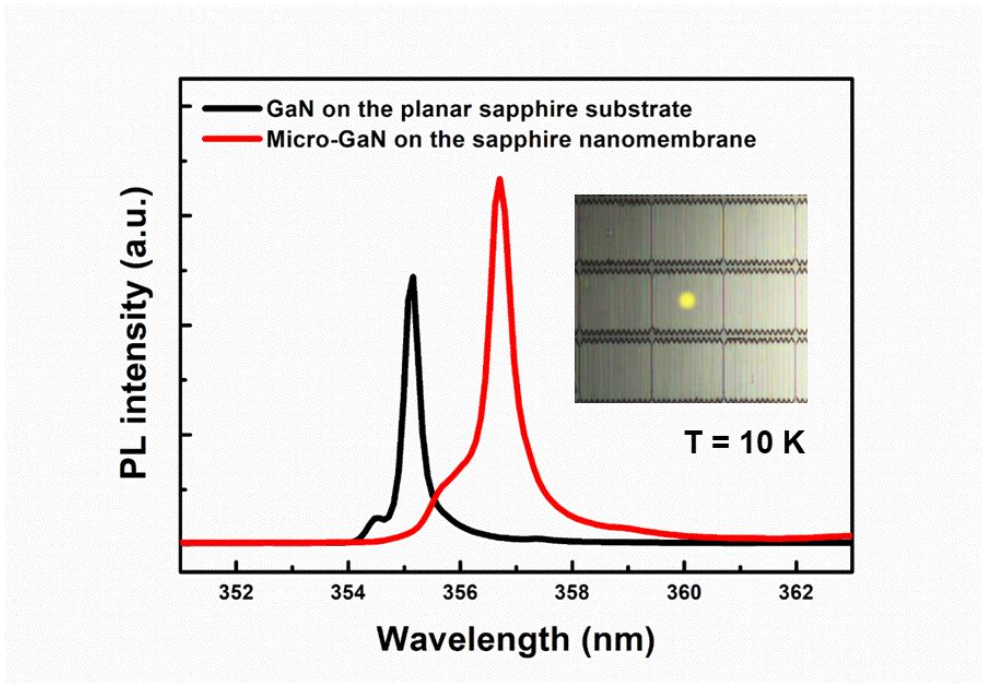
Figure 4.19. Micro-PL spectra of GaN layers grown on the planar sapphire substrate and the sapphire nano-membrane.

4.4 Summary

In summary, we proposed the designed pattern to grow a discrete micro-GaN array with various size. For the fabrication of sapphire nano-membrane structure, microwave plasma asher was used as PR removal method. Depending on the thickness and density of the ALD membrane, the quality of the porous membrane varied, and thus the degree of diffusion of PR was changed, resulting in the change of the rate of PR removal. Discrete micro-GaN arrays were successfully grown on the thin sapphire nano-membrane by using faster lateral growth rate over vertical growth rate. Different growth rates of growth facets determine the shape of GaN die by convex growth. Threading dislocation density of chip-sized GaN is reduced by 40% as compared with the GaN on planar sapphire substrate. Also, the PL peak intensity of micro-GaN on sapphire nano-membrane increased by 36.5% compared to that of GaN on planar sapphire substrate.

4.5. Bibliography

[1] H. X. Jiang, and J. Y. Lin, "Nitride micro-LEDs and beyond - a decade progress review", *Opt. Express* **21**, A475 (2013).

[2] T. Wu, C.-W. Sher, Y. Lin, C.-F. Lee, S. Liang, Y. Lu, S.-W. H. Chen, W. Guo, H.-C. Kuo, and Z. Chen, "Mini-LED and micro-LED: promising candidate for the next generation display technology", *Appl. Sci.* **8**, 1557 (2018).

[3] E. Virey, "MicroLED displays: hype and reality, hopes and challenges", *Yole Development*, (2017).

[4] F. Olivier, A. Daami, C. Licitra, and F. Templier, "Shockley-Read-Hall and Auger non-radiative recombination in GaN based LEDs: A size effect study:, *Appl. Phys. Lett.* **111**, 022104 (2017).

[5] D. Hwang, A. Mughal, C. D. Pynn, S. Nakamura, and S. P. DenBaars, "Sustained high external quantum efficiency in ultrasmall blue III-nitride micro-light-emitting diodes", *Appl. Phys. Express* **10**, 032101 (2017).

[6] M. S. Wong, D. Hwang, A. I. Alhassan, C. Lee, R. Ley, S. Nakamura, and S. P. DenBaars, "High efficiency of III-nitride micro-LEDs by sidewall passivation using atomic layer deposition", *Opt. Express* **26**, 21325 (2018).

[7] S. S. Konoplev, K. A. Bulashevich, and S. Y. Karpov, "From large-size to micro-LEDs: scaling trends revealed by modeling", *Phys. Status Solidi A* **215**, 1700508 (2018).

[8] P. Tian, J. J. D. McKendry, Z. Gong, B. Guilhabert, I. M. Watson, E. Gu1, Z. Chen, G. Zhang, and M. D. Dawson, "Size-dependent efficiency and efficiency droop of blue InGaN micro-light emitting diodes", *Appl. Phys. Lett.* **101**, 231110 (2012).

[9] F. Olivier, S. Tirano, L. Dupré, B. Aventurier, C. Largeron, and F. Templier, "Influence of size-reduction on the performance of GaN-based micro-LEDs for display applications" *J. Lumin.* **191**, 112 (2017).

[10] P. Tian, J. J. D. McKendry, J. Herrnsdorf, S. Watson, R. Ferreira, I. M. Watson, E. Gu, A. E. Kelly, and M. D. Dawson, "Temperature-dependent efficiency droop of blue InGaN micro-light emitting diodes", *Appl. Phys. Lett.* **105**, 171107 (2014)

[11] F. Templier, "GaN-based emissive microdisplays: A very promising technology for compact, ultra-high brightness display systems", *Journal of the SID* **24**, 669 (2016).

[12] F. Olivier, A. Daami, L. Dupré, F. Henry, B. Aventurier, and F. Templier, "25-4: Investigation and Improvement of 10μm Pixel-pitch GaN-based Micro-LED Arrays with Very High Brightness", *SID 2017 Digest* **48**, 1, 353 (2017).

[13] L. Li, C. Liu, Y. Su, J. Bai, J. Wu, Y. Han, Y. Hou, S. Qi, Y. Zhao, H. Ding, Y. Yan, L. Yin, P. Wang, Y. Luo, and X. Sheng, "Heterogeneous Integration of Microscale GaN Light-Emitting Diodes and Their Electrical, Optical, and Thermal Characteristics on Flexible Substrates", *Adv. Mater. Technol.* **3**, 1700239 (2018).

[14] J. Zhu, T. Takahashi, D. Ohori, K. Endo, S. Samukawa, M. Shimizu, and X.-L. Wang, "Near-Complete Elimination of Size-Dependent Efficiency Decrease in GaN

Micro-Light-Emitting Diodes", *Phys. Status Solidi A* **216**, 1900380 (2019)

[15] M. Wong, C. Lee, D. J. Myers, D. Hwang, J. A. Kearns, T. Li, J. S. Speck, S. Nakamura, and S. P. DenBaars, "Size-independent peak efficiency of III-nitride micro-light-emitting-diodes using chemical treatment and sidewall passivation", *Appl. Phys. Express* **12**, 097004 (2019).

[16] J. Smith, R. Ley, M. S. Wong, Y. H. Baek, J. H. Kang, C. H. Kim, M. J. Gordon, S. Nakamura, J. S. Speck, and S. P. DenBaars, "Comparison of size-dependent characteristics of blue and green InGaN microLEDs down to 1 μm in diameter", *Appl. Phys. Lett.* **116**, 071102 (2020)

[17] L. Liu, and J. H. Edgar, "Substrates for GaN epitaxy", *Mater. Sci. Eng. R.* **37**, 61 (2002).

[18] D. Moon, J. Jang, D. Choi, I.-S. Shin, D. Lee, D. Bae, Y. Park, and E. Yoon, "An ultra-thin compliant sapphire membrane for the growth of less strained, less defective GaN", *J. Cryst. Growth* **441**, 52 (2016).

[19] J. Kim, S. Lee, J. Oh, J. Ryu, Y. Park, S.-H. Park, and E. Yoon, "Highly polarized photoluminescence from c-plane InGaN/GaN multiple quantum wells on stripe-shaped cavity-engineered sapphire substrate", *Sci. Rep.* **9**, 8282 (2019).

[20] Q. Sun, C. D. Yerino, B. Benjamin, J. Han, M. E. Coltrin, " Understanding and controlling heteroepitaxy with the kinetic Wulff plot: A case study with GaN", *J. Appl. Phys.* **110**, 053517 (2011).

[21] J. Jang, D. Yang, D. Moon, D. Choi, H. J. Lim, S. Kang, D. Bae, H. N. Han, Y.

Park and E. Yoon, "Solid-phase epitaxy of a cavity-shaped amorphous alumina nanomembrane structure on a sapphire substrate", *J. Cryst. Growth* **498**, 130 (2018).

[22] D. Zubia, and S. D. Hersee, "Nanoheteroepitaxy: The Application of nanostructuring and substrate compliance to the heteroepitaxy of mismatched semiconductor materials", *J. Appl. Phys.* **85**, 6492 (1999).

[23] R. Lizarraga, E. Holmström, S. C. Parker, and C. Arrouvel, "Structural characterization of amorphous alumina and its polymorphs from first-principles XPS and NMR calculations", *Phys. Rev. B* **83**, 094201 (2011).

[24] F, W, Dynys, and J. W. Halloran, "Alpha Alumina Formation in Alum-Derived Gamma Alumina", *J. Am. Ceram. Soc.* **65**, 442 (1982).

Chapter 5. A core-shell-like micro-LED array grown on sapphire nano-membrane

5.1 Introduction

Micro-light-emitting diodes (micro-LEDs) is attracting much attention for next-generation display technology due to their superior characteristics, compared to current technologies such as liquid-crystal display and organic light-emitting diode display.[1-3] High brightness, long lifetime, and low energy consumption are necessary to outdoor and large-area displays. Especially, for the virtual and augmented reality (VR and AR) applications, high response rates and high pixel densities are essential for fast scene transitions and natural imaging without discomfort.[4,5] Because there are limitations in these requirements with the conventional display technologies, micro-LEDs draw a lot of attention for the next-generation display technology to deal with the new emerging markets.[5] Besides, micro-LEDs also exhibit enhanced light extraction, uniform current spreading, and heat dissipation due to their small configuration.[6-9] Therefore, since Jiang et al. demonstrated the first micro-LEDs with diameter of 12 μm[10,11], researches on micro-LEDs have been widely conducted throughout academia and industry as shown in Fig 5.1.[6-9,12-23] A micro-LED array driven by complimentary metal-oxide-semiconductor circuitry and a full color micro-LED array with active matrix operation were reported in 2009 and 2011, respectively.[12,13] In 2016, the 6.5 μm x 6.5 μm-sized blue and green micro-LED array with 2.2 x 10^7 cd/m^2 were demonstrated.[17] However, there are some issues for micro-LEDs sush as low

external quantum efficiency (EQE), leakage current, and costly and time-consuming transfer process onto a display backplane, etc.[3] Conventional micro-LED fabrication is done by plasma etching of the LED epitaxial film grown on large substrates for chip singulation. As the size of micro-LEDs shrinks, the wasted fraction of epitaxial wafers increases, and so-called kerf loss becomes unacceptable for mass production. Moreover, the non-radiative recombination at exposed sidewalls of multiple quantum wells (MQWs) significantly reduces the EQE of the micro-LEDs and generates leakage current paths. F. Oliviere et al. repoted influence of size-reduction on the performances of micro-LED as shown in Fig. 5.2.[18] For manufacturing micro-LED displays, transfer of micro-LED to backplane of display is required. Although the pick-and-place technology is a representative method of transferring micro LEDs, it is not suitable for mass production, and there are many difficulties in the process, especially as small displays become. Small displays such as VR and AR that are close to the human eye require high resolution, so monolithic hybridization transfer method is required as shown in Fig. 5.3.

In this chapter, we demonstrated a sapphire nano-membrane array for growth of a discrete micro-LED array with size of 4 μm × 16 μm without the harmful plasma etching process. Each multi-faceted micro-LED was grown on each sapphire nano-membrane without merging with adjacent ones. Figure 5.4 shows expected micro-LED shape with self-passivation by p-GaN. Since the MQW on the sidewalls is protected by p-GaN, it is expected to have high internal quantum efficiency (IQE), and since the TIP structure, which is widely known to be advantageous for light extraction[24], is naturally formed, the light extraction efficiency (LEE) is also expected to increase. Threading dislocation density (TDD) in the micro-LEDs grown on sapphire nano-membranes was reduced by 59.6%, compared to that grown on a

conventional sapphire substrate. Improved IQE was also observed from the temperature-dependent photoluminescence (PL) measurement. From the cathodoluminescence (CL) measurements, two orders of magnitude stronger emission at 435 nm was observed from the c-plane than that from semi-polar sidewall facets. The InGaN/GaN MQWs were formed both on the c-plane and semi-polar facets, and forming a core-shell-like, self-passivated micro-LED, hopefully minimizing the concentration of non-radiative recombination centers and leakage current paths. Sapphire nano-membrane technology is expected to provide a powerful platform for micro-LED fabrication process without plasma etching for chip singulation.
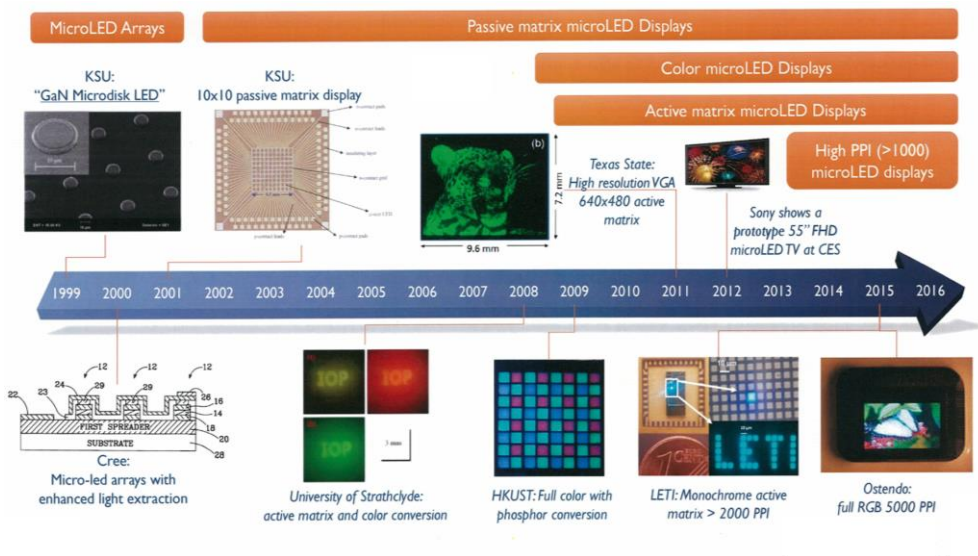
Figure 5.1. Micro-LED displays technology evolution.[3]
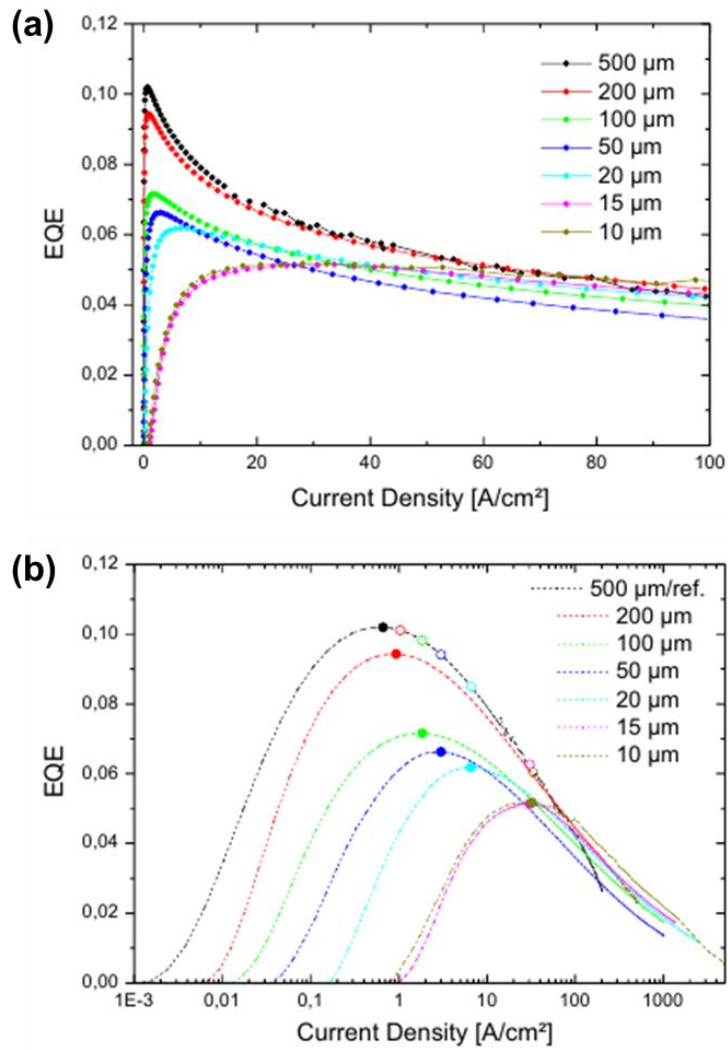
Figure 5.2. (a) EQE as a function of current density for different LED. (b) EQE curves showing experimental (solid circles) and expected maximum (empty circles).[18]
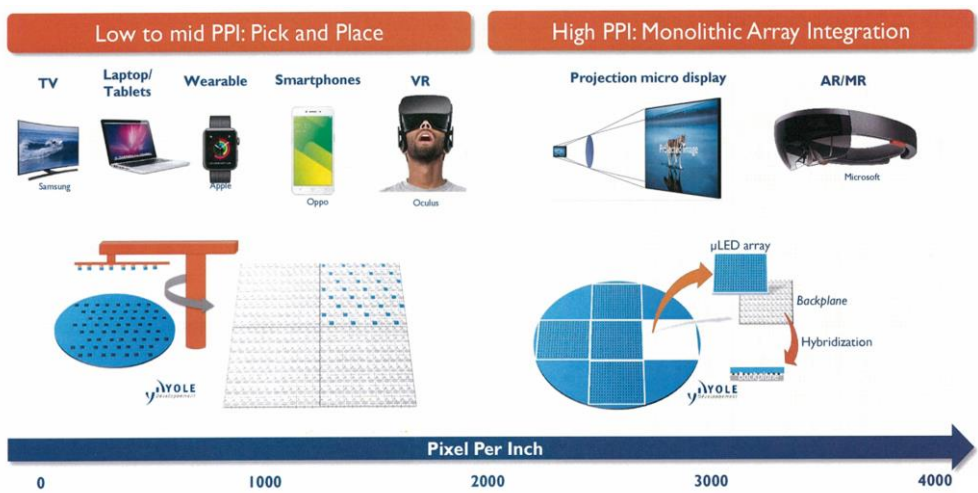
Figure 5.3. Micro-LED transfer technology.[3]
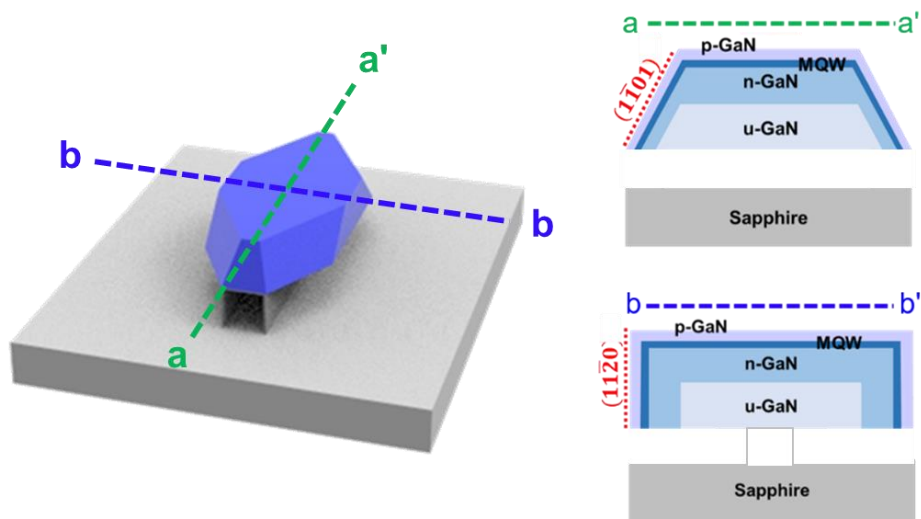
Figure 5.4. Expected micro-LED shape with MQWs at both top and sidewalls of a micro-LED die.

5.2 Experimental procedure

The schematic sequence for the fabrication of a sapphire nano-membrane array and the subsequent growth of a discrete micro-LED array are shown in Fig. 5.5, and described in detail in follows.

5.2.1 Fabrication of a sapphire nano-membrane array

A stripe-shaped PR pattern was firstly defined on a 2-inch c-plane sapphire substrate by a maskless patterning system (Nano System Solutions, DL-1000 HP) along the sapphire $[11\bar{2}0]$ direction. The width and height of the stripe were 2 μm, and the spacing between them was 5 μm. Subsequently, a 120 nm-thick amorphous alumina layer was deposited by ALD at 110 °C using trimethylaluminum and H_2O as precursors of Al and O, respectively. The second PR pattern (width: 16 μm, pitch: 20 μm) was formed along the direction perpendicular to the first stripe pattern to selectively expose the alumina layer. After the exposed amorphous alumina was etched by 85.0% H_3PO_4 at 50 °C, all PR was removed by acetone, resulting in a cavity-incorporated membrane array. The sample was subsequently annealed at 1150 °C for 2 hours in an air ambient furnace to crystallize amorphous alumina nano-membrane into single crystalline sapphire (α–phase) by solid-phase epitaxy, as described in detail elsewhere.[25,26] The sapphire nano-membrane became epi-ready states by wet cleaning and thermal treatment with rms roughness of 0.8 nm. Through the densification of alumina membrane during the crystallization, the thickness and width of top membrane were reduced to about 100 nm and 1.7 μm, respectively.

5.2.2 Epitaxial growth of a micro-LED array

An un-doped GaN array was grown for 40 min at 1040 °C and 40 kPa in a metal-organic chemical vapor deposition (MOCVD) chamber. Micro-LED epitaxial layers including an n-type GaN layer, 15 period InGaN/GaN superlattices (SLs), an InGaN stress relaxation layer, 3 period InGaN/GaN MQWs, an InGaN quantum barrier layer[27], and a p-type GaN layer were subsequently regrown on the un-doped GaN array in another MOCVD chamber. The n-type GaN layer was grown for 10 min at 1030 °C and 53 kPa. Thicknesses of un-doped GaN, n-type GaN, and p-type GaN were estimated to 1.1 μm, 0.3 μm, and 0.1 μm, respectively. An array of 4 μm × 16 μm micro-LEDs were formed on the sapphire nano-membrane array after the regrowth. For comparison, a reference LED epitaxial layer was grown on a planar sapphire substrate in the same batch. However, the LED structure of the reference sample is not identical to the micro-LED sample. The quantum well thickness as well as In content in InGaN well would be slightly different due to the differences in 2-dimensional growth (reference sample) and 3-dimensional growth on sapphire nano-membrane structures.

5.2.3 Characterization

The fabrication of sapphire nano-membrane array and the growth of micro-LED array were observed by field emission scanning electron microscope (FE-SEM), Hitachi S-4800. Raman spectra were taken from a LabRAM HV Evolution system using a 633 nm laser to analyze the stress states of un-doped GaN layers. Temperature-dependent PL were measured by Dongwoo Optron micro-PL system

with a 325 nm He-Cd laser to estimate IQE. The laser spot size of micro PL system used in this study was 3 μm. Cross-section TEM images of the micro-LEDs on sapphire nano-membranes were observed by Titan G2 80-200. Cross-section STEM measurements were also conducted to observe the core-shell-like micro-LEDs at all facets. TDD (deduced from CL dark spot density), monochromatic CL images, and spatially-resolved CL spectra from each facet of micro-LEDs were analyzed by Gatan Mono-CL4 with an acceleration voltage of 5 kV at room temperature.
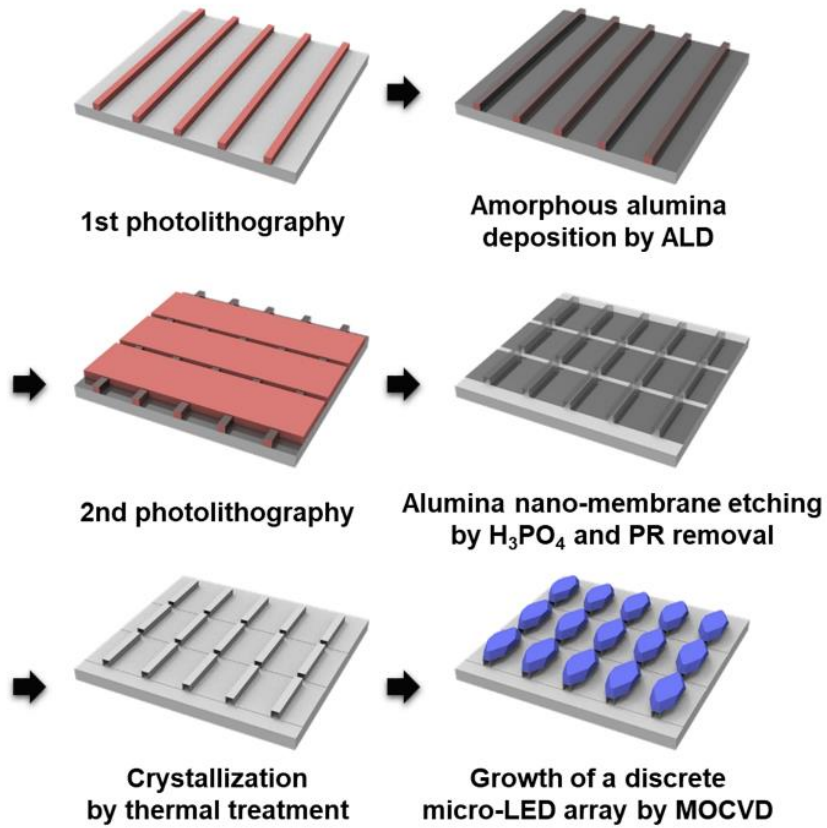
Figure 5.5. Schematic diagram for the fabrication of a sapphire nano-membrane array and the subsequent growth of a discrete micro-LED array.

5.3 Results and discussion

5.3.1 Fabrication of a sapphire nano-membrane array

Plan-view and cross-section scanning electron microscope (SEM) images of the ALD alumina-deposited first photoresist (PR) pattern are shown in Fig. 5.6(a) and 5.6(b), respectively. It was found that the stripe PR pattern was successfully formed and the amorphous alumina was conformally deposited over all exposed surface, preserving the stripe geometry. Subsequently, 4 μm-thick second PR pattern was formed in perpendicular direction with respect to the first PR pattern, exposing the top and side surface of the ALD alumina layer deposited on the first stripe PR pattern, as shown in Fig. 5.6(c) and 5.6(d). After the wet etching of exposed alumina by H_3PO_4, PR both above and underneath the alumina was removed, and the cavity-incorporated amorphous alumina nano-membrane array was fabricated, as shown in Fig. 5.6(e) and 5.6(f). The width and height of the first PR pattern and the spacing between them were designed to grow a discrete micro-LED array, considering the anisotropic growth behaviors of GaN.[28,29] After the subsequent thermal treatment, the amorphous alumina nano-membrane array was crystallized into sapphire (α-phase Al_2O_3) nano-membrane array by solid-phase epitaxy[25,26], as shown in Fig. 5.6(g) and 5.6(h). Due to the densification of alumina membrane during crystallization, the thickness and width of top membrane were reduced to about 100 nm and 1.7 μm, respectively. The top surfaces of the sapphire nano-membrane array were later used as templates for the growth of a discrete micro-LED array.
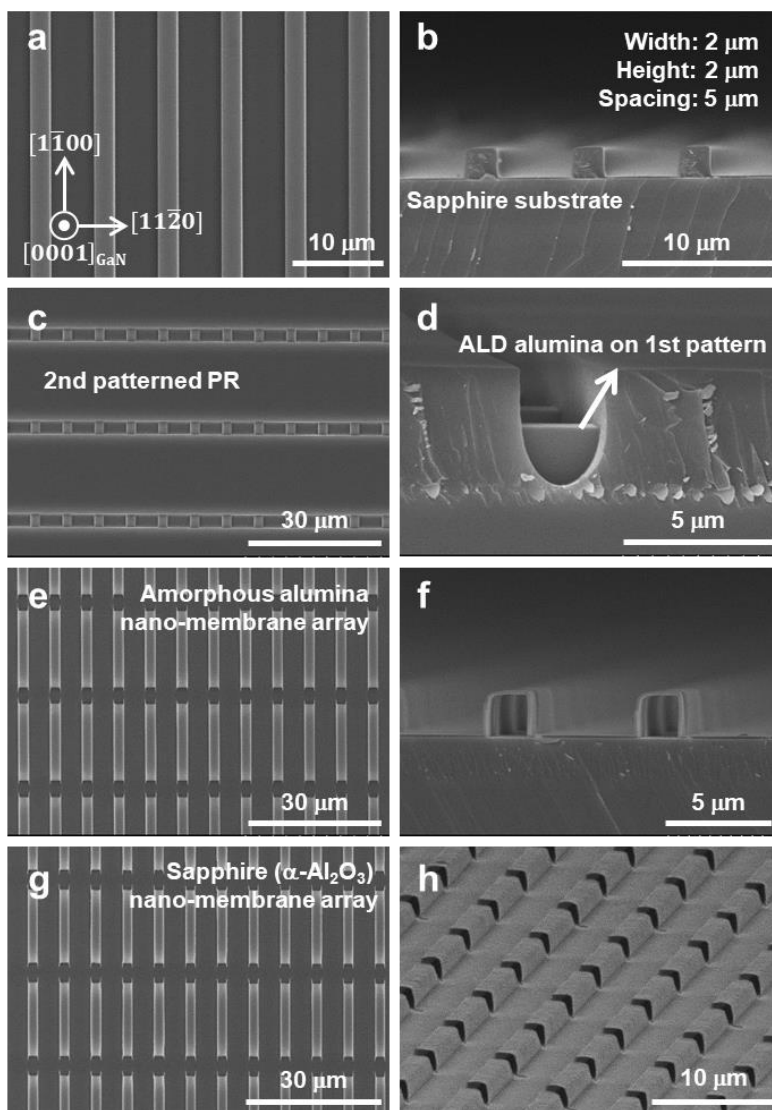
Figure 5.6. SEM images for the fabrication process of a sapphire nano-membrane array. (a) Plan-view and (b) cross-section SEM images of ALD alumina layer deposited on the first stripe-shaped PR pattern. (c) Plan-view and (d) cross-section SEM images of the second PR pattern on the ALD alumina layer. (e) Plan-view and (f) cross-section SEM images of a cavity-incorporated alumina nano-membrane array. (g) Plan-view and (h) cross-section SEM images of a sapphire nano-membrane array after thermal treatment.

5.3.2 Epitaxial growth of a discrete micro-LED array

Figures 5.7(a) and 5.7(b) show plan-view and bird's eye-view SEM images of an array of un-doped GaN template grown on the array of sapphire nano-membrane after 40 min growth, respectively. An array of 3 μm-wide un-doped GaN template was obtained after the pendeo-epitaxy of GaN along the $[11\bar{2}0]$ direction of GaN. Note that (0001), $\{11\bar{2}0\}$, and $\{1\bar{1}01\}$ facets were clearly observed. During the subsequent growth of an n-type GaN at a slightly different growth condition (lower temperature and higher pressure), $\{11\bar{2}2\}$ facets appeared instead of $\{11\bar{2}0\}$ facets[30], as shown in Fig. 5.7(c) and 5.7(d). Relative growth rates of GaN facets and its configuration are greatly affected by the MOCVD growth conditions.[31] Under the convex growth mode, $\{11\bar{2}2\}$ facet with slower growth rate appeared instead of $\{11\bar{2}0\}$ facet with higher growth rate during the n-GaN growth at relatively lower temperature and higher pressure.[28] The $\{11\bar{2}2\}$ facets prevailed throughout the subsequent growth of LED structures. Due to the proper design for dimensions of the sapphire nano-membrane array (i.e., width, length of the sapphire nano-membrane, pitches in two orthogonal directions), the micro-LEDs were isolated with respect to adjacent micro-LEDs. Note that GaN was also grown on the spacing region between the sapphire nano-membrane array; however, GaN growth was hindered since the majority of incoming Ga and N flux was more or less directed toward the GaN templates grown on the sapphire nano-membranes located at an elevated position (higher than ~2 μm with respect to the spacing region). Therefore, the precise design for the sapphire nano-membrane array is quite essential to construct a discrete micro-LED array. The shape of micro-LEDs with semi-polar

$\{11\bar{2}2\}$ and $\{1\bar{1}01\}$ facets is very effective in light extraction due to reduced total internal reflection, similarly to the truncated inverted pyramid structures.[24,32] In addition to the enhanced light extraction due to nano- and micro-structures, the inclined semi-polar facets is also expected to further enhance the light extraction.
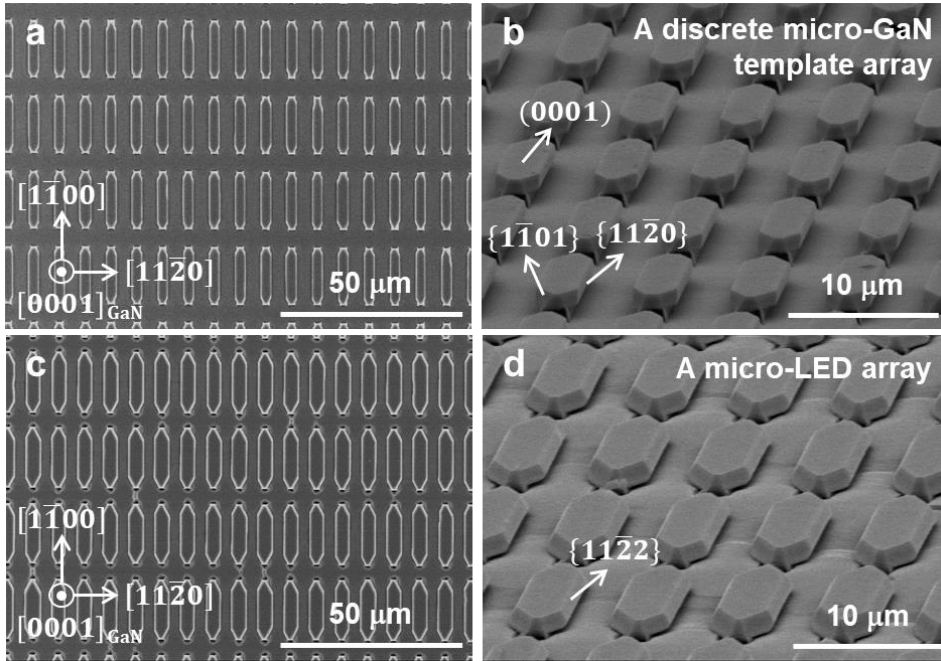
Figure 5.7. SEM images of epliayers on sapphire nano-membrane array. (a) Plan-view and (b) bird's eye view SEM images of discrete micro-sized un-doped GaN template array. (c) Plan-view and (d) bird's eye view SEM images of discrete micro-LEDs array grown on saphire nano-membrane array.

5.3.3 Characterization of a core-shell-like micro-LED array

Structural and optical properties of the un-doped GaN template and the micro-LED were analyzed by micro-Raman spectroscopy, CL, and micro-PL measurements. Figure 5.8 shows Raman spectra from a free-standing GaN, an un-doped GaN template on a sapphire nano-membrane, and an un-doped GaN on a thick planar sapphire substrate. For in-depth investigation on the stress variation in the un-doped GaN on sapphire nano-membrane, Raman spectroscopy measurements were carried out at two positions, i.e., GaN above membrane (indicated by green dot) and pendeo-epitaxy GaN (indicated by blue dot), as shown in inset of Fig. 5.8. The peaks of E2-high mode were observed at 568.4 cm^{-1} from GaN at both positions, and at 570.6 cm^{-1} for GaN on planar sapphire substrate. Considering the stress coefficient of GaN (4.3 cm^{-1}/GPa)[33], the residual compressive stresses in the un-doped GaN grown on sapphire nano-membrane and planar sapphire substrate were calculated to be 139 MPa and 651 MPa, respectively. Although the extents of stress relaxation of 78.6% were slightly lower, compared to our previous results (95.7%) for ultra-thin (26 nm) sapphire nano-membrane[25], considerable stress relaxation were observed. Figures 5.9(a) and 5.9(b) show panchromatic CL images from LEDs on planar sapphire substrate and the micro-LEDs grown on sapphire nano-membrane, respectively. The locations of the sapphire nano-membranes were indicated with green boxes as shown in Fig. 5.9(b). TDDs from micro-LEDs in the green boxes were as high as 2.87×10^8 cm^{-2}, which was reduced by 37.3%, compared to that in the reference sample of 4.58×10^8 cm^{-2}, as shown in Table 5.1. Misfit dislocation is generated at the interface between epitaxial layer and substrate when the epitaxial layer thickness increases beyond so-called critical thickness. As the thickness of

substrate decreases, the lattice mismatch strain in epilayer dramatically decreases due to strain partitioning. The ultra-thin nano-membrane substrate shared the part of strain in the epitaxial layer and effectively reduced the number of misfit dislocations at the GaN/nano-membrane interfaces[25], leading to the less defective GaN islands/interface and resultant reduction of TDD in the epitaxial layer.[34,35] These results are in good agreement with the stress states in GaN measured by Raman spectroscopy in Fig. 5.8. Nearly TDD-free regions were observed from the pendeo-epitaxy GaN regions due to absence of vertical propagation of threading dislocations.[36] Average TDD was measured to be 1.85×10^8 cm^{-2}, which was reduced by 59.6%, compared to the reference sample. Figure 5.10 shows Arrhenius plots of the integrated PL intensity from both micro-LED on sapphire nano-membrane and reference sample over the temperature ranges of 10 K to 300 K. The IQE was estimated from the ratio of integrated PL intensity at 10 K and 300 K by assuming that the IQE is 100% at a low temperature of 10 K.[37] The IQE of the micro-LEDs on sapphire nano-membrane was enhanced a factor of 1.44, compared to the reference sample. The inset of the Fig. 5.10 shows PL spectra of the samples measured at 300 K. About 3.3 times higher integrated PL intensity was observed from the micro-LED on sapphire nano-membrane than that of the reference sample at room temperature. The improvement in both IQE and integrated PL intensity was attributed to the stress relaxation and reduced TDD in the micro-LEDs grown on sapphire nano-membranes. The PL peak position from the micro-LEDs on sapphire nano-membranes was red-shifted by 0.12 eV, compared to that from the reference sample. The red-shift could be attributed to the higher indium incorporation into the InGaN wells[38,39], whose temperature was slightly lower due to the lower thermal conductivity of the cavity-incorporated nano-membrane structures. Using the

sapphire nano-membrane array, both blue-shift induced by reduction of QCSE and the red-shift due to higher indium incorporation were superimposed. The apparent PL red-shift indicates that the higher indium incorporation was dominant in this study. The PL full width at half maximum (FWHM) from the micro-LEDs on sapphire nano-membranes and reference sample were 0.17 eV and 0.10 eV, respectively. The origin of the larger FWHM will be discussed later. Additional PL peak around 382 nm fitted with the emission from the semi-polar facets as shown in CL images in Fig. 5.13. The laser spot size of micro PL system used in this study was 3 μm so that emission from the sidewalls could be detected from the micro PL measurements.

To observe the core-shell-like MQWs on all facets of the micro-LED, transmission electron microscopy (TEM) analysis was conducted. Figure 5.11(a) shows a cross-section TEM image of a single micro-LED viewed along $[1\bar{1}00]_{GaN}$ direction. We found that a discrete micro-LED was grown on a sapphire nano-membrane without merging with the GaN grown on the spacing region. The magnified scanning TEM (STEM) images in Fig. 5.11(b) and 5.11(c) showed that the p-type GaN layer and the InGaN/GaN MQWs were formed on all polar and semi-polar facets, implying the formation of a core-shell-like micro-LED. The red lines in insets of Fig. 5.11(b) and 5.11(c) indicate the location where cross-section images were taken. It was worth noting that thicknesses of MQWs on (0001) plane near the edge gradually decreased toward both sidewalls of $\{11\bar{2}2\}$ and $\{1\bar{1}01\}$, respectively, as shown in Fig. 5.11(b) and 5.11(c). The broader PL spectrum from the micro-LEDs on sapphire nano-membranes discussed above could be explained in terms of inhomogeneous indium composition and thickness deviation in (0001) facets. Funato et al. reported the inhomogeneous indium distributions in MQWs grown on (0001) facets in the micro-structures with semi-polar and non-polar

facets.[36] Cross-section STEM images of (0001), $\{11\bar{2}2\}$, and $\{1\bar{1}01\}$ facets clearly show the differences in growth rate at various facets as shown in Fig. 5.12(a), 5.12(b), and 5.12(c), respectively. The thicknesses of InGaN wells were measured to be 3.01 ± 0.13 nm, 1.36 ± 0.11 nm, and 1.35 ± 0.15 nm on (0001), $\{11\bar{2}2\}$, and $\{1\bar{1}01\}$ facets, respectively.

Figures 5.13(a), 5.13(b), 5.13(c), and 5.13(d) show plan-view SEM image, monochromatic CL images at 375 nm, 387 nm, and 435 nm, respectively, from a micro-LED on a sapphire nano-membrane. The monochromatic CL measurements clarified the emission from all facets as shown in Fig. 5.13(b), 5.13(c), and 5.13(d). Emissions with shorter wavelengths were measured from the facets in order of $\{11\bar{2}2\}$, $\{1\bar{1}01\}$, and (0001), in good agreement with the results in the literature.[40-43] The emissions with various wavelengths were attributed to the differences in growth rates and indium incorporation on each facet.[43,44] In addition, the thinner InGaN quantum well in semi-polar facets reduced the QCSE and leads to an increased emission energy, which is consistent with the CL results. Points on each facet of the micro-LED in Fig. 5.13(a) indicates positions where spatially-resolved CL measurement were conducted, and the corresponding CL spectra were shown in Fig. 5.14. Peak wavelengths of the spatially-resolved CL spectra from each facet were corresponded to the monochromatic CL images shown in Fig. 5.13(b), 5.13(c), and 5.13(d), respectively. Two orders of magnitude stronger emission was observed from (0001) plane at 435 nm than that from semi-polar $\{11\bar{2}2\}$ and $\{1\bar{1}01\}$ planes. This result is different from emission properties of similar micro-sized light emitters with $\{11\bar{2}2\}$, $\{1\bar{1}01\}$, and (0001) facets obtained from the selective growth by using a dielectic-patterned GaN/sapphire substrate.[43] Hwang et al.

reported superior optical properties from $\{11\bar{2}2\}$ facets compared to those from (0001) facet, which was explained by less QCSE at the semi-polar $\{11\bar{2}2\}$ facet.[43] In our structures; however, the weaker CL signals from the semi-polar facets were attributed to the extremely thin InGaN wells as observed in the STEM measurements, since carriers in the very thin MQWs can be easily escape. Moreover, the ultra-thin sapphire nano-membrane significantly reduced the compressive stress in GaN, leading to reduction of QCSE in (0001) facet and resultant increase in overlap of electron and hole wave functions. The strong CL emission mostly from the c-plane of the micro-LED on sapphire nano-membrane may be an important characteristic for the realization of micro-LED displays. The results suggest that the proper n- and p-metal design in micro-LEDs on sapphire nano-membranes would suppress the emission from semi-polar with shorter wavelength and generate the emission only from (0001) plane.
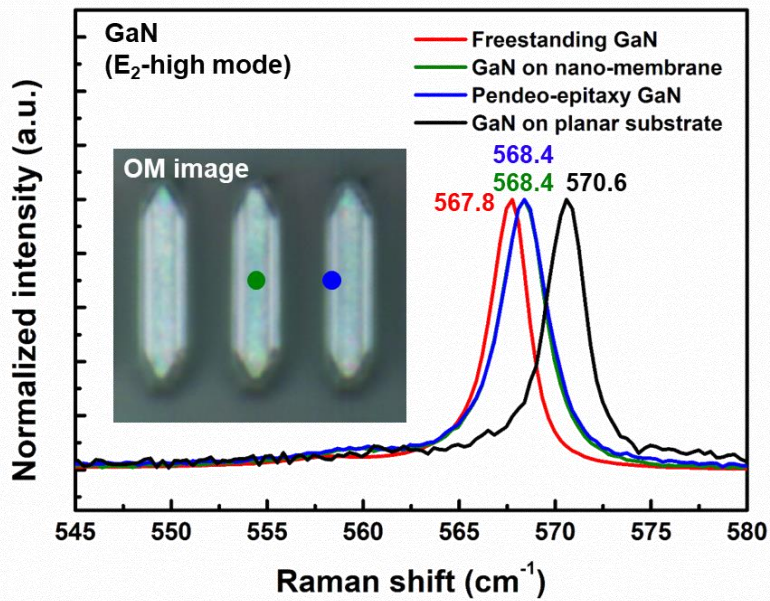
Figure 5.8. Raman spectra from freestanding GaN, micro-sized un-doped GaN on sapphire nano-membrane, and un-doped GaN on planar sapphire substrate.
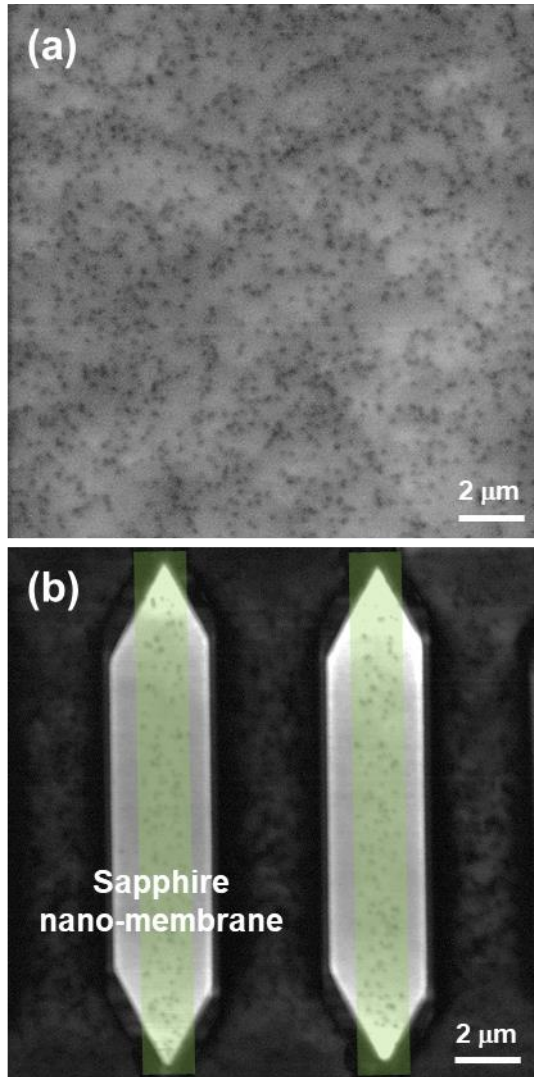
Figure 5.9. Panchromatic CL images of (a) a LED film on planar sapphire substrate and (b) micro-LEDs grown on sapphire nano-membrane.

Table 5.1. Calculated threading dislocation density of LEDs on planar sapphire substrate and micro-LEDs on sapphire nano-membrane from CL results.

Samples	Threading dislocation density (TDD) (cm^{-2})	
LEDs on planar sapphire substrate	4.58×10^8	
Micro-LEDs on sapphire nano-membrane	1.85×10^8 (average)	
	Membrane region 2.87×10^8	Pendeo-GaN 0
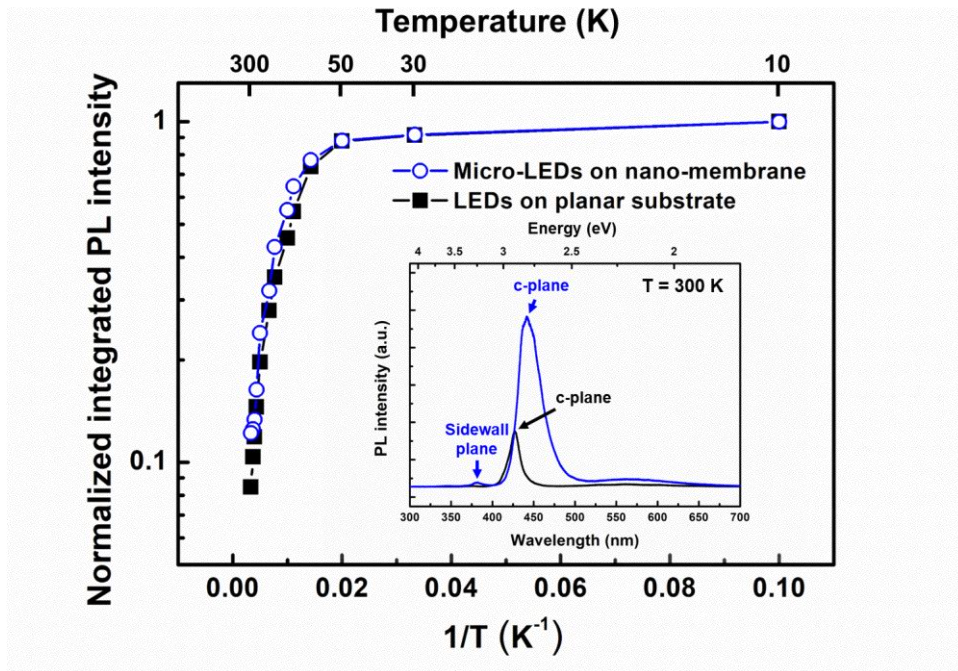
Figure 5.10. Ahrrenius plots of temperature dependent PL from micro-LEDs on sapphire nano-membrane and LEDs on planar substrate. The inset figure shows PL spectra measured at 300 K from micro-LEDs on sapphire nano-membrane and LEDs on planar substrate.
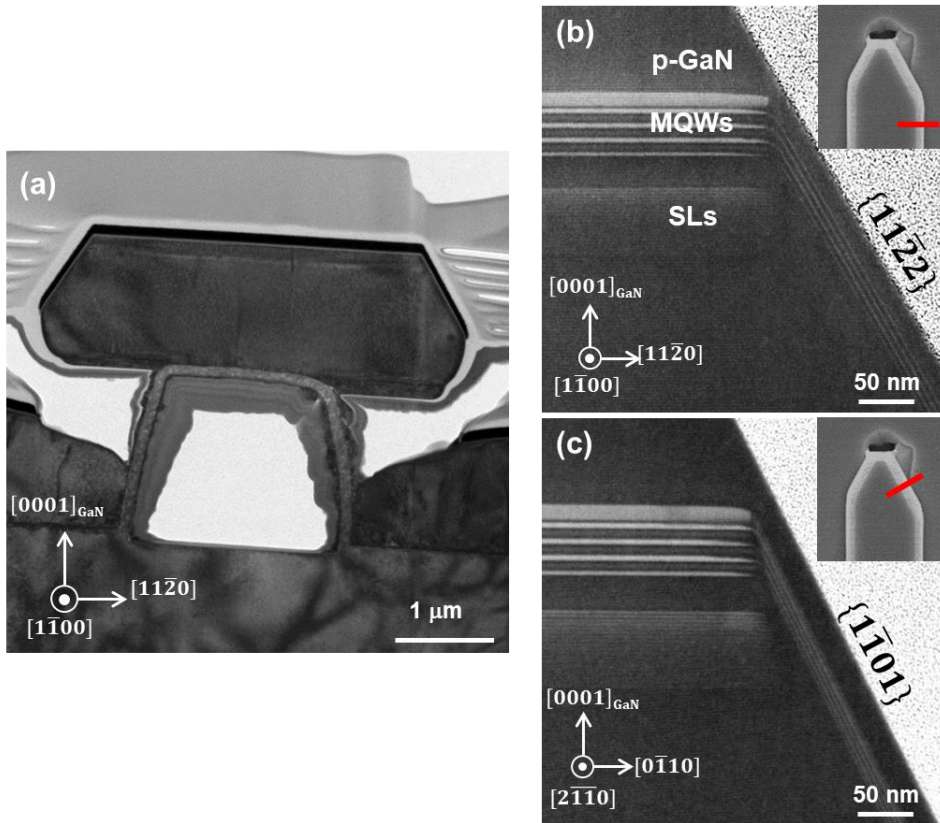
Figure 5.11. Cross-section TEM and STEM images of a core-shell-like micro-LED. (a) Cross-section TEM image of single micro-LEDs on sapphire nano-membrane with zone axis of $[1\bar{1}00]$ direction of GaN. Cross-section STEM images with zone axis of (b) $[1\bar{1}00]$ direction and (c) $[2\bar{1}\bar{1}0]$ direction of GaN.
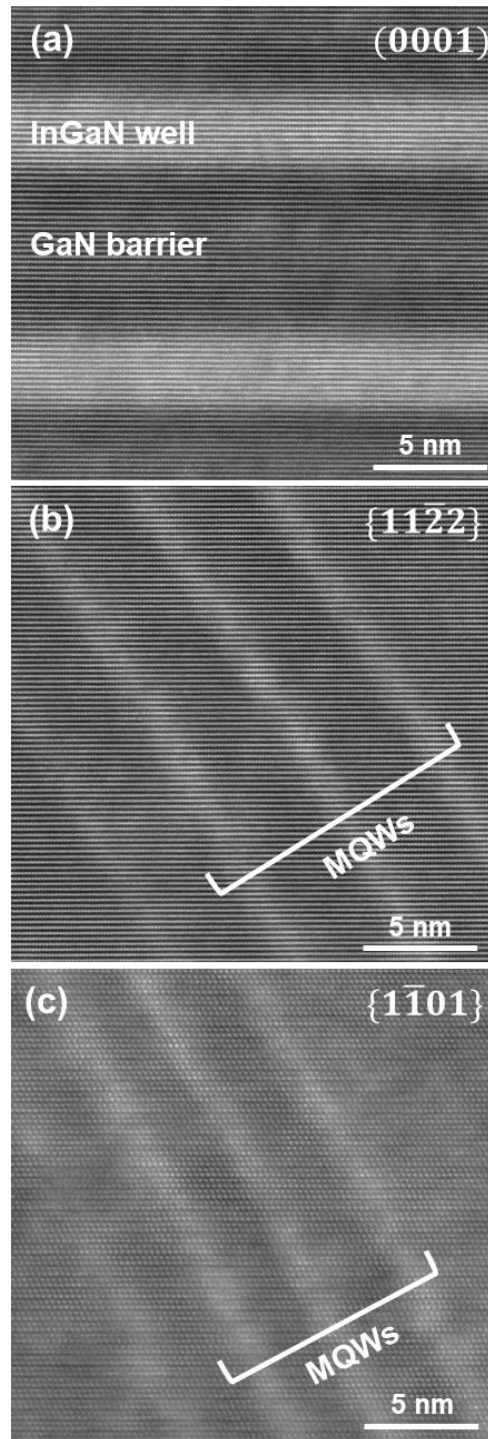
Figure 5.12. STEM images of InGaN/GaN MQWs on facets of (a) (0001), (b) {11$\bar{2}$2}, and (c) {1$\bar{1}$01}.
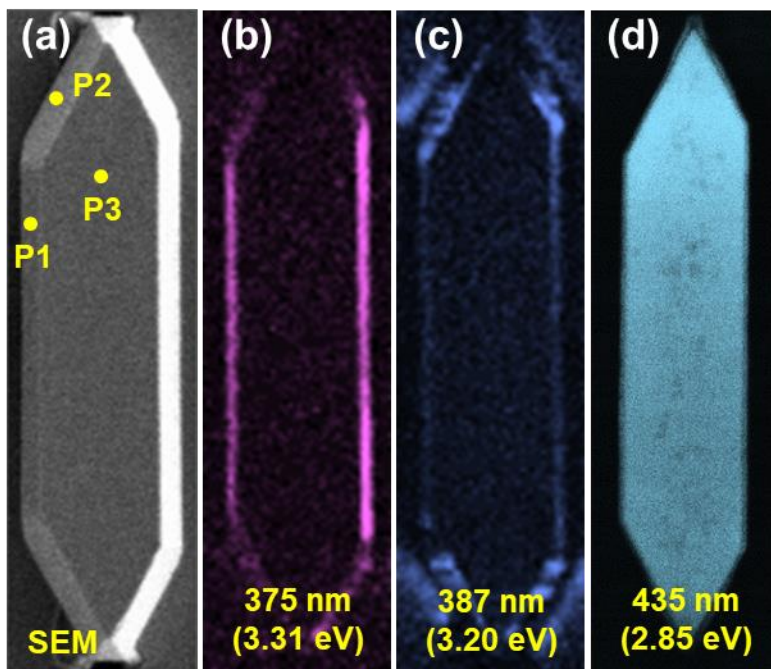
Figure 5.13. Plan-view SEM image and CL emission properties of single micro-LED
(a) Plan-view SEM image of single micro-LED grown on sapphire nano-membrane.
Monochromatic CL images measured at wavelengths of (b) 375 nm, (c) 387 nm, and
(d) 435 nm.
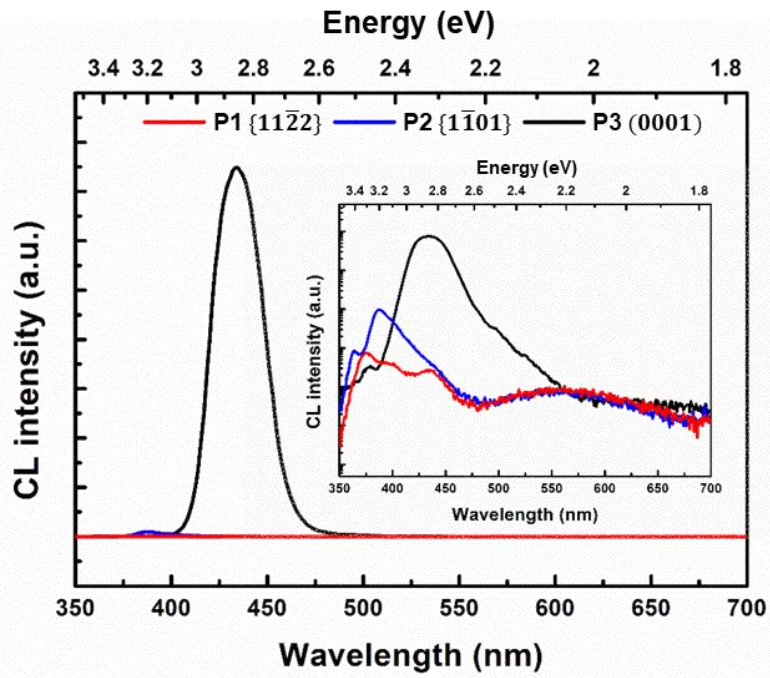
Figure 5.14. Spatially-resolved CL spectra measured at $\{11\bar{2}2\}$, $\{1\bar{1}01\}$, and (0001) facets. The inset figure shows the CL spectra in log scale.

5.3.4 Transfer of a micro-LED array for device fabrication

Figure 5.15 shows schematic diagram for the fabrication of a vertical-type micro-LED device. Before transfer of a micro-LED array, p-metal pattern was formed on c-plane micro-LED array and Ag-based p-ohmic metal (ITO 20 nm / Ni 0.5 nm / Ag 250 nm / Ni 100 nm / Ti 20 nm / Ni 20 nm / Au 90 nm) was deposited on a micro-LED array by e-beam evaporator as shown in Fig 5.16. After metal lift-off process, the sapphire substrate with a micro-LED array was flipped over to a p-metal deposited SiO_2/Si wafer (Ti 20 nm / Ni 40 nm / Au 60 nm / Sn 120 nm / Au 30 nm). Au/Sn eutectic bonding was used for bonding between micro-LEDs and target wafer. Figure 5.17 shows SEM images of a micro-LED array on target wafer successfully transferred by wafer bonder at 300 ℃ and 10 kgf for 20 min. The leg part of thin sapphire nano-membrane was broken by mechanical force, resulting in the monolithic transfer of a micro-LED array. The mechanical lift-off (MLO) has the advantage of being simpler and capable of processing in large quantities compared to existing substrate separation technologies such as laser lift-off (LLO) or chemical lift-off (CLO). In addition, since monolithic transfer of a micro-LED array is simply possible, it is very advantageous to apply to small displays such as VR/AR. Figure 5.18 shows cross-section TEM images of a transferred micro-LED array by mechanical lift-off. As shown in the magnified TEM image, the leg of the membrane was broken and the upper part of the sapphire nano-membrane was transferred together. In order to make contact with the n-metal, it is necessary to remove the transferred membrane. After the transfer, 150 nm-thick Al_2O_3 was deposited by ALD for electrical isolation and the remained membrane and un-GaN was subsequently etched by PR patterning and dry etching. The dielectric SiO_2 layer was formed by

sputtering and lift-off process for planarization and semi-transparent n-metal (In 20 nm / ITO 200 nm) was deposited on the exposed n-GaN.

Figure 5.19 shows electroluminescence (EL) spectra of a 4 μm × 16 μm membrane LED as a function of injection current density. The inset graph shows peak wavelength as a function of injection current density for the membrane micro-LED and 10 μm × 10 μm dry-etched conventional micro-LED. In a dry etched micro-LED, due to the screening effect by quantum confined Stark effect (QCSE), blue shift of the peak wavelength was observed according to the injection current density, whereas in the membrane micro-LED, the peak shift was hardly seen. Due to the strain partitioning of the sapphire nano-membrane, the compressive stress applied to the GaN thin film is greatly reduced, thereby reducing the QCSE, resulting in almost no peak shift. The little peak shift according to the injection current density is a very important characteristic required for a display. Therefore, micro-LED growth on sapphire nano-membrane can be a powerful breakthrough in micro-LED display applications.
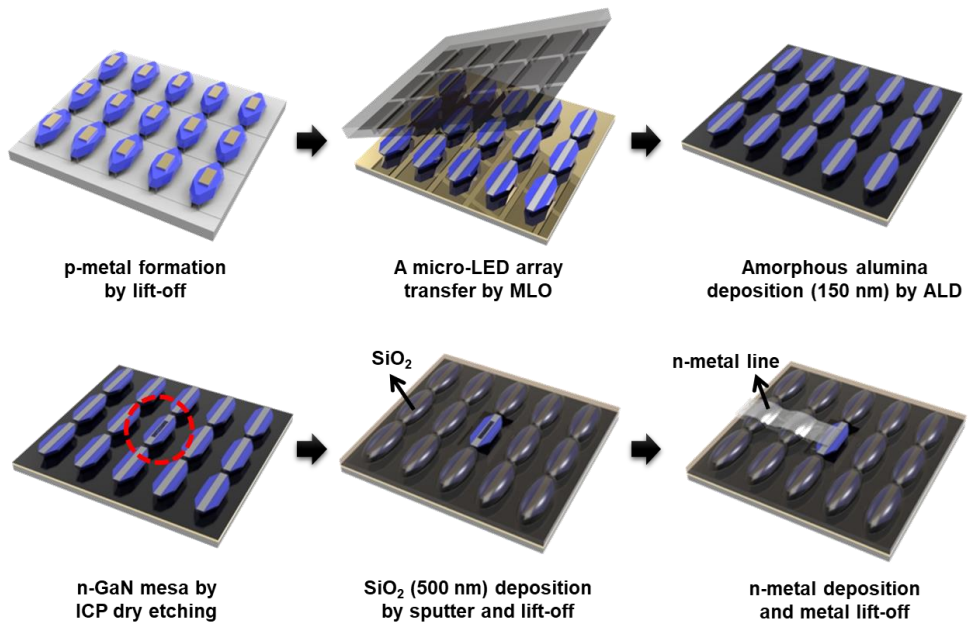
Figure 5.15. Schematic diagram for the fabrication of a vertical-type micro-LED device by transfer with mechanical lift-off.
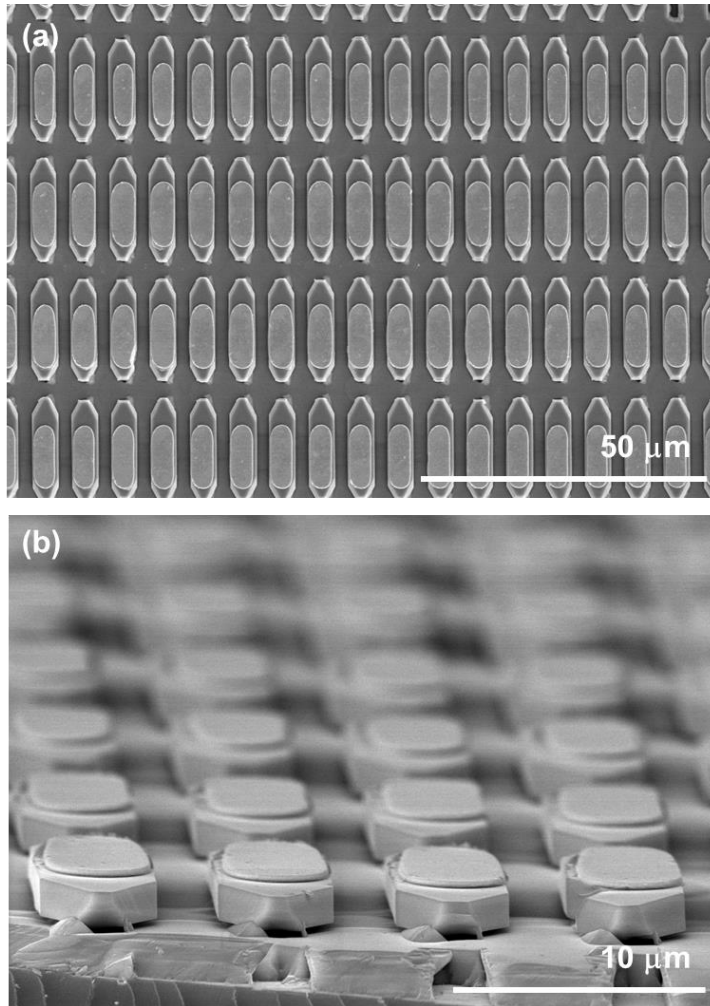
Figure 5.16. (a) Plan-view and (b) bird's eye view SEM images of a micro-LED array after p-metal deposition and metal lift-off.
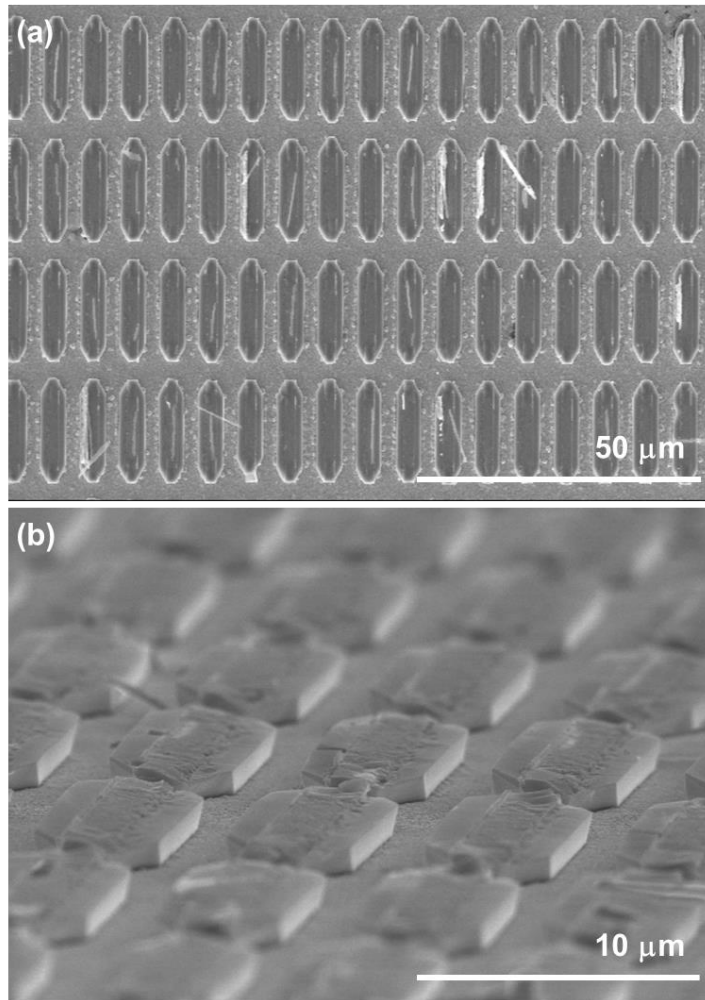
Figure 5.17. (a) Plan-view and (b) bird's eye view SEM images of a transferred micro-LED array by mechanical lift-off.
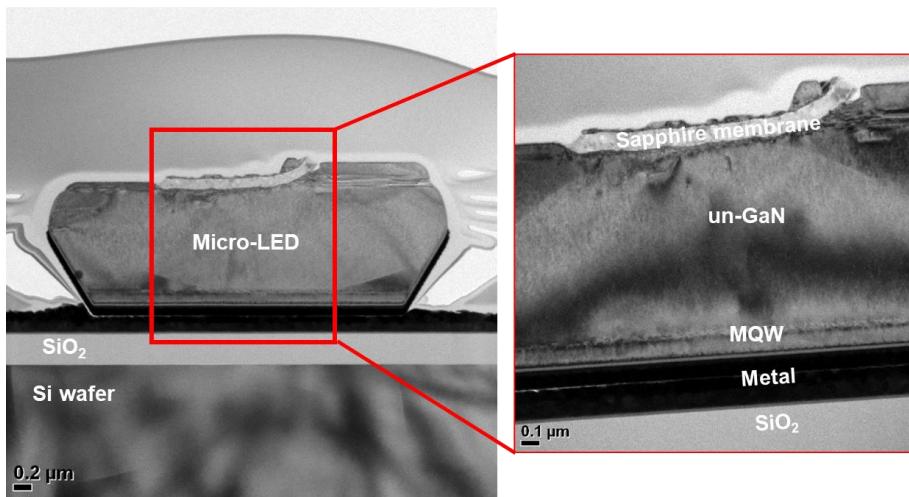
Figure 5.18. Cross-section TEM images of a transferred micro-LED array by mechanical lift-off and remained sapphire nano-membrane.
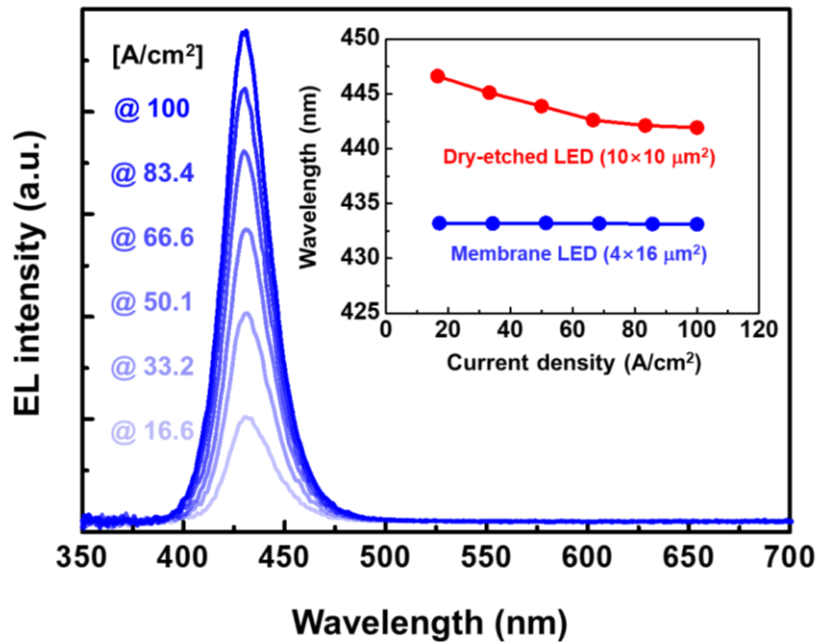
Figure 5.19. EL spectra of a membrane LED as a function of injection current density. The inset graph is peak wavelength as a function of injection current density for the membrane LED and dry-etched LED.

5.4 Summary

In this chapter, A core-shell-like micro-LED array with multi-facets was successfully grown on a 100 nm-thick sapphire nano-membrane array without harmful plasma etching. The micro-LED on sapphire nano-membrane was individually formed and MQWs was not exposed by self-passivation of p-GaN. Raman analysis showed that compressive stress in GaN layer was reduced by 78.6% in the un-GaN. The CL measurement yielded a TDD of 1.85×10^8 cm^{-2}, which was reduced by 59.6%, compared to the LED on planar sapphire substrate. TD-PL measurement confirmed that IQE increased by 1.44 times, and PL intensity was improved by a factor of 3.3 compared to planar sapphire substrate. Strong CL emission at 435 nm was observed was observed from c-plane MQWs due to reduction of QCSE, whereas negligible CL emissions were measured from semi-polar sidewall facets. Vertical-type micro-LED devices were demonstrated by transferring micro-LED array through mechanical lift-off. Although optimization of fabrication process is needed, unique characteristics such as single blue emission and no peak shifts in EL spectra were observed, which is superior characteristic for display technology.

5.5. Bibliography

[1] J. Day, J. Li, D. Y. C. Lie, C. Bradford, J. Y. Lin, and H. X. Jiang, "III-nitride full-scale high-resolution microdisplays,", *Appl. Phys. Lett.* **99**, 031116 (2011).

[2] H. X. Jiang and J. Y. Lin, "Nitride micro-LEDs and beyond – a decade progress review", *Opt. Express* **21**, A475 (2013).

[3] T. Wu, C.-W. Sher, Y. Lin, C.-F. Lee, S. Liang, Y. Lu, S.-W. H. Chen, W. Guo, H.-C. Kuo, and Z. Chen," Mini-LED and micro-LED: promising candidate for the next generation display technology", *Appl. Sci.* **8**, 1557 (2018).

[4] G Haas, "Microdisplays for wearable augmented reality - OLED vs LED based systems", *SID Symp. Dig. Tech. Pap.* **50**, 713 (2019).

[5] E. Virey, "MicroLED displays: hype and reality, hopes and challenges." *Yole Development,* (2017).

[6] S. X. Jin, J. Li, and H. X. Jiang, "InGaN/GaN quantum well interconnected microdisk light emitting diodes", *Appl. Phys. Lett.* **77**, 3236 (2000),

[7] H. W. Choi, C. W Jeon, M. D. Dawson, P R. Edwards, R. W. Martin, S. Tripathy, "Mechanism of enhanced light output efficiency in InGaN-based microlight emitting diodes", *J. Appl. Phys.* **93**,5978 (2003).

[8] Z. Gong, S. Jin, Y. Chen, J. McKendry, D. Massoubre, I. M. Watson, E. Gu, and M. D. Dawson, "Size-dependent light output, spectral shift, and self-heating of 400 nm InGaN light-emitting diodes", *J. Appl. Phys.* **107**, 013103 (2010).

[9] T. -I. Kim, Y. H Jung, J. Song, D. Kim, Y. Li, H. -S. Kim, I. -S. Song, J. J. Wierer, H. A. Pao, Y. Huang, and J. A. Rogers, "High-efficiency, microscale GaN light-emitting diodes and their thermal properties on unusual substrates", *Small* **8**, 1643 (2012).

[10] S. X. Jin, J. Z. Li, J. Y. Lin, and H. X. Jiang, "GaN microdisk light emitting diodes", *Appl. Phys. Lett.* **76**,631 (2000).

[11] H. X. Jiang, S. X. Jin, J. Li, J. Shakya, J. Y. Lin, "III-nitride blue microdisplays", *Appl. Phys. Lett.* **78**, 1303 (2001).

[12] J. J. D. McKendry, B. R. Rae, Z. Gong, K. R. Muir, B. Guilhabert, D. Massoubre, E. Gu, D. Renshaw, M. D. Dawson, and R. K. Henderson, "Individually addressable AllnGaN micro-LED arrays with CMOS control and subnanosecond output pulses", *IEEE Photon. Tech. Lett.* **21**, 811 (2009).

[13] Z. J. Liu, K. M. Wong, W. C. Chong, and K. M. Lau, "Active matrix programmable monolithic light emitting diodes on silicon (LEDOS) displays", *SID Symp. Dig. Tech. Pap.* **42**, 1215 (2011).

[14] C.-W. Sun, C.-H. Chao, H.-Y. Chen, Y.-H. Chiu, W.-Y. Yeh, M. H. Wu, H.-H. Yen, and C.-C. Liang, "Development of micro-pixellated GaN LED array", *SID Symp. Dig. Tech. Pap.* **42**, 1042 (2011).

[15] P. Tian, J. J. D. McKendry, Z. Gong, B. Guilhabert, I. M. Waatson, E. Gu, Z. Chen, G. Zhang, and M. D. Dawson, "Size-dependent efficiency and efficiency droop of blue InGaN micro-light emitting diodes", *Appl. Phys. Lett.* **101**, 231110 (2012).

[16] P. Tian, J. J. D. McKendry, J. Herrnsdorf, S. Watson, R. Ferreira, I. M. Watson, E. Gu, A. E. Kelly, and M. D. Dawson, "Temperature-dependent efficiency droop of blue InGaN micro-light emitting diodes", *Appl. Phys. Lett.* **105**, 171107 (2014).

[17] F. Templier, "GaN-based emissive microdisplays: A very promising technology for compact, ultra-high brightness display systems", *J. Soc. Info. Disp.* **24**, 669 (2016).

[18] F. Olivier, S. Tirano, L. Dupré, B. Aventurier, C. Largeron, and F. Templier, "Influence of size-reduction on the performance of GaN-based micro-LEDs for display applications", *J. Lumin.* **191**, 112 (2017).

[19] F. Olivier, A. Daami, C. Licitra, and F. Templier, "Shockley-Read-Hall and Auger non-radiative recombination in GaN based LEDs: A size effect study". *Appl. Phys. Lett.* **111**, 022104 (2017).

[20] S.-C. Haung, H. Li, Z.-H. Zhang, H. Chen, S. C. Wang, and T.-C. Lu, "Superior characteristics of microscale light emitting diodes through tightly lateral oxide-confined scheme", *Appl. Phys. Lett.* **110**, 021108 (2017).

[21] D. Hwang, Mughal, C. D. Pynn, S. Nakamura, and S. P. DenBaars, "Sustained high external quantum efficiency in ultrasmall blue III-nitride micro-light-emitting diodes", *Appl. Phys. Express* **10**, 032101 (2017).

[22] M. S. Wong, D. Hwang, A. I. Alhassan, C. Lee, R. Ley, S. Nakamura, and S. P. DenBaars, "High efficiency of III-nitride micro-LEDs by sidewall passivation using atomic layer deposition", *Opt. Express* **26**, 21324 (2018)

[23] S. S. Konoplev, K. A. Bulashevich, and S. Y. Karpov, "From large-size to micro-LEDs: scaling trends revealed by modeling", *Phys. Status Solidi A* **215**, 1700508 (2018).

[24] M. R. Krames, M. Ochiai-Holcomb, G. E. Höfler, C. Carter-Coman, E. I. Chen, I.-H. Tan, P. Grillot, N. F. Gardner, H. C. Chui, J.-W. Huang, S. A. Stockman, F. A. Kish, and M. G. Craford, "High-power truncated-inverted-pyramid $(Al_xGa_{1-x})_{0.5}In_{0.5}P$/GaP light-emitting diodes exhibiting >50% external quantum efficiency", *Appl. Phys. Lett.* **75**, 2365 (1999).

[25] D. Moon, J. Jang, D. Choi, I. -S. Shin, D. Lee, D. Bae, Y. Park, and E. Yoon, "An ultra-thin compliant sapphire membrane for the growth of less strained, less defective GaN", *J. Cryst. Growth* **441**, 52 (2016).

[26] J. Jang, D. Yang, D. Moon, D. Choi, H. J. Lim, S. Kang, D. Bae, H. N. Han, Y. Park and E. Yoon, "Solid-phase epitaxy of a cavity-shaped amorphous alumina nanomembrane structure on a sapphire substrate", *J. Cryst. Growth* **498**, 130 (2018).

[27] E.-H. Park, J. Jang, S. Gupta, I. Rerguson, S.-K. Jeon, J.-G. Kim, J. -S. Lee, C.-H. Kim, and J. S. Park, "The effect of the last quantum barrier on the internal quantum efficiency of InGaN-light emitting diodes", *Appl. Phys. Lett.* **93**, 101112 (2008).

[28] Q. Sun, C. D. Yerino, B. Leung, J. Han, and M. E. Coltrin, "Understanding and controlling heteroepitaxy with the kinetic Wulff plot: A case study with GaN", *Nucl. Instrum. Methods Phys. Res. B* **206** 357 (2003).

[29] B. Beaumont, P. Vennéguès, and P. Gibart, "Epitaxial lateral overgrowth of

GaN", *Phys. Status Solidi B* **227**, 1 (2001).

[30] K. Nishizuka, M. Funato, Y. Kawakami, Sg. Fujita, Y. Narukawa, and T. Mukai, "Efficient radiative recombination from (1122)-oriented multiple quantum wells fabricated by the regrowth technique", *Appl. Phys. Lett.* **85**, 3122 (2004).

[31] Hiramatsu, K. et al. "Recent progress in selective area growth and epitaxial lateral overgrowth of III-nitrides: Effect of reactor pressure in MOVPE growth", *Phys. Status Solidi* **176**, 535 (1999).

[32] K. A. Bulashevich, S. S. Konoplev, and S, Y, Karpov, "Effect of die shape and size on performance of III-nitride micro-LEDs: a modeling study", *Photonics* **5**, 41 (2018).

[33] S. Tripathy, S. J. Chua, P. Chen, and Z. L. Miao, "Micro-Raman investigation of strain in GaN and $Al_xGa_{1-x}N$/GaN heterostructures grown on Si(111)", *J. Appl. Phys.* **92**, 3503 (2002).

[34] V. Narayanan, K. Lorenz, W. Kim, and S. Mahajan, "Origins of threading dislocations in GaN epitaxial layers grown on sapphire by metalorganic chemical vapor deposition", *Appl. Phys. Lett.* **78**, 1544 (2001).

[35] R. A. Oliver, M. J. Kappers, and C. J. Humphreys, "Insights into the origin of threading dislocations in GaN/Al_2O_3 from atomic force microscopy", *J. Cryst. Growth* **289**, 506 (2006).

[36] K. Linthicum, T. Gehrke, D. Thomson, E. Carlson, P. Rajagopal, T. Smith, D. Batchelor, and R. Davis, "Pendeo epitaxy of gallium nitride thin films", *Appl. Phys.*

Lett. **75**, 196 (1999).

[37] Y. Kawakami, K. Omae, A. Kaneta, K. Okamoto, T. Izumi, S. Sajou, K. Inoue, Y. Narukawa, T. Mukai, and Sg. Fujita, "Radiative and nonradiative recombination processes in GaN-based semiconductors", *Phys. Status Solidi A* **183**, 41 (2001).

[38] N. Yoshimoto, T. Matsuoka, T. Sasaki, and A. Katsui, "Photoluminescence of InGaN films grown at high temperature by metalorganic vapor phase epitaxy", *Appl. Phys. Lett.* **59**, 2251 (1991).

[39] Y. Guo, X. L. Lin, H. P. Song, A. L. Yang, X. Q. Xu, G. L. Zheng, H. Y. Wei, S. Y. Yang, Q. S. Zhu, and Z. G. Wang, "A study of indium incorporation in In-rich InGaN grown by MOVPE", *Appl. Surf. Sci.* **256**, 3352 (2010).

[40] M. Funato, T. Kotani, T. Kondou, Y. Kawakami, Y. Narukawa, and T. Mukai, "Tailored emission color synthesis using microfacet quantum wells consisting of nitride semiconductors without phosphors", *Appl. Phys. Lett.* **88**, 261920 (2006).

[41] C. Cho, I, K Park, M. -K. Kwon, J. -Y. Kim, S. -J, Park, D. R. Jung, and K. W. Kwon, "Phosphor-free white light-emitting-diode using InGaN/GaN multiple quantum wells grown on microfacets", *Proc. of SPIE* **7058**, 70580N (2008).

[42] K. M. Song, D. -H. Kim, J. -M. Kim, C. -Y. Cho, J. Choi, K. Kim, J. Park, and H. Kim, "White light emission of monolithic InGaN/GaN grown on morphology-controlled, nanostructured GaN templates", *Nanotechnology* **28**, 225703 (2017).

[43] S. Hwang, Na Han, H. Jeong, J. H. Park, S. -H. Lim, J. -H. Cho, Y. -H. Cho, H. J. Jeong, M. S. Jeong, and J. K. Kim, "Optical and facet-dependent carrier

recombination properties of hendecafacet InGaN/GaN microsized light emitters",
Cryst. Growth Des. **17**, 3649 (2017).

[44] Y. C, Sim, S. -H. Lim, Y. –S. Yoo, M. -H. Jang, S. Choi, H. –S. Yeo, K. Y. Woo, S. Lee, H. G. Song, and Y. -H. Cho, "Three-dimensional GaN dodecagonal ring structures for highly efficient phosphor-free warm white light-emitting diodes", *Nanoscale* **10**, 4686 (2018).

Chapter 6. Conclusions

In this study, the sapphire nano-membrane have been proposed to solve the current issues in micro-LEDs such as high cost, low EQE, and difficulty in the transfer process and to obtain the high quality GaN epitaxial layers.

Firstly, the growth behavior of GaN grown on the sapphire nano-membrane was observed in various orientations. In order to grow a discrete GaN array, stripe-shaped sapphire nano-membrane structures were fabricated in various directions and the lateral to vertical growth rate of growth facets of GaN was measured. The GaN layer grown on the membrane had (0001), $\{11\bar{2}0\}$, $\{11\bar{2}2\}$, and $\{1\bar{1}01\}$ growth facets along the orientation and the growth behavior was determined according to the growth rate of each facet. Lateral to vertical growth rate ratio decreased from 0° stripe pattern, which is parallel to $[11\bar{2}0]_{sapphire}$, to 30° distorted stripe pattern and increased again with 60°. The growth of GaN deposited in the spacing region was interrupted by the GaN layer on the membrane when the lateral growth rate was high. These growth features showed the potential to grow separate GaN layers.

Secondly, a discrete micro-GaN array with various sizes was grown on a sapphire nano-membrane structure by using different growth rates for each growth facet of GaN. To fabricate a micro-chip-sized sapphire nano-membrane that is closed on all sides, a method of ashing PR was introduced, and all of the PR was successfully removed by changing the thickness and density of the membrane. The micro-GaN layers with sizes of 14×14 and 50×50 μm^2 was grown separately from each other and did not merge with GaN grown on the spacing region, so it is expected to be advantageous when it is detached from the substrate. Threading dislocation

density (TDD) of chip-sized GaN was reduced by 40% and the PL intensity increased by 36.5% as compared with the GaN on planar sapphire substrate. This study provides opportunities to realize high quality GaN epitaxial layers and fabricate micro-LEDs without chip singulation process.

Lastly, a core-shell-like micro-LED array with multi-facets was grown on a 100 nm-thick sapphire nano-membrane array. Without harmful plasma etching for chip singulation, the core-shell-like micro-LED with size of 4×16 μm^2 was individually formed on each sapphire nano-membrane. Significant stress relaxation of 78.6% in the un-doped GaN and considerable TDD reduction of 59.6% in the micro-LED were observed due to the compliant sapphire nano-membrane structure used in this study. IQE was enhanced by a factor of 1.44, and PL intensity was improved by a factor of 3.3 from the micro-LEDs on sapphire nano-membranes compared to the LED on planar sapphire substrate. Strong CL emission at 435 nm was observed from c-plane MQWs, whereas negligible CL emissions were measured from semi-polar sidewall facets. The discrete micro-LED arrays successfully transferred to target wafer by mechanical lift-off to fabricate vertical-type micro-LED devices. This study is expected to provide a platform technology to realize high-efficiency micro-LEDs by using sapphire nano-membrane, which is suitable for next-generation display technology.

국 문 초 록

　3족 질화물 기반 반도체는 고품질, 높은 효율, 긴 수명 등의 장점을 가지고 있어 지난 수십 년 동안 발광 다이오, 레이저, 태양전지 등 광전자 소자 응용 분야에서 상당한 관심을 받고 있다. 질화갈륨 기반 에피층은 경제적, 기술적인 이유로 동종 기판을 사용한 에피 성장이 불가능하여 주로 Si, SiC 및 Sapphire와 같은 이종 기판에서 성장한다. 그 중에서 사파이어 기판은 고품질, 투명성 및 고온 안정성으로 인해 광범위하게 사용하는데 에피층과의 격자 상수 차이와 열팽창 계수 차이로 인해 많은 문제점들이 발생하게 된다. 격자상수 차이로 인하여 광소자 효율에 직접적으로 영향을 미치는 고밀도의 전위 결함이 에피층 내에 생성되고 열팽창 계수 차이로 인하여 고온에서의 에피층 성장 후 상온 냉각 시에 기판 휨 현상과 함께 박막에 큰 압축 응력이 작용하게 된다. 이는 질화갈륨 기반 광소자의 구현을 방해한다.

　마이크로 발광 다이오드는 기존 디스플레이 기술인 액정 표시 장치나 유기 발광 다이오드에 비해 고휘도, 빠른 응답 속도, 초고해상도 구현 가능, 낮은 전력 소모 등 우수한 특성을 가지고 있어 차세대 디스플레이 기술로 각광받고 있다. 특히, 앞으로 많은 수요가 기대되는 가상 현실과 증강 현실과 같은 분야에서는 디스플레이가 사람의 눈에 가까워지며, 초고화질의 마이크로 디스플레이를 요구하고 있다. 하지만, 낮은 외부양자 효율, 높은 수준의 누설 전류 및 미숙한 마이크로 발광 다이오드 전사

기술 등이 상용화에 걸림돌이 되고 있다. 기존 마이크로 발광 다이오드 제작은 기판 위에 발광 다이오드 에피층을 성장한 후, 개별 마이크로 발광 다이오드를 형성하기 위하여 플라즈마 식각 공정을 이용한다. 이는 활성층 역할을 하는 다중양자우물 구조를 외부에 드러나게 하여 비발광 재결합을 증가시키고 따라서 낮은 외부양자효율과 높은 수준의 누설 전류를 발생하게 한다.

본 연구에서는 사파이어 나노멤브레인 구조가 형성된 기판을 제안하여 고품질의 질화갈륨 에피층을 얻고 마이크로 발광 다이오드의 문제점들을 해결하고자 하였다. 사파이어 나노멤브레인 위의 질화갈륨 성장은 유기금속화학증착법을 이용하여 연구하였다.

질화갈륨 에피층의 성장은 성장 방향과 성장 조건에 따라 다양한 모습으로 성장하며, 여러 결정면들이 나타난다. 사파이어 나노멤브레인 위에 원하는 형태의 마이크로 질화갈륨 에피층을 성장하기 위해, 먼저 사파이어 나노멤브레인 위 질화갈륨의 성장 양상을 이해하는 연구를 진행하였다. 사파이어 나노멤브레인 제작은 포토리소그래피, 원자층 증착 장비를 활용한 비정질 알루미나 증착, 포토리지스트 제거, 후속 열처리 공정을 통한 결정화로 진행된다. 비정질 알루미나층은 열처리 과정에서 고상에피택시를 통해 사파이어 기판과 같은 단결정 알파상 알루미나층으로 결정화된다. 성장 방향에 따른 성장 거동을 파악하기 위해, 스트라이프 패턴의 각도를 다양하게 바꾸며 질화갈륨의 성장을 관찰하였다. 사파이어 [11$\overline{2}$0] 방향의 스트라이프 형태 사파이어 나노멤브레인에서 가장 빠른 측면 성장 속도를 볼 수 있었고, 30도 회전할 때마다 측면 성장 속도

가 최고와 최소를 반복하는 것을 확인하였다. 방향에 따라 다르게 형성되는 질화갈륨 결정면들의 성장 속도를 측정하여 질화갈륨의 성장 형태가 달라지는 것을 이해할 수 있었다. 또한, 멤브레인 패턴 사이의 바닥 영역에서 성장한 질화갈륨도 관찰하였다. 측면 성장이 원활하게 진행된 멤브레인 위 질화갈륨층에 의하여 바닥 영역으로의 갈륨 확산이 저해되었고, 이는 사파이어 나노멤브레인을 부러뜨려 질화갈륨층을 기판에서 떼어낼 수 있다는 가능성을 보여주었다.

다음으로, 사파이어 나노멤브레인 위 성장 양상에 대한 이해를 토대로 패턴을 설계하여 서로 분리된 마이크로 크기의 질화갈륨층을 성장하였다. 사파이어 나노멤브레인이 막힌 구조이기 때문에 포토리지스트를 제거하기 위한 산소 플라즈마 방법을 제안하였다. 멤브레인의 두께와 밀도를 조절하며 포토리지스트의 제거 속도를 관찰하였고 결과적으로 적합한 조건을 이용하여 다양한 크기의 사파이어 나노멤브레인을 성공적으로 제작할 수 있었다. 측면 성장 속도가 가장 빠른 방향과 가장 느린 방향을 이용하여 패턴의 방향과 크기를 적절히 설계하였고 원하는 영역에서만 질화갈륨층이 합쳐지게 하여 서로 분리된 마이크로 크기의 질화갈륨이 성장하게 하였다. 마이크로 크기의 질화갈륨층은 평면 사파이어 기판에서 성장한 질화갈륨에 비해 관통전위 밀도가 40% 감소하였고, 광 발광 세기는 36.5% 증가하였다.

마지막으로, 100 nm 두께의 사파이어 나노멤브레인 위에 마이크로 발광 다이오드 어레이를 해로운 플라즈마 식각 공정 없이 성장하였다. 서로 분리되어 성장한 마이크로 발광 다이오드의 측면 다중양자우물 층은

p형 질화갈륨에 의해 보호되는 것을 확인하였고 이는 플라즈마 식각 공정으로 인한 광 효율의 저하를 막을 수 있을 것으로 기대된다. 사파이어 나노멤브레인 위에 성장한 마이크로 발광 다이오드의 관통전위 밀도는 평면 사파이어 기판 위에 성장한 발광 다이오드에 비해 59.6% 감소하였다. 또한, 내부양자효율이 44% 향상되었고 광 발광 세기가 3.3배 증가한 것을 관찰하였다. 435 nm의 음극 발광 방출이 c면 다중양자우물에서 측정된 반면, 측면의 반극성면에서 무시할 수 있는 수준의 방출이 관측되었다. 코어쉘 형태의 다중양자우물이 모든 면에 형성되어 있어 비복사 표면 재결합을 감소시키고 누설 전류 경로를 줄이게 된다. 본 연구를 통해, 사파이어 나노멤브레인 기술이 마이크로 발광 다이오드를 위한 획기적인 플랫폼 기술로 발전될 가능성을 기대한다.